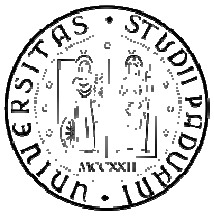

UNIVERSITA' DEGLI STUDI DI PADOVA

DIPARTIMENTO DI PEDIATRIA

SCUOLA DI DOTTORATO DI RICERCA

Medicina Dello Sviluppo e Scienze Della Programmazione

INDIRIZZO: Malattie Rare, Genetica, Biologia e Biochimica

XXIV CICLO

Study of mechanism of action of the phototoxicity of drugs and of new natural compounds endowed with antiproliferative activity

Direttore della Scuola : Ch.mo Prof. Giuseppe Basso

Coordinatore d'indirizzo: Ch.mo Prof. Giorgio Perilongo

Supervisore : Dott. Giampietro Viola

Dottoranda: Maria Antonella Linardi

2009-2011

INDEX

SUMMARY

Study of mechanism of action of the phototoxicity of drugs and of new natural compounds endowed with antiproliferative activity

In recent years it has been observed an increase of clinical cases on the phototoxicity of drugs, this fact is probably due to changes in lifestyle and to a greater number of drugs present on the market. In this study we have examined the mechanisms of phototoxicity of Fluvastatin and the Pitavastatin two HMG-CoA reductase inhibitors. Initially it was observed that these drugs when in aqueous solution, can form different photoproducts, after the irradiation with UVA . The photoproducts were separated by HPLC and characterized by mass spectrometry and NMR. For the fluvastatin it was isolated a photoproduct in sufficent quantity (FP6), while for pitavastatin were isolated two photoproduct (PP3 and PP4). The phototoxicity of these drugs and that of their photoproduct were tested on the human keratinocytes cell line NCTC 2544. The cell phototoxicity was evaluated by the MTT test after 72h from the irradiation, in presence of the two drugs and submitted at different doses of UVA and different concentrations. The photoproducts were also evaluate for they potential phototoxicity. The results obtained show a reduction in the cell viability dependent of the dose of UVA administered and of the concentration of drug used, and interestingly it was noted that the photoproducts are much more phototoxic than the parent compound. After through the use of the flow cytometry it was demonstrate that these drugs and their photoproduct are able to induce necrosis as a major made of cell death as a result of the incorporation of the propidium in the irradiated cell in the presence of the compounds examined . Furthermore, this was confirmed also by a strong depletion of the cellular ATP level and by the absence of mitochondrial depolarization. Moreover further experiments have shown an increase of intracellular calcium due to a damage induced to the cell membrane after the phototoxic insult. To confirm this hypothesis we have observed after treatment high levels of membrane lipids peroxidation. This data suggest that the phototoxic mechanism of these drugs are mediatates by the formation of photoproducts and/or reactive species (radicals, ROS) have the membrane cell as target over which they exercise their photoxic effects.

Another study carried out in this thesis regards the analysis of natural compounds as anticancer agents. The substances present in nature have for centuries known for

their healing proprieties and in the last years have become very important for the research and the development of new drugs, in fact many of them have a natural origin. The compounds evaluated were extracted from Ferula the *ferula communis*, *ferulago campestris* and of the *ferula glauca*, a plant belonging to the family of Umbrellifere. These plants have been much studied for their antimicrobial, estrogenic, and antiviral activity and for their cytotoxic properties. Initially was evaluated the cytotoxicity of different compounds on six cell line, three lines from solid tumors and three leukemia cell lines. From this screening we have identified four compounds structurally related to daucane esters endowed with high cytotoxicity activity especially on the leukemic cell lines. The activity of the four compound was analyzed on the cell cycle and for their proapoptotic activity . Of these four compounds, all showed a block of cell cycle in the G1 phase but only two have a high proapoptotic activity, so we proceeded to further study these compounds named DE 8, and DE 11. In the leukemia T-cell line Jurkat, it was evaluated the ROS production (reactive oxygen species) and it was examined the mitochondrial potential, and it was observed after one hour of incubation, a high ROS production while the depolarization of mitochondrial potential occurred later at longer times, indicating that the ROS production is due to the molecule itself, and not as a result of the mitochondrial depolarization. To confirm that the cell death occurred for the early ROS production, the cells were incubated with well-known scavenger of ROS such as N-acetylcisteine, Tocoferol e Butylhydroxyanisol. The results obtained have showed a significant increase of the cellular survival in the cell treated with DE-8 togheter with the inhibitor of ROS, respect to the cells treated alone with the compound. The cell were incubated also with the an Pancaspase inhibitor, Z-Vad, demonstrating also in this case un increase of the cellular viability, suggesting that the apoptosis is caspase- dependent.

RIASSUNTO

Studio del meccanismo d'azione della fototossicità di farmaci e di nuovi composti naturali ad azione antiproliferativa

Negli ultimi anni è stato osservato un aumento di casi clinici riguardanti la fototossicità dei farmaci, e questo fatto probabilmente è dovuto a cambiamenti di stile di vita e a un maggior numero di farmaci presenti sul mercato. In questo studio sono stati esaminati i meccanismi di fototossicità di due farmaci inibitori della HMG-CoA riduttasi: la Fluvastatina e la Pitavastatina.

Inizialmente è stato osservato che questi farmaci in soluzione acquosa, sono in grado di formare dei fotoprodotti, in seguito ad irradiazione con raggi UVA. Questi fotoprodotti sono stati separati attraverso HPLC e caratterizzati mediante spettrometria di massa e NMR. Per quanto riguarda la fluvastatina è stato isolato un fotoprodotto (FP6) in quantità sufficiente, mentre per la pitavastatina sono stati isolati due fotoprodotti (PP3 e PP4). La fototossicità di questi farmaci e dei loro fotoprodotti, è stata testata su una linea di cheratinociti umani NCTC-2544. La fototossicità cellulare è stata valutata attraverso il test del MTT dopo 72 ore dall'irradiazione, in presenza dei due farmaci e dei loro fotoprodotti sottoposti a diverse dosi di UVA. I risultati ottenuti mostrano una riduzione della vitalità cellulare dipendente dalla dose di UVA somministratisi e dalla concentrazione utilizzata e in maniera interessante è stato notato che i fotoprodotti risultano essere molto più fototossici del farmaco di partenza. Successivamente grazie all'uso della citometria a flusso, è stato dimostrato che questi farmaci e i loro fotoprodotti sono in grado di indurre necrosi come meccanismo principale di morte cellulare, come risulta dalla rapida incorporazione di ioduro di propidio nelle cellule irradiate in presenza dei composti in esame. Ciò è stato inoltre confermato anche da una forte deplezione dei livelli cellulari di ATP senza che vi sia alcuna depolarizzazione del potenziale mitocondriale. Ulteriori studi hanno mostrato un incremento di calcio a livello citoplasmatico dovuto a un ingresso di calcio extracellulare causato probabilmente da danni indotti alla membrana cellulare in seguito all'insulto fototossico. A conferma di questa ipotesi abbiamo osservato dopo trattamento un elevato livello di perossidazione dei lipidi di membrana. Questi dati suggeriscono che questi farmaci attraverso la formazione di fotoprodotti e/o specie

reattive (radicali ROS) presentano come bersaglio la membrana cellulare sulla quale esercitano i loro effetti fototossici.

Un altra ricerca svolta in questo dottorato ha riguardato lo studio di composti naturali come antitumorali. Le sostanze presenti in natura sono da secoli conosciute per le loro proprietà curative e negli ultimi anni sono divenuti molto importanti per la ricerca e lo sviluppo di nuovi farmaci infatti molti di essi hanno origine naturale. I composti valutati sono stati isolati dalla Ferula, dalla *ferula communis, ferulago campestris* e dalla *ferula glauca*, una pianta facente parte della famiglia delle Umbrellifere. Queste piante sono state molto studiate per la loro attività antimicrobica estrogenica, antivirale e con proprietà citotossiche, *in vitro* antilesmanica e antiproliferativa. Inizialmente è stata valutata la citotossicità dei diversi composti su sei linee cellulari: 3 linee provenienti da tumori solidi e 3 linee leucemiche. Da questo screening sono stati individuati quattro composti strutturalmente correlati a Daucano Esteri che presentano una buona attività citotossica elevata attività citotossica soprattutto sulle linee leucemiche. Successivamente è stata analizzata l'attività dei quattro composti sul ciclo cellulare e la loro attività proapoptotica Di questi quattro composti tutti hanno mostrato un blocco del ciclo cellulare in fase G1 ma solo due presentano un' elevata attività proapototica così si è proceduto allo studio approfondito solo di due composti denominati DE-8 e DE-11.

E' stata valutata la produzione di ROS (Reactive Oxygen Species) ed è stato esaminato il potenziale mitocondriale, andando così ad osservare che già dopo 1h dall'incubazione con il composto si aveva un elevata produzione di ROS mentre la depolarizzazione del potenziale mitocondriale avveniva successivamente , a tempi più lunghi, indicando che la produzione di ROS era dovuta alla molecola in se e non come conseguenza della depolarizzazione mitocondriale.

Per confermare che la morte cellulare avveniva per la produzione precoce di ROS le cellule sono state incubate con scavenger dei ROS quali N-acetilcisteina, Tocoferolo e Butilidrossianisolo. I risultati ottenuti hanno dimostrato un significativo aumento della sopravvivenza cellulare delle cellule trattate con DE-8 insieme ad inibitori dei ROS rispetto alle cellule trattate solo con il composto. Successivamente le cellule sono state incubate anche con un inibitore pancaspasico, lo Z-Vad, dimostrando anche in questo caso un aumento della vitalità cellulare, suggerendo che l'apoptosi è caspasi dipendente.

PART 1: THE PHOTOXICITY OF DRUGS

Introduction

The solar spectrum consists of electromagnetic energy with a wavelength that goes from 200 to 1800 nm. the wavelengths between 400-760 nm include the visible, that goes from 760-1800 nm include the infrared and then the ultraviolet that goes between 200-400 nm.

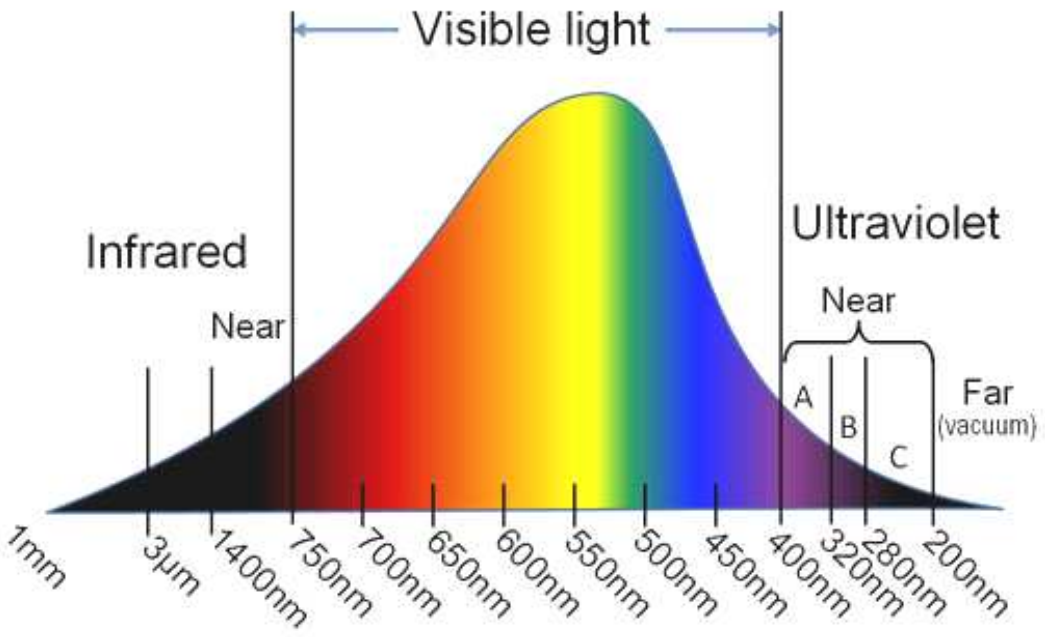

Figure 1. *Rapresentative solar spectrum*

Ultraviolet light, , is able to pass through the different layers of the atmosphere, it is characterized by its short wavelength and reach earth. The wavelengths of the ultraviolet region of the solar spectrum, are imperceptible to the human eye, but they are an inherent part of our everyday life. Ultraviolet radiations was divided in three region.UVA (320-400 nm) are the responsibility of the suntan and are considered the harmless UVB (290-320) are responsible for sunburn and photocarcinogenicity;. UVC (200-290 nm) are the most biologically active in fact they have antimicrobial and mutagenic activity.; but they are not relevant to human health because they are totally absorbed from atmosphere *(Greenhill et al 1990)*.

UVB frequencies are absorbed in the first layers of the skin composed by dead cells of stratum corneum; however UVA radiations are able to reach the blood vasculature system. The dated interest of photochemists for the properties of the electronically excited states of compounds of pharmaceutical use has been rapidly increasing during the last decade. *(Van Henegouwen et al).*

Xenobiotic species such as pharmaceutical products transported through the blood system will eventually reach superficial areas in the body where they will readily absorb the incident radiation. A wide range of photophysical and photochemical reactions may occur at this instance, reaction for which the organism has not evolved to protect itself. For instance in a biological system photochemical reaction of a compound such as decomposition, isomerization or rearrangement can occur and unstable photoproducts can react with endogenous molecules resulting in a biological effect. *(Van Henegouwen et al).*

Decomposition can also involve formation of radicals, which whether or not, coupled to oxygen, can damage biomolecules. An example of this phenomena is represented by chlorpromazine, which upon UVA irradiation decomposes into the corresponding radical which *in vivo* can covalently bound to lipid and proteins. Another documented reactions of xenobiotics or drugs is the photoreaction with endogenous molecules. This type of reaction is represented by the well known effect of psoralens used in the so called PUVA (psoralen plus UVA therapy) in which the irreversible binding of a photoexcited molecule of psoralen to DNA takes place (*Dall'Acqua et al 2004).* Energy transfer to endogenous molecules can also occur; this is exemplified by singlet oxygen formation from molecular oxygen. This phenomena is also exploited in photodynamic therapy of cancer.

The xenobiotics incident sunlight interactions can be very detrimental for living tissue since they can result in photoallergic and phototoxic responses. Photosensitization is defined as a process in which reactions to normally ineffective radiation doses are induced in a system by the introduction of a specific, radiation-absorbing substance (the photosensitizer), which causes another substance (the substrate) to be changed by radiation. When used to describe the reaction of skin to an exogenous chemical and UV or visible radiation, the term includes both phototoxic and photoallergic reactions.

Phototoxicity is an acute reaction that can be caused by a single treatment with a chemical and UV or visible radiation. *In vivo*, the reaction can be evoked in all subjects provided that the concentration of chemical and dose of light are appropriate. "Acute" includes both immediate and delayed (e.g. after 48 hours) reactions. *(Viola et al 2006).*

The term photoirritation is used to describe phototoxic reactions in skin which are produced with topically applied substances following exposure to light. Photoallergies are the response to a chemical modification of a substrate into allergen, for example drug-protein adduct formation following drug photoexcitation. The allergen will promote the formation of a specific antibody against its structure. Upon subsequent light exposure, an inflammatory antibody-antigen reaction will be elicited. From a mechanistic point of view it is generally accepted that photoallergy involves covalent binding of a drug derived hapten to a protein which results in the formation of the full antigen (*Lovell W.W. 1993)*. The hapten can be a stable photoproduct of the drug or a short lived photochemical intermediate for example a free radical. In the latter case the binding process must occur within a very short period of time, which requires that the precursor reaction partners must be in close proximity. Moreover many drugs may have the potential to photodamage DNA leading to photogenotoxic effects such as mutagenicity, chromosomal damage and eventually cause tumors (*Lovell W.W. 1993)*. Nowadays clinical data show an increase of the number of these phenomena, probably caused by changes in lifestyle and increased consumption of drugs. Therefore has been developed many models to product the potential phototoxicity and better undertand the mechanism of action on in vitro and in vivo. The tests in vitro are very important because shown a potential drug phototoxicity and can determine the correlation between the structure of the drug and its action phototoxic. Phototoxicity could be due to the formation of radicals or reactive oxygen species (ROS) and inorganic ions that cause cellular damage. This damage is related with the chemical structure of the compound. Usually the are damaged the subcellulare organelles or structures that are DNA, cell membrane and lysosomes *(Fasani et al 2002)*.

References

Bensasson, R.V., Land, E.J. and Truscott, T.G. *Excited States and Free Radicals in Biology and Medicine*, Oxford University Press, Oxford. 1993

Dall'Acqua, F., Viola, G. and Vedaldi, D. Molecular basis of psoralen photochemotherapy In *CRC Handbook of Organic photochemistry and Photobiology.* (Hoorspool, W.M. and Lenci, F. Eds.) CRC Press Boca Raton USA, 2004 pp.1-17.

Fasani E., Mella M., Andrea Ricci A., Monti S., Albini A. *Reattività foto indotta di farmaci e sua relazione con la foto stabilità di preparati farmaceutici e con effetti foto sensibilizzanti* Istituto Superiore di Sanità 2002.

Greenhill JV, McLelland MA. *Photodecomposition of drugs.* In Progress in medicinal Chemistry1990.27:1-4.

Lovell, W.W. A *scheme for in vitro screening of substance for photoallergenic potential* Toxic. In Vitro 1993 **7**, 95-102.

Van Henegouwen B. , G.M.J. Medicinal Photochemistry Phototoxic and Phototherapeutic Aspects of Drugs *In Advances in Drug Research*, (Testa, B. and Mayer, U. eds.) Academic Press,New York, 1997 Vol. **29**, pp. 79-17.

Viola G. Dall'Acqua F. *Photosensitization of Biomolecules by Phenothiazine Derivatives Current* Drug Targets, 2006, 7, 1135-1154

The Phototoxicity Of Fluvastatin, An HMG-CoA Reductase Inhibitor, Is Mediated By The Formation Of A Benzocarbazole-Like Photoproduct

Giampietro Viola*[1], Pawel Grobelny†, Maria Antonella Linardi*, Alessia Salvador‡, Giuseppe Basso*, Jadwiga Mielcarek§, Stefano Dall'Acqua‡, Daniela Vedaldi‡, Francesco Dall'Acqua‡

**Department of Pediatrics, Laboratory of Oncohematology, University of Padova, Italy*

†*Department of Pharmaceutical Technology, Poznan University of Medical Sciences, Grunwaldzka 6, 60-780 Poznań, , Poland*

‡ D*epartment* of Pharmaceutical Sciences, University of Padova, Italy,

§*Department of Inorganic and Analytical Chemistry, Poznan University of Medical Sciences, Grunwaldzka 6, 60-780 Poznań, , Poland*

----------*Toxicological Sciences 2010 118(1):236-50*----------

Abstract

In this paper we have investigated the mechanism of phototoxicity of fluvastatin, an HMG-CoA reductase inhibitor, in human keratinocytes cell line NCTC-2544. Fluvastatin underwent rapid photodegradation upon UVA irradiation in buffered aqueous solution as shown by the changes in absorption spectra. Interestingly, no isosbestic points were observed but only a fast appearance of a spectral change, indicative of the formation of a new chromophore. The isolation and characterization of the main photoproduct revealed the formation of a polycyclic compound with a benzocarbazole-like structure. This product was also evaluated for its phototoxic potential. Cell phototoxicity was evaluated by MTT test after 72 h from the irradiation in the presence of fluvastatin. The results showed a reduction of the cell viability in a concentration and UVA dose dependent manner. Surprisingly, the photoproduct showed a dramatic decrease of the cell viability which occurred at concentrations of an order of magnitude lower than the parent compound.

Flow cytometric analysis indicated that fluvastatin and its main photoproduct induced principally necrosis as revealed by the large appearance of propidium iodide positive cells and confirmed also by the rapid drop in cellular ATP levels. Interestingly, a rapid

increase of intracellular calcium followed by an extensive cell lipid membrane peroxidation and a significant oxidation of model proteins were induced by fluvastatin and its photoproduct, suggesting that these compounds exerted their toxic effect mainly in the cellular membranes. On the basis of our results, the phototoxicity of fluvastatin may be mediated by the formation of benzocarbazole-like photoproduct that acts as strong photosensitizer.

Keywords: *Fluvastatin; Phototoxicity; Photoproduct; Necrosis; Lipid peroxidation; Protein oxidation.*

Introduction

There is a significant number of reports indicating that a variety of drugs can elicit undesired side effects, such as phototoxicity, photoallergy or photocarcinogenicity (Beijersbergen van Henegouwen, 1997 ; Stahlmann and Lode 1999; Ferguson 2002; Elisei *et al*., 2004; Viola and Dall'Acqua, 2006)

Absorption of sunlight by drug molecules leads to their excited states. This can proceed further to afford drug-derived reactive intermediates or under aerobic conditions reactive oxygen species (ROS). Any of the above short-lived chemical entities may be able to interact with various cellular components, ultimately producing photodamage (Cosa, 2004; Stadtman and Levine 2003; Girotti, 2001).

The 3-hydroxy-3-methylglutaryl Coenzyme A (HMG-CoA) reductase inhibitors (commonly known as *statins*) are used in the treatment of hypercholesterolemia and are among the most commercially successful drugs (Alexander *et al.* 2009; Shaw *et al.* 2009). They interfere with the synthesis of cholesterol by competitively inhibiting the HMG-CoA reductase, the rate-limiting step in *de novo* cholesterol synthesis. In 1987 with the introduction of lovastatin, the statin drug first became available and since then, there has been a constant effort to introduce new, improved anti-cholesterol compounds.

Lovastatin, pravastatin and simvastatin are natural derived inhibitors of HMG-CoA reductase, while atorvastatin, fluvastatin, rosuvastatin, pitavastatin and glenvastatin are fully synthetic compounds. Among natural statins, lovastatin has been described to cause UVA-induced cellular damage in the human keratinocytes (Quiec *et al.*, 1995), although the compound does not absorb light in the UVA range and therefore it cannot act as photosensitizers. The mechanism(s) by which lovastatin could enhance the cellular photodamage is yet not clearly elucidated. It was speculated that this

phenomenon was most likely to be explained by lysosomal membrane destabilization and cholesterol deprivation from plasma membrane. Simvastatin is also known to elicit the chronic actinic dermatitis (Holme *et al*., 2002). However, its phototoxic mechanism has been not investigated by in vitro laboratory assays up to now.

The entirely synthetic HMG-CoA reductase inhibitors are structurally distinct from the natural derivatives and they are considered to undergo photochemical decomposition. Hitherto, research has been mainly limited to very few reports (Montanaro *et al*., 2009; Cermola *et al.* 2006; Astarita *et al*., 2007, Mielcarek *et al*., 2005; Grobelny *et al*., 2009, Cermola *et al*., 2007).

Fluvastatin (FLV), shown in Figure 1, is a reversible, competitive and highly specific inhibitor of HMG-CoA, and is widely used in the treatment of hypercholesterolemia. The presence of the double bound in the heptanoic acid chain of the compound results in two stereomeric form, *E* and *Z*-isomers. The active *trans* form is used in the therapy. The drug is considered to be extremely sensitive to light and must be protected from it during storage. Nevertheless, an exhaustive search of the literature indicates that very little attention has been paid to the photochemical behavior of statins, including FLV. A recent study (Cermola *et al*., 2007) reports the structure elucidation of photoproducts formed after solar and UV exposure of the drug in aqueous media, indicating that photocyclization and photooxygenation are the main reactions involved in the formation of the observed products. Therefore, it would be pertinent at this stage to conduct experiments on the phototoxic potential of fluvastatin. Thus, the aim of this work is to evaluate the phototoxic potential of FLV and its main photoproduct in a cultured NCTC-2544 keratinocytes. In order to gain insight into the mechanism of phototoxicity, we have extended our studies on the photochemical damage on protein model *in vitro*..

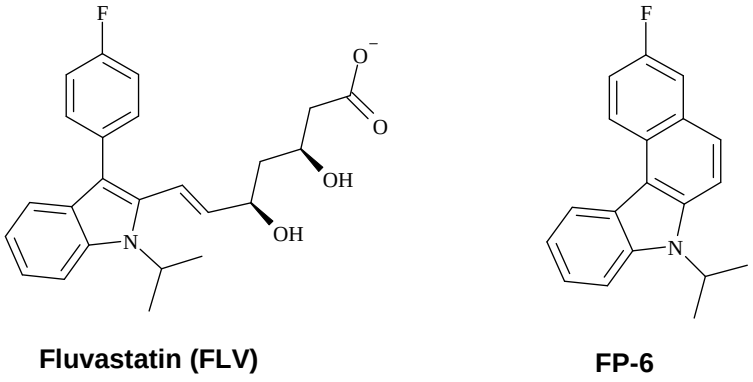

Fluvastatin (FLV) **FP-6**

Figure 1. *Structures of fluvastatin (FLV) and its main photoproducts FP6*

2 Materials and methods

2.1 Chemicals. Fluvastatin sodium, FLV, [R*,S*-(E)]-(±)-7-[3-(4-fluorophenyl)-1-(1-methylethyl)-1H-indol-2-yl]-3,5- dihydroxy-6-heptenoic acid monosodium salt was obtained from Zydus Cadila, India. Thiobarbituric acid (TBA), sodium azide (NaN_3), N-N'-dimethylthiourea (DMTU), superoxide dismutase (SOD), catalase (CAT), bovine serum albumin (BSA), human serum albumin (HSA), RibonucleaseA (RNAseA), 2,6-di-tert-butylhydroxyanisole (BHA) and glutathione reduced form (GSH) were purchased from Sigma-Aldrich (Milano, Italy).

2.2 Irradiation procedure. Two HPW 125 Philips lamps, mainly emitting at 365 nm, were used for irradiation experiments. The spectral irradiance of the source was 4.0 mW cm^{-2} as measured at the sample level by a Cole-Parmer Instrument Company radiometer (Niles, IL, USA) equipped with a 365-CX sensor.

2.3 HPLC Analysis and isolation of photoproduct FP-6. HPLC analyses were carried out on an Agilent 1200 liquid chromatography system (Agilent, Waldron, Germany) consisted of quaternary solvent delivery system, on-line degasser, autosampler and a diode array detector. Fluvastatin was irradiated in and its photoproducts were separated at room temperature on a Gemini C18 column (250 mm × 4.6 mm, 5 μm particle size, Phenomenex, Cheshire, UK). The mobile phase consisted of solvent A (methanol) and solvent B (triethylamine buffer, pH 6.0). Gradient started at 58% v/v A held for 5 minutes ramping up to 65% A over 1 minute, then held for 10 minutes isocratic separation. Subsequently ramping up to 95% A held for 5 minutes.

The flow rate was 1.0 ml/min and sample injection volume was 5 µl. The chromatographic data were recorded and processed with an Agilent ChemStation workstation. Irradiations of fluvastatin in aqueous buffered solution gave yield of around 25% in terms of FP6 photoproduct. XTerra MS C18 (100 mm × 19 mm, 5 µm) preparative column was employed for isolation of photoproduct FP6. The mobile phase consisted of solvent A (methanol) and solvent B (water). The gradient elution described above was utilized. Flow rate was 5.0 ml/min and detection was carried out at 330 nm. The fraction corresponding to FP6 was checked for purity by means of analytical HPLC. Peaks of minor components were detected, but the impurities content never exceeded 2% of the total signal intensity.

2.4 Cellular phototoxicity. Phototoxicity experiments were carried out on a immortalized, non tumorigenic cell line of human keratinocytes (NCTC- 2544) and a cell line of murine fibroblasts (3T3). Both lines were grown in DMEM medium (Sigma-Aldrich Milan, Italy), supplemented with 115 units/mL of penicillin G, 115 µg/ml streptomycin, and 10% fetal calf serum (Invitrogen, Milan, Italy). The generation time of NCTC-2544 is approximately 21h. Individual wells of a 96-well tissue culture microtiter plate (Falcon, Becton-Dickinson) were inoculated with 100 µl of complete medium containing $5x10^3$ NCTC-2544 or 3T3 in exponential growth. The plates were incubated at 37 °C in a humidified 5% CO_2 incubator for 18 hours prior to the experiments. After medium removal, 100 µl of the drug solution, dissolved in DMSO and diluted with Hank's Balanced Salt Solution (HBSS pH=7.2), were added to each well and incubated at 37 °C for 30 minutes and then irradiated. After irradiation, the solution was replaced with the medium, and the plates were incubated for 72 hours. After this period control cells reached a confluency of about 90% and the cell viability was assayed by the MTT [(3-(4,5-dimethylthiazol-2-yl)-2,5 diphenyl tetrazolium bromide)] test as previously described (Viola *et al.* 2007). Analogous experiments were performed in the presence of different additives.

2.5 Cell cycle analysis. For flow cytometric analysis of DNA content, $5x10^5$ NCTC-2544 cells in exponential growth were irradiated as described above and after different times, the cells were trypsinized and together with floating cells, centrifuged and fixed with ice-cold ethanol (70%). The keratinocytes were then treated with lysis buffer containing RNAseA, and subsequently stained with propidium iodide. Samples were analyzed on a Beckman Coulter Cytomic FC500 flow cytometer. For cell cycle

analysis, DNA histograms were analyzed using MultiCycle™ for Windows (Phoenix Flow Systems, CA, USA).

2.6 Externalization of phosphatidylserine. Surface exposure of phosphatidylserine (PS) by apoptotic cells was measured by flow cytometry with a Coulter Cytomics FC500 (Beckman Coulter) by adding Annexin-V-FITC to cells according to manufacturer's instructions (Roche Diagnostic, Monza, Italy). Simultaneously, the cells were stained with PI. Excitation was set at 488 nm and the emission filters were set at 525 nm for FITC fluorescence and in the range 560-680 nm for PI fluorescence.

2.7 Assessment of mitochondrial changes and production of reactive oxygen species. The mitochondrial membrane potential was measured with the lipophilic cation 5,5',6,6' tetrachlo-1,1',3,3'-tetraethylbenzimidazol-carbocyanine (JC-1, Molecular Probes Eugene, OR, USA) (Salvioli et al. 1997). Briefly, after different times from the irradiation, the cells were collected by centrifugation and resuspended in HBSS containing the JC-1 at a concentration of 2.5 μM. The cells were then incubated at 37 °C for 10 min, centrifuged and resuspended again in HBSS. The fluorescence was directly recorded with the flow cytometer (Coulter Cytomics FC500).

The production of Reactive Oxygen Species (ROS) by flow cytometry using hydroethidine (HE) and 2',7'-dichlorodihydrofluorescein diacetate (H_2DCFDA) (Rothe and Valet, 1990). All of these fluorescent probes were purchased from Molecular Probes (Eugene, OR, USA). After 24 hours from the irradiation, the cells were trypsinized and collected by centrifugation and resuspended in HBSS containing the fluorescence probes HE or H_2DCFDA at the concentration of 2.5 μM, and 0.1μM respectively. As above, the cells were then incubated at 37 °C for 30 min, centrifuged and resuspended again in HBSS. The fluorescence was directly recorded with the flow cytometer using as excitation wavelength 488 nm and emission at 585 nm for HE and at 525 nm for H_2DCFDA.

2.8 Detection of DNA fragmentation by Agarose Gel. Total genomic DNA was extracted from irradiated keratinocytes by a commonly used salting out protocol. One μg of DNA obtained was subsequently loaded on a 0.8% agarose gel at 50V for 6h in TAE buffer. After staining in ethidium bromide solution, the gel was washed with water and the DNA bands were detected under UV radiation with a ImageQuant 300 transilluminator (GE Healthcare) equipped with a CCD camera.

2.9 ATP assay. Cells were irradiated in the presence of FLV or its photoproduct. After different times from the irradiation, cells were collected and counted then the ATP content per 100000 cells was determined using the CellTiter-Glo luminescent assay (Promega, Milano, Italy) according to manufacturer instruction, using a Victor^{3TM} luminometer (Perkin Elmer). Data are normalized to ATP content in non irradiated cells.

2.10 Intracellular calcium measurement. Intracellular calcium in NCTC-2544 cells was measured by flow cytometry using the Ca^{2+} -sensitive fluorescent dye Fluo-4/AM (Molecular Probes). Briefly, irradiated cells after different times were washed and incubated with 2.5 μM Fluo-4/AM in complete medium at 37 °C for 30 min. The cells were then trypsinized, washed two times and resuspended in HBSS. The intracellular calcium was analyzed immediately for Fluo-4/AM fluorescence intensity by flow cytometry.

2.11 Lysosomal integrity assay. Cells were irradiated in the presence of FLV or the photoproduct and after different times the cells were collected by centrifugation and resuspended in DMEM containing the fluorescent probe LysoTracker RED DND-99 (Molecular Probes) at the concentration of 50 nM and incubated at 37 °C for 30 min. After this period, the cells were washed and analyzed by flow cytometry**.** As positive control we incubate the cells with H_2O_2 (Antunes *et al.* 2001) at the concentration of 100 μM for 1h at 37 °C and then analyzed as described before.

2.12 Detection of the intracellular glutathione content (GSH). Cellular GSH levels were analysed using 5-chloromethylfluorescein diacetate (CMFDA, Molecular Probes) (Hedley and Chow, 1994). Cell were irradiated in the presence of FLV and incubated for 12 and 24 h respectively. Cells were harvested centrifuged and incubated in the presence of a solution of CMFDA 5 μM at 37 °C for 30 min. Cytoplasmic esterases convert non-fluorescent CMFDA to fluorescent 6-chloromethylfluorescein which can then react with glutathione. Fluorescence intensity was determined by flow cytometry.

2.13 Caspase-3 assay. Caspase-3 activation in NCTC-2544 cells was evaluated by flow cytometry using a human active caspase-3 fragment antibody conjugated with FITC (BD Pharmingen). Briefly after irradiation, the cells were collected by centrifugation and resuspended in Perm/Wash^{TM}(BD Pharmingen) buffer for 20 min

washed and then incubated with the antibody for 30 min. After this period, the cells were washed and analyzed by flow cytometry.

2.14 Cellular localization studies. NCTC-2544 cells were allowed to attach in a sterile Petri dishes and treated with FLV and FP6 at the concentration of 100 μM and 50 μM respectively for 2 h, then washed with HBSS, and incubated for further 30 min in the presence of JC-1 a fluorescence probe which stains mitochondria (Salvioli et al., 1997) or LysoTracker RED as fluorescent probe to stain lysosomes (Yuan et al., 2002). Cellular fluorescence images were acquired with an video-confocal microscope (NIKON), using a Nir Apo 60X/1.0W water immersion objective (NIKON). Emission filter settings were used to separate the emission of the probes from that of the test compounds.

2.15 Lipid peroxidation: TBARS assay. Lipid peroxidation was measured using a thiobarbituric acid assay as described previously (Morliere *et al.*, 1991). A standard curve of 1,1,3,3-tetraethoxypropane was used to quantify the amount of produced malonaldehyde. Data are expressed in terms of nanomoles of TBARS normalized to the total protein content, measured in an aliquot of the cell extract.

2.16 Protein oxidation. Solutions of Bovine serum albumin (BSA), Ribonuclease A (RNAseA) and Human serum albumin (HSA), (0.5 mg/ml) in phosphate buffer 10 mM were irradiated in the presence of the test compounds for various time in a quartz cuvette. At different time, an aliquot of the solution was taken and the degree of protein oxidation was monitored spectrophotometrically, as described previously (Levine *et al.*, 1990), by derivatization with 2,4-dinitrophenylhydrazine (DNPH).

2.17 Statistical analysis. Unless indicated differently, the results are presented as mean ± S.E.M. The differences between irradiated and non irradiated sample were analysed, using the two-sided Student's *t* test.

3 Results

3.1 Isolation and characterization of the photoproducts.

Fluvastatin showed absorption maxima in the UVA range (320-400 nm), and underwent rapid photodegradation upon UVA irradiation in buffered aqueous solution as previously reported (Mielcarek *et al.* 2005; Cermola *et al.* 2007). No distinct isosbestic points were observed but just after low UVA doses (0.5-2.5 J cm^{-2}), the

appearance of a spectral change was detected, indicative of the formation of a new chromophore or multiple products (Supplementary data).

More importantly a detailed kinetic analysis, carried out by HPLC (Figure 2), showed that FLV was completely degradated yielding multiple products, after 7.5 J cm^{-2} of UVA, corresponding to 30 min of irradiation in our conditions. The UV spectra of FP1 - FP2 and FP3 - FP4 presented in Figure 2 were indistinguishable with λ_{max} 260 nm and 280 nm respectively, suggesting that the pair of the photoproducts possessed similar structure of chromophore. In addition, the UV spectrum of FP6 was very similar to that of FP3, except for a slight red shift of λ_{max} and much more different polarity. We assumed similar structure of the chromophores differing only in an additional side chain responsible for polarity. However, the majority of them appear to be unstable. Fractions corresponding to six photoproduct (FP1-FP6) were isolated. The dried fractions were dissolved in methanol and analysed by mass spectrometry. The mass spectra were recorded over the range 100 – 1000 m/z in the positive mode (Supplementary Data).

We focused our attention on the isolation and characterization of product FP6 since this compound was formed in high quantity and after prolonged irradiation was the only product found (Cermola *et al.* 2007). Isolated fraction corresponding to FP6 was dissolved in methanol (MeOH-d_4) and subjected to ^{1}H-NMR and ^{1}H,^{1}H COSY-NMR analyses. NMR spectra (see supplementary data) indicated a structure consistent with a tetracyclic compound namely 9-fluoro-5-(1-methylethyl)-benzo[*c*]carbazole depicted in Figure 1. These findings are in excellent agreement with the paper of Cermola *et al.* (2007), who reported the isolation and a detailed characterization of fluvastatin photoproducts after solar and UVA irradiation in aqueous solution (Supplementary data).

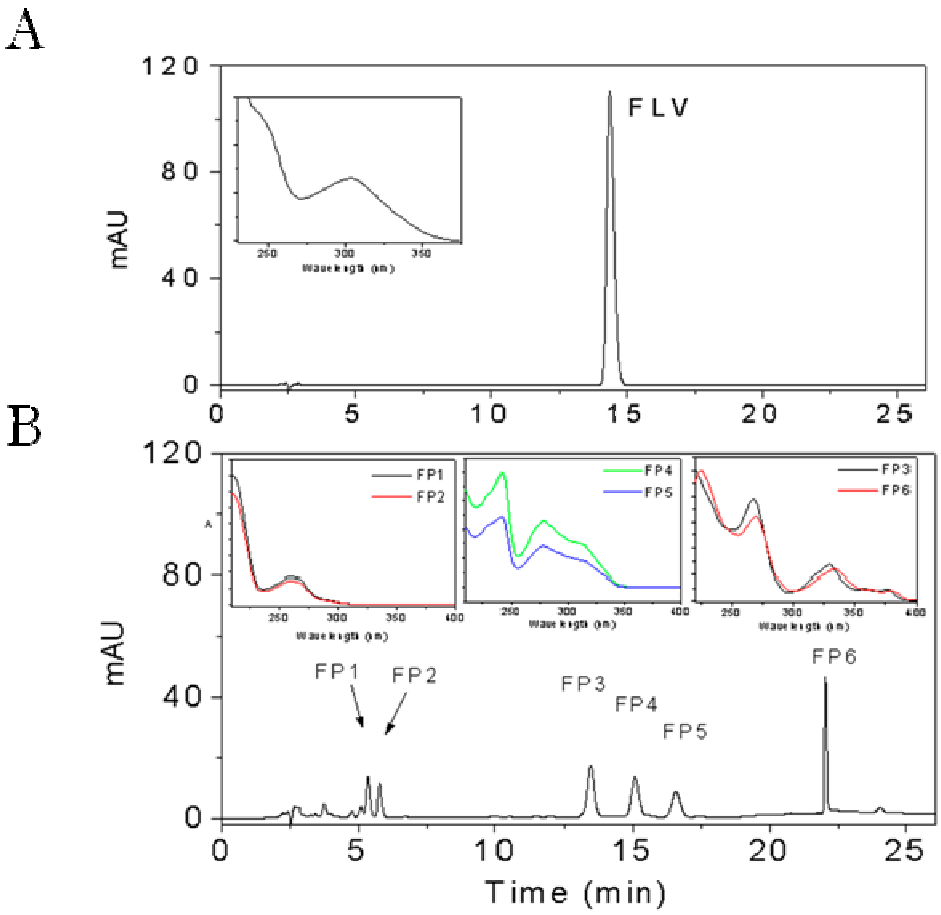

Figure 2. *Representative HPLC chromatograms obtained from aqueous solution of FLV exposed to 0 (panel A) or 7.5 J cm⁻² of UVA (panel B). The inset in the chromatogram represents absorption spectra of FLV (panel A) and its photoproducts FP1-FP6 (panel).*

3.2 Cellular phototoxicity.

The phototoxicity of FLV was evaluated in a cell line of immortalized human keratinocytes NCTC-2544 by use of the MTT assay carried out 72 hours after irradiation. Figure 3 (panel A) shows the reduction of viability obtained in NCTC-2544 cells at different concentration and different UVA doses. As can be observed, a concentration and UVA dose-dependent reduction of cell viability is induced by FLV. The calculated GI_{50} were >100 μM, 99.1μM 18.5 μM and 5.5 μM at the UVA doses of 1.25, 2.50, 3.75 and 7.5 J cm^{-2} respectively. In the same experimental conditions but in the absence of irradiation, FLV did not show any decrease of viability.

In the same model, photoproduct FP6 was tested. FP6 did not affect cell viability without irradiation but on the contrary, after irradiation a dramatic reduction of cell viability can be observed for this compound in comparison to the parent one, as

showed in Figure 3 (panel B). In this case, the calculated GI_{50} were 3.7 μM ,1.9 μM and 1.3 μM at the UVA doses of 1.25, 2.50, and 3.75 J cm^{-2} respectively.

Analogous experiments were performed also in 3T3 fibroblast cell line a well known *in vitro* model to evaluate the phototoxic potential of a drug (Spielmann *et al.* 1998).

Also in this cell line we have observed a clear reduction of cell viability that is both UVA dose and concentration dependent. In comparison to human keratinocytes, 3T3 appear more sensible to the phototoxic action of FLV since the GI_{50} in this cell line are lower than that observed in NCTC-2544 cells (82.8 μM, 31 μM, 8.5μM at at the UVA doses of 1.25, 2.50, and 3.75 J cm^{-2} respectively). On the contrary the sensitivity of 3T3 to FP6 appear similar to NCTC-2544 cells in fact the GI_{50} are in this case 11.5μM, 6.8μM and 3.1μM at the UVA doses of 1.25, 2.50, and 3.75 J cm^{-2} respectively, although also in this case a remarkable increase of phototoxicity, was observed in comparison to the lead compound. Altogether these data suggest that the phototoxicity of FLV could be mediated by the formation of this photoproduct.

With the purpose to evaluate which reactive species are involved in the mechanism(s) of photoinduced cell toxicity, analogous experiments were performed, irradiating NCTC-2544 cells with FLV and FP6 in the presence of different scavengers as previously reported (Elisei *et al.* 2004; Viola *et al.* 2007). The additives used were NaN_3 (a singulet oxygen scavenger), superoxide dismutase (SOD, scavenger of $O^{\bullet -}$), catalase (CAT, scavenger of H_2O_2), mannitol and DMTU (scavengers of $^{\bullet}OH$) and 2,6-di-tert-butylhydroxyanisole (BHA) and GSH, (free radical scavengers). The concentrations of the compounds and the UVA doses were chosen on the basis of the results presented in Figure 3.

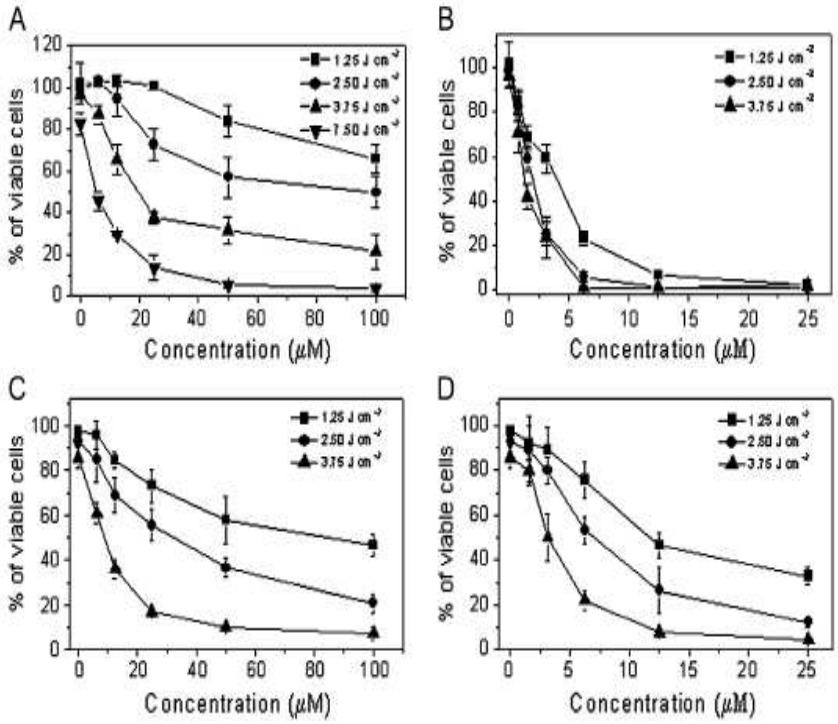

Figure 3. *Percentage of viability of NCTC-2544 human keratinocytes (panels A and B) and 3T3 murine fibroblast (panel C and D) after UVA irradiation in the presence of FLV (panels A and C) and photoproduct FP6 (panels B and D). Cell were irradiated at the indicated different UVA doses and at different concentrations of drugs. Cell viability was measured by MTT test after 72 h after irradiation. Data represent mean ± S.E.M for at least four independent experiments.*

It can be observed from Table 1 that the photoinduced cell death by FLV and FP6 is efficiently counteract by SOD, GSH, BHA and mannitol, indicating that superoxide anion, free and hydroxyl radicals may be involved in the mechanism of action.

Table 1. *Effects of different scavengers on the phototoxicity induced in NCTC-2544 cells, by fluvastatin and FP6.*

Treatment (concentration, UVA dose)	Scavenger (concentration)	% cell viability
Fluvastatin (25 μM, 3.75 J cm^{-2})	none	36.8 ± 4.5
	BHA (10 μM)	37.4 ± 4.6
	NaN_3 (20 mM)	33.0 ± 4.0
	DMTU (1 mM)	39.9 ± 4.9
	GSH (1mM)	66.6 ± 7.1**
	CAT (1000 UI/ml)	37.1 ± 4.4
	SOD (2000 UI/ml)	59.1 ± 8.4*
	Man (10 mM)	88.9 ± 8.7**
FP6 (5 μM, 1.25 J cm^{-2})	none	65.6 ± 5.2
	BHA (10 μM)	89.4 ± 6.4*
	NaN_3 (20 mM)	62.6 ± 5.4
	DMTU (1 mM)	88.2 ± 4.6*
	GSH (1mM)	96.3 ± 7.5**
	CAT (1000 UI/ml)	67.6 ± 3.9
	SOD (2000 UI/ml)	77.1 ± 4.6*
	Man (10 mM)	87.3 ± 6.2*

The cell viability was measured 72 h from the treatment with the MTT test.

**p<0.05 **p<0.01 vs none Student's t test (n=5)*

3.3 Assessment of the mode of cell death.

To characterize the mode of cell death (necrosis or apoptosis) photoinduced by FLV and its photoproduct FP6, a biparametric cytofluorimetric analysis was performed to quantify the precise extent of apoptosis versus necrosis using propidium iodide, which stains DNA and is permeable only to dead cells, and fluorescent immunolabeling of the protein Annexin-V, which binds to phosphatidylserine in a highly selective manner. This phospholipid flips from the inner to the outer leaflet of the plasma membrane during apoptosis. Positive staining with Annexin-V correlates with the loss of plasma membrane polarity but precedes the complete loss of membrane integrity that accompanies the later stages of cell death resulting from either apoptosis and necrosis. In contrast, PI can only enter cells after the loss of their membrane integrity. Thus, dual staining with Annexin-V and PI allows clearly to discriminate between unaffected

cells (Annexin-V$^-$/PI$^-$), early apoptotic cells (Annexin-V$^+$/PI$^-$), late apoptotic cells (Annexin-V$^+$/PI$^+$) and necrotic cells (Annexin-V$^-$/PI$^+$)(Vermes *et al.* 1995).

Figure 4 (panel A), shows as representative, four biparametric histograms in which the effect of FLV at 6 and 24 h from the irradiation is depicted. It is quite evident that FLV early induced, an accumulation of PI positive cells in comparison to the irradiated control and these latter further increase at 24 h indicating the formation of necrotic cells. As positive control, we submitted the cells to rapid cycles of freeze/thawing, and the histograms depicted in Figure 4 (panels B and C) show that the cell population after this treatment were composed exclusively of necrotic cells (*i.e.*, Annexin-V$^+$/PI$^+$).

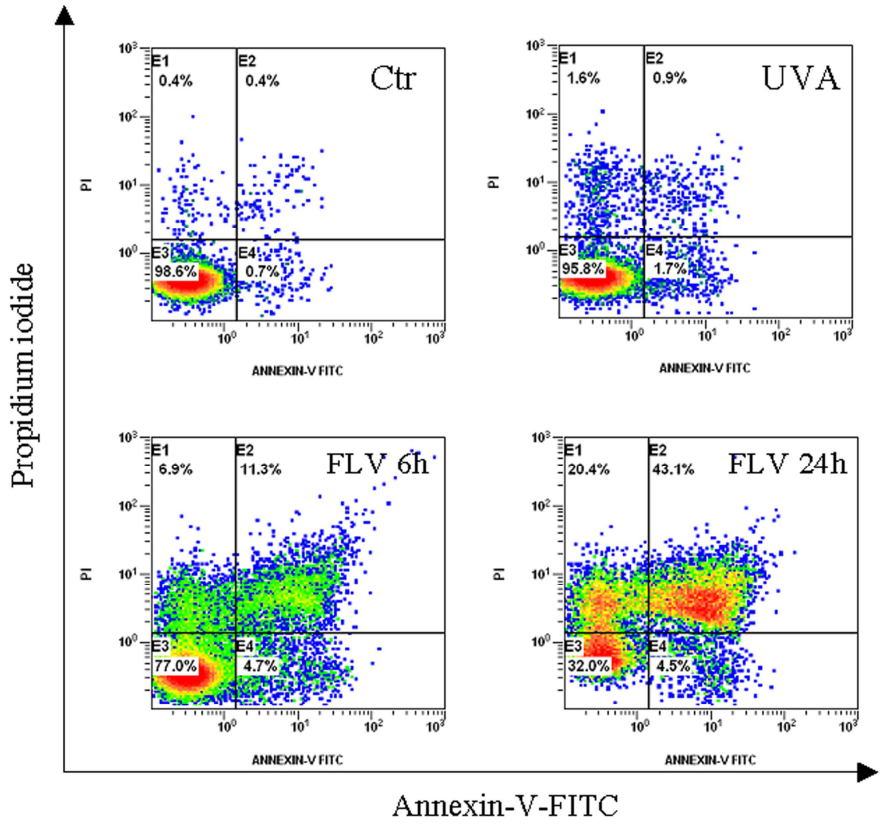

Figure 4. *Determination of the mode of cell death using Annexin-V and PI staining and flow cytometric analysis. Panel A. Representative biparametric histograms obtained after 6 and 24 h after the irradiation (3.75 J cm^{-2}) of NCTC-2544 in the presence of FLV 50 μM. Panels B and C. Representative histograms of necrotic NCTC generated by one (panel B) or two cycles (panel C) of a rapid freeze/thaw exposure of the cells*

A complete picture of results is presented in Figure 5 for FLV at the concentration of 50 and 25 μM and in Figure 6 for FP6 at the concentration of 10 and 5 μM. It can be

observed that we did not observed A^+/PI^- cells at any time point investigated but, on the contrary, a large percentage of PI positive cells was found indicating a rapid permeabilization of the cell plasma membrane that leads to a necrotic cell death.

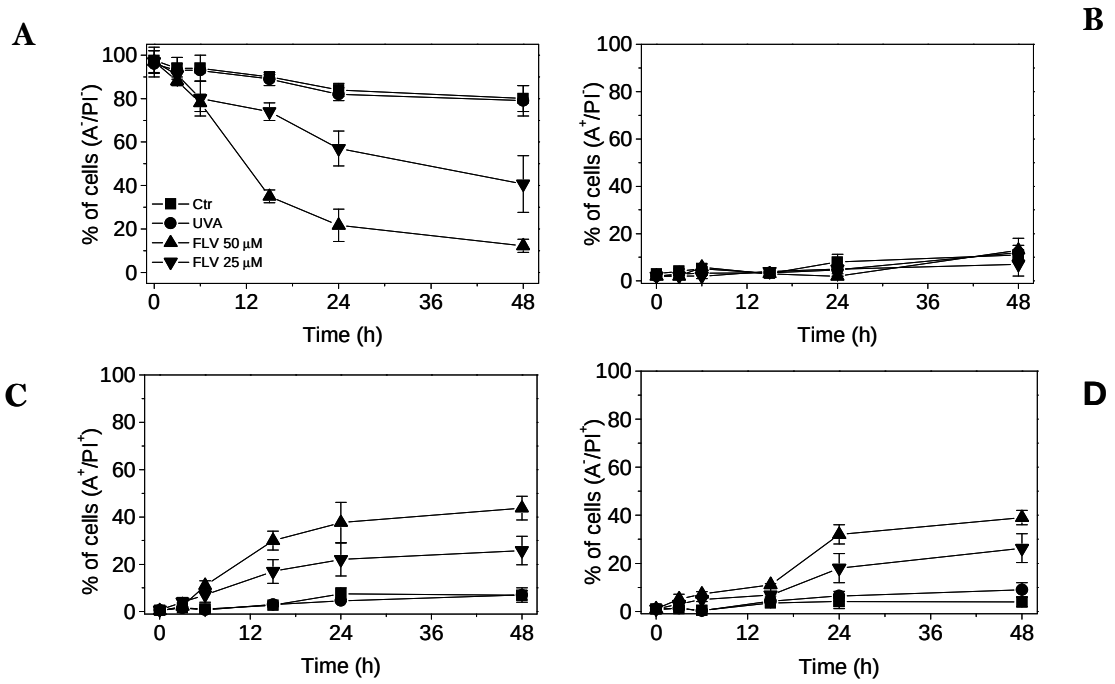

Figure 5. *NCTC-2544 were irradiated in the presence of FLV at the indicated concentration and after different times the cells were collected and stained with Annexin-V-FITC and Propidium iodide (PI) and analysed by flow cytometry. The results are expressed as percentage of cells found in the different region of the biparametric histograms showed in Figure 4. Panel A: A^-/PI^- cells; Panel B: A^+/PI^-; Panel C: A^+/PI^+; Panel D A^-/PI^+. Data represent mean ± S.E.M of three independent experiments.*

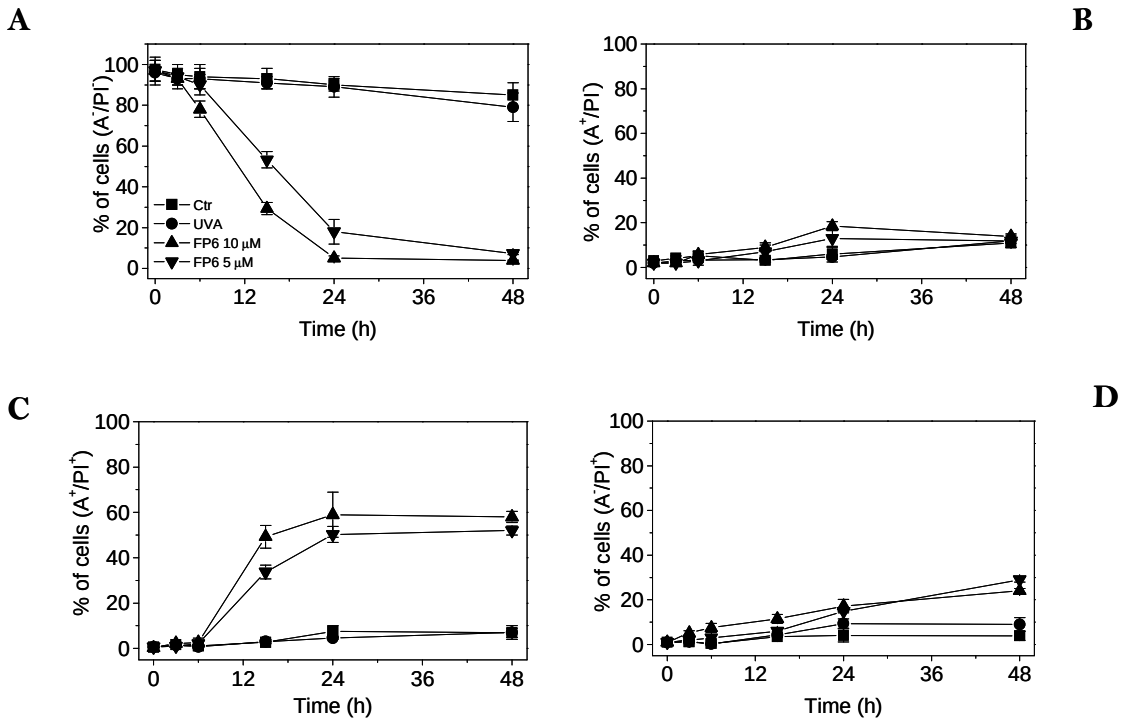

Figure 6. *NCTC-2544 were irradiated in the presence of FP6 at the indicated concentration and after different times the cells were collected and stained with Annexin-V FITC and Propidium iodide (PI) and analysed by flow cytometry . The results are expressed as percentage of cells found in the different region of the biparametric histograms showed in Figure 4. Panel A: A⁻/PI⁻ cells; Panel B: A⁺/PI⁻; Panel C: A⁺/PI⁺; Panel D A⁻/PI⁺. Data represent mean ± S.E.M of three independent experiments*

The mode of cell death was also followed by two most common endpoint analysis such as morphological changes and analysis of DNA fragmentation (Galluzzi *et al*., 2009). As shown in Figure 7 (panel A), visual inspection by contrast phase microscopy of the morphology of NCTC-2544 cells irradiated in the presence of FLV (50 μM) or FP6 (10 μM) revealed the presence of cellular swelling and rupture of the plasma membrane which are typical signs of necrotic type of cell death. Furthermore, agarose gel electrophoresis of DNA extracted from keratinocytes irradiated in the presence of FLV and FP6 (Figure 7, panel B) showed a non specific degradation resulting in a "smear" of randomly degraded DNA in the samples treated, indicative of a necrotic cell death. In addition, we evaluated the activity of caspase-3 since this enzyme is essential to the propagation of the apoptotic signal after the exposure to many DNA-damaging agents, anticancer drugs and it is activated in most cases of photodynamic therapy with a number of different photosensitizers (Kumar 2007; Porter and Janicke, 1999; Oleinick *et al.* 2002). As depicted in figure 7 (panel C) flow cytometric analysis of

NCTC-2544 irradiated in the presence of FLV and FP6 did not show any activation of caspase-3.

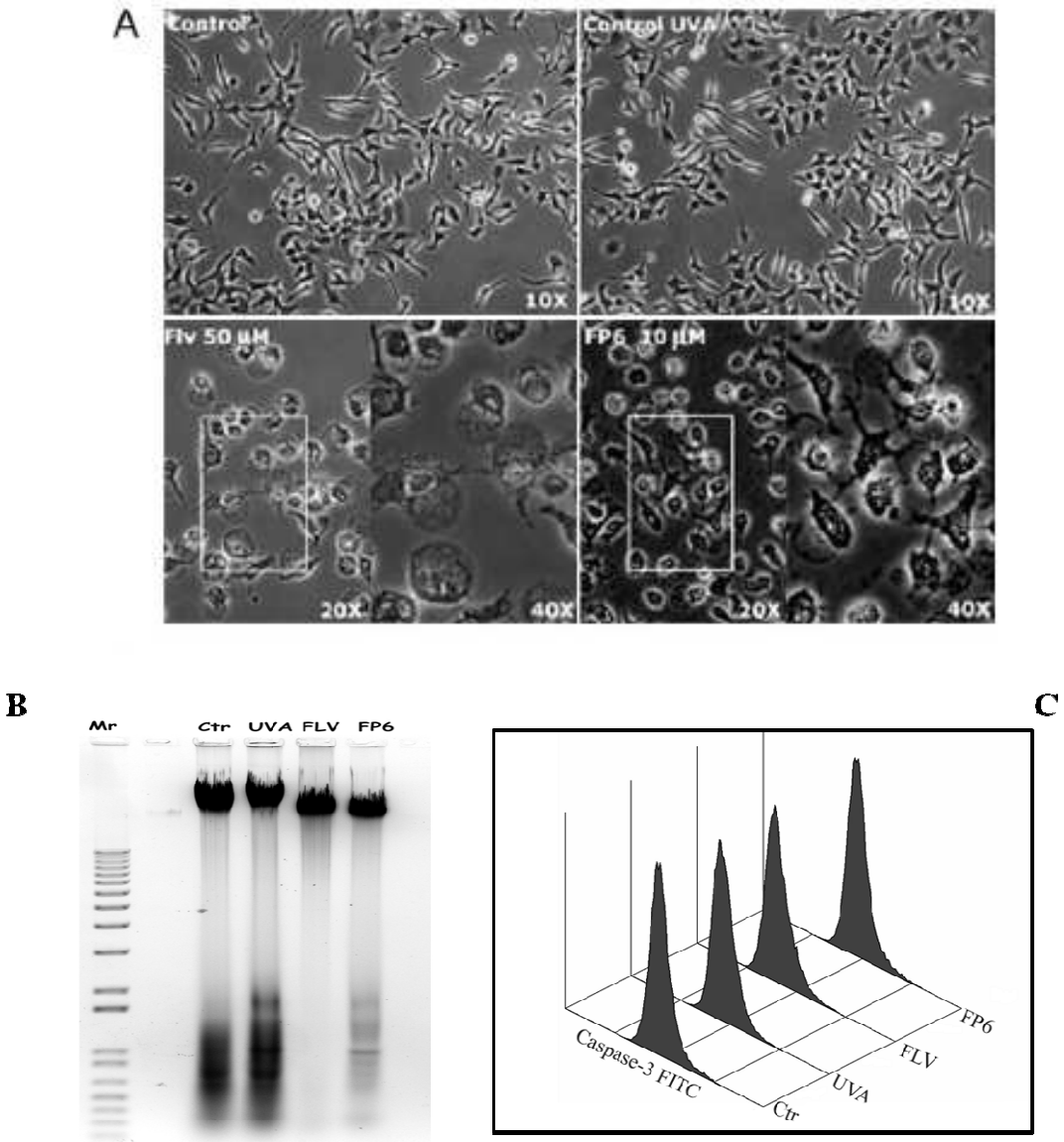

Figure 7. *Panel A. Cell micrographs taken after 24 h from the irradiation (3.75 J cm^{-2}) in the presence of FLV and FP6 at the indicated concentrations; Panel B. Agarose gel electrophoresis of chromosomal DNA extracted from NCTC-2544 cells 24 h after the irradiation (3.75 J cm^{-2}) in the presence of FLV (50µM) and FP6 (10 µM) or after 24 of treatment with Doxorubicin 5 µM . Lane 1: Ctr; lane 2. UVA; Lane 3: FLV 50 µM; Lane 4: FP6 (10 µM) Lane M indicated size marker DNAs; Panel C. Flow cytometric analysis of Caspase-3 activity after irradiation in the presence of FLV (50µM) and FP6 (10 µM). After 24 h of treatment, cells were harvested, and stained with an anti-human active Caspase-3 fragment monoclonal antibody conjugated with FITC. Representative histograms of three different experiments are shown*

3.4 ATP assay.

Apoptosis is an energy dependent process in which the decrease of ATP below critical levels may impede the execution of apoptosis and promote necrosis (Eguchi *et al.* 1997; Leist *et al.* 1997). In fact, necrosis is characterized by a rapid drop in ATP and given the potentially pivotal role attributed to ATP in the necrosis, we measured cellular ATP levels following irradiation with FLV and FP6.

Using a luciferase based assay for cellular ATP content, a dramatic depletion of ATP levels was detected in keratinocytes irradiated cells in the presence of 50 μM FLV (Figure 8). Similarly, the irradiation with 10 μM FP6 dramatically decreases ATP levels in comparison to non irradiated cells: this was already seen after 6h from irradiation and a further reduction was detected at 24h reaching levels of around 10%. Taken together, these data suggested that the rapid and pronounced ATP depletion was a concurrent event that accompanied the loss of cell viability.

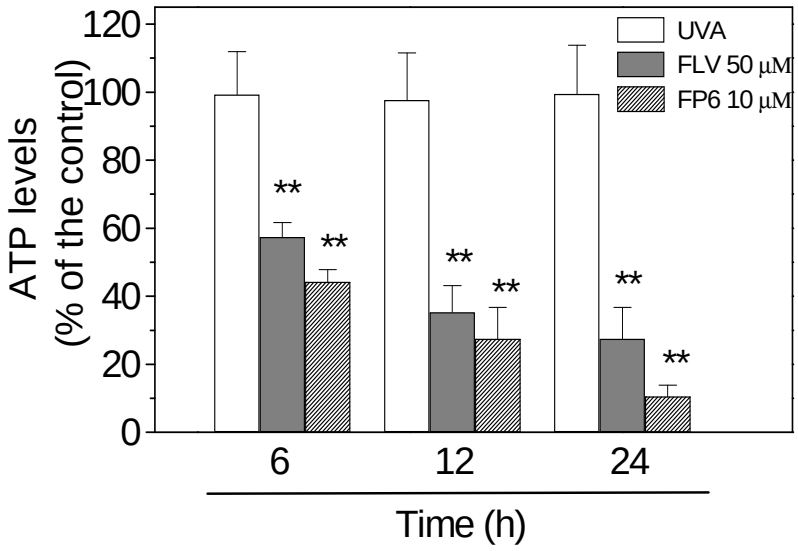

Figure 8. *ATP levels were measured in NCTC-2544 cells after different times from the irradiation (3.75 J cm^{-2}) in the presence of FLV (50 μM) and FP6 (10 μM). Data represent mean ± S.E.M of three independent experiments. **p<0.01 vs UVA irradiated cells.*

3.5 Analysis of Cell cycle.

To investigate the effects of FLV and FP6 upon UVA irradiation on the cell cycle, NCTC-2544 cells were treated with the test compounds at different concentrations

and at the light dose of 3.75 J cm^{-2}. After 12, 24 and 48 h from the irradiation, the cells were fixed and labelled with propidium iodide. The different phases of the cell cycle were analysed by flow cytometry.

Irradiation of keratinocytes with the FLV and its photoproduct induced only a modest increase of the S phase along with a reduction of G1 phase (Table 2) in particular at 24 h. More importantly, it is interesting to note that the percentage of the cell population with hypodiploid DNA content peak (subG1) reached a maximum values of 10-20% at 24 h. This peak represents those cells with a DNA content less than G1, usually considered as apoptotic cells slightly increased in the treated samples in comparison to the controls.

Table 2. *Effect of FLV and FP6 on the cell cycle of NCTC-2544*

	% G1[a]	G2/M	S	Apoptotic Cells[b] (Sub-G1)
Ctr 12 h	65.1±2.0	11.0 ±1.9	25.6±1.7	1.8 ±0.1
UVA alone 12 h	64.6 ±3.0	10.0±1.5	25.4±2.1	1.3 ±0.3
FLV 12 h 50 µM	61.0 ±4.0	7.7 ±2.5	31.3 ±4.1	6.9 ±1.5
FP6 12 h 10 µM	58.9 ±5.2	19.8 ± 1.5	32.3 ±3.5	2.5 ±0.7
Ctr 24 h	63.2±3.4	11.6±1.2	25.2±2.8	1.0 ±0.3
UVA alone 24 h	66.9±3.5	14.1 ±3.1	19.0 ±1.5	5.4 ±1.9
FLV 24 h 50 µM	43.9 ±2.7	15.6±1.0	40.4±3.0	12.1±4.3
FP6 24 h 10 µM	60.4±11.1	10.1±5.8	29.5±5.7	20.9±5.5
Ctr 48 h	62.8 ±1.2	10.4 ±2.9	26.8 ±1.6	5.0±1.5
UVA alone 48 h	63.4 ±2.7	9.8 ± 0.5	26.6 ±2.3	5.2±1.0
FLV 48 h 50 µM	52.5 ±5.6	17.8 ±2.1	29.7 ±3.5	6.6±2.1
FP6 48 h 10 µM	50.5 ±2.5	19.5 ±1.5	30.9 ±6.2	10.5 ±3.1

[a] *The percentage of each phase of the cell cycle was calculated on living cells*

[b] *Percentage of the cell population with hypodiploid DNA content peak (apoptotic cells)*

3.6 Mitochondrial and lysosomal integrity assessment.

To investigate which cellular sites are involved in the phototoxicity induced by FLV and FP6, we focused our attention on mitochondria and lysosomes. It has been previously shown that mitochondrial and/or lysosomial alterations are involved in cell death caused by many photosensitisers including fluoroquinolones, phenothiazines, antimalarial drugs and porphyrins (Oudreaogo *et al.*,1999; Viola and Dall'Acqua 2006; Viola *et al.*, 2007; Kessel and Luo, 2001). In an attempt to evaluate the intracellular

localization of FLV and its photoproduct in NCTC-2544 cells, we used two fluorescent probes: JC-1, a lipophilic cation commonly used for the assessment of the mitochondrial potential (Salvioli *et al.*, 1997), and Lyso tracker RED, a fluorescent dye that specifically stains lysosomes (Yuan *et al.*, 2002), while the test compounds emit in the blue region. Both fluorescences can be easily separated using suitable bandpass optical filters. It can be observed in Figure 9 that both FLV and FP6 were found to incorporate into NCTC-2544 cells and distribute within the cytoplasm after incubation but without a specific disposition into subcellular structures as evidenced by the loss of overlapping with JC-1 and LysoTracker Red.

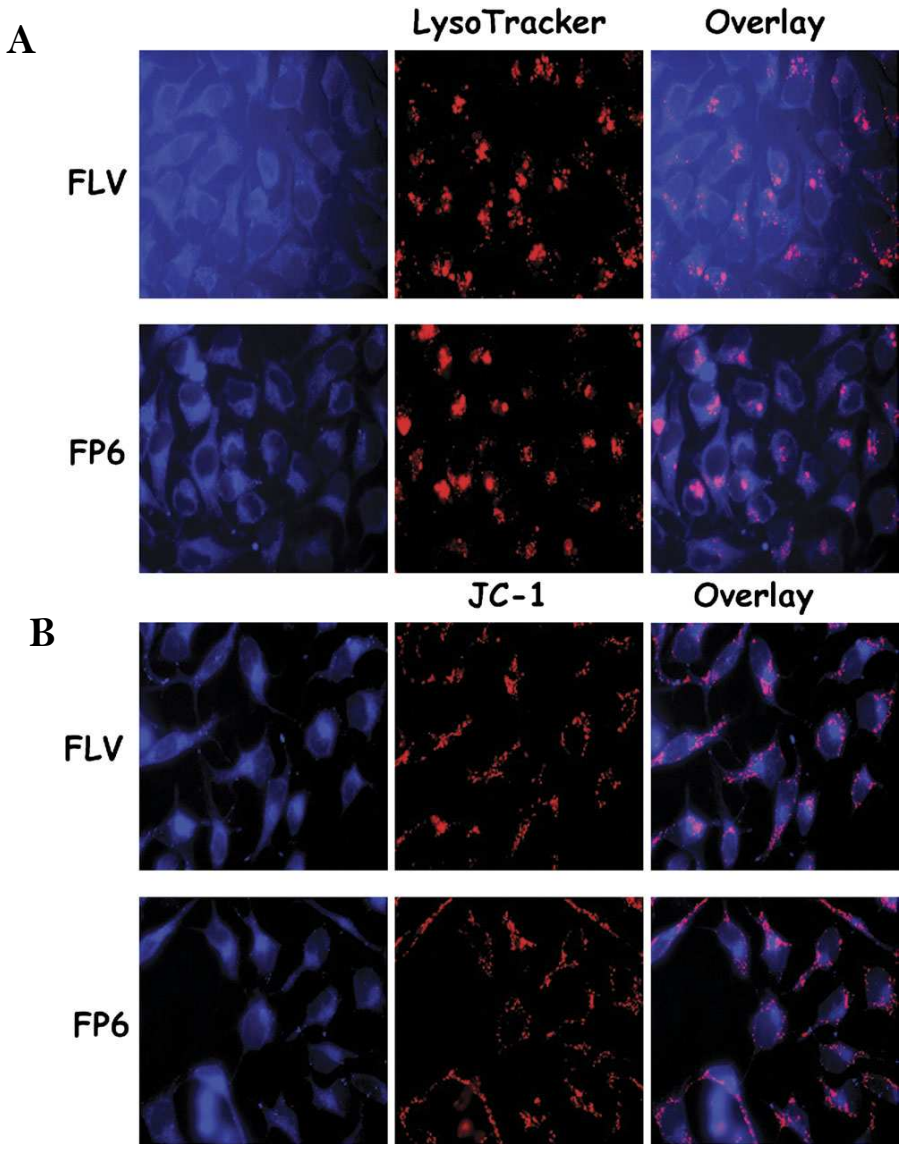

Figure 9. *Panel A Fluorescence microphotographs showing the intracellular localization of FLV and FP6 in NCTC-2544 cells in the presence of LysoTracker RED. Intracellular localization of FLV and FP6. Panel B. Fluorescence microphotographs showing the intracellular localization of FLV and FP6 in NCTC-2544 cells in the presence of JC-1;*

Further experiments to assess changes in mitochondrial functions after irradiation in the presence of FLV and FP6 were performed measuring mitochondrial potential ($\Delta\psi_{mt}$), by flow cytometry, using the JC-1 dye which is considered a reliable probe to assess such events (Salvioli *et al.*, 1997). Flow cytometric analysis of NCTC-2544 cells after 12, 24 or 48 h from the irradiation in the presence of the compounds showed no significant variations (Supplementary data) of $\Delta\psi_{mt}$ in comparison to the irradiated control, indicating the non involvement of this organelle in the photoinduced cell

death. To confirm that mitochondria were not involved in the photokilling mechanism, we also evaluated the mitochondrial production of ROS by two fluorescent probes, hydroethidine (HE) and 2',7'-dichlorodihydrofluorescein diacetate (H_2DCFDA) by flow cytometry (Rothe and Valet 1990; Nohl *et al.* 2005). In agreement, only a slight increase of ROS production was observed for cell irradiated with FLV and FP6.

In order to investigate the integrity of lysosomes after irradiation with the test compounds, flow cytometric analysis was performed using the fluorescent acidotropic dye LysoTracker Red. As showed in Figure 10 (panels A and B), the irradiation of the cells in the presence of FLV led to a reduction of LysoTracker fluorescence that occurred just after 6h from it, indicating alterations of the lysosomal membrane permeability. Interestingly, this effect did not occur with FP6, if not at later time in comparison to FLV probably due to a different disposition of the photoproduct.

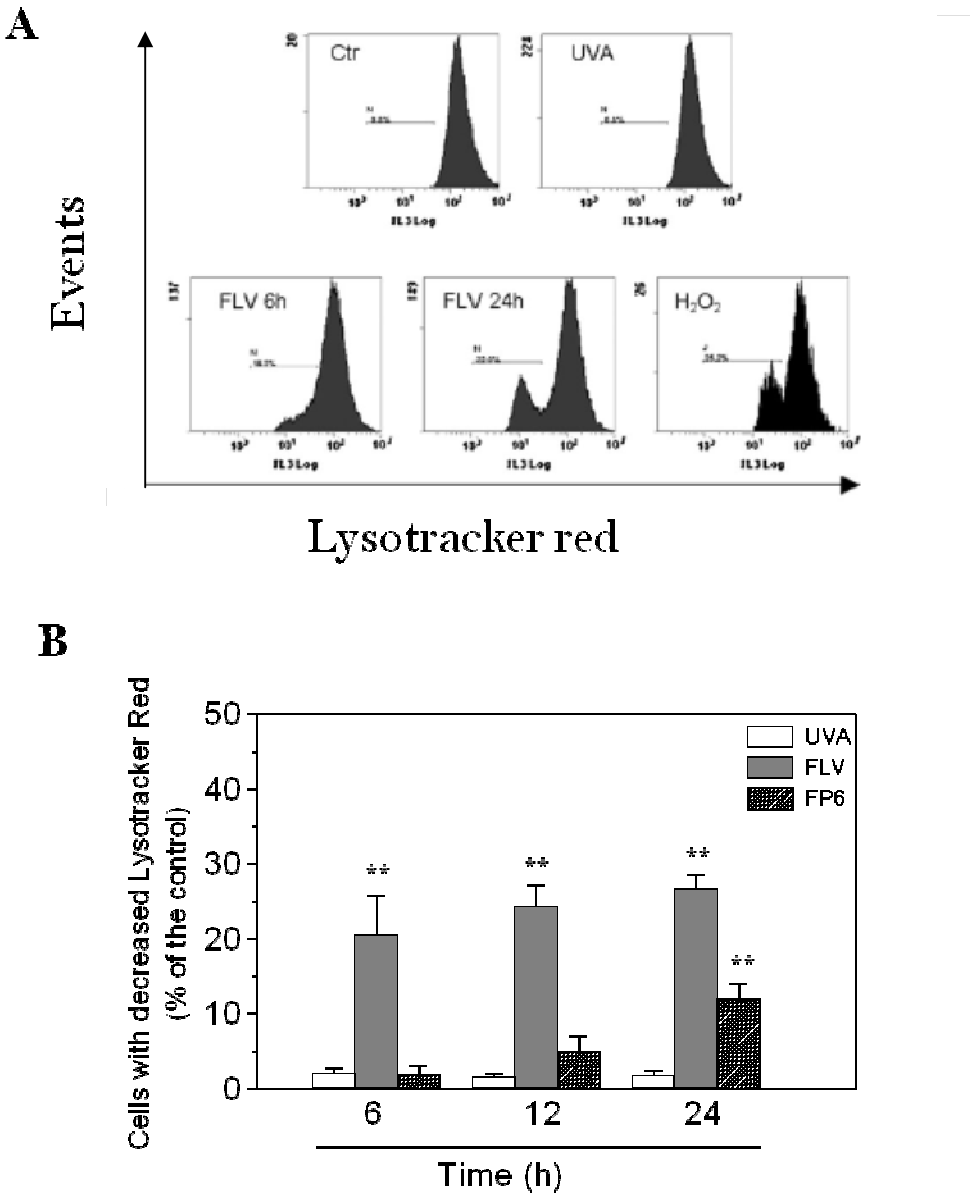

Figure 10. *NCTC cell were irradiated in the presence of FLV or FP6 and after the indicated times stained with LysoTracker RED and analysed by flow cytometry. Representative histograms from three independent experiments are shown (panel A); the marker indicates the percentage of cells with damaged lysosomes. As positive control, cell treated with H_2O_2 at the concentration of 100 mM for 1h were also showed; Panel B: percentage of cell with reduced Lysotracker fluorescence. Data are expressed as mean ± S.E.M. of three independent experiments **p<0.01 vs UVA irradiated cells.*

3.7 Intracellular Ca^{2+} Measurement.

It has been demonstrated that the overload of intracellular Ca^{2+} is associated with necrotic cell pathway (Golstein and Kroemer, 2006). To verify whether a calcium signal is involved in the photoinduced cell death mechanism activated by FLV and

FP6, we used the Ca^{2+}- sensitive dye Fluo-4/AM to investigate whether FLV and FP6 induce an increase in intracellular Ca^{2+} concentration in NCTC-2544 cells. The cells displayed an increase in Fluo-4/AM fluorescence intensity just after one hour from irradiation and the intensity was two-three times greater that the irradiated controls for both FLV and its photoproduct (Figure 11).

To verify the source of calcium, we performed similar experiment using a calcium free medium containing 1mM EGTA. The results showed (Figure 11, panel C) that in these experimental conditions a significant decrease of fluorescence occurred indicating that the increased intracellular calcium is due to calcium influx from the extracellular sites without calcium release from internal stores.

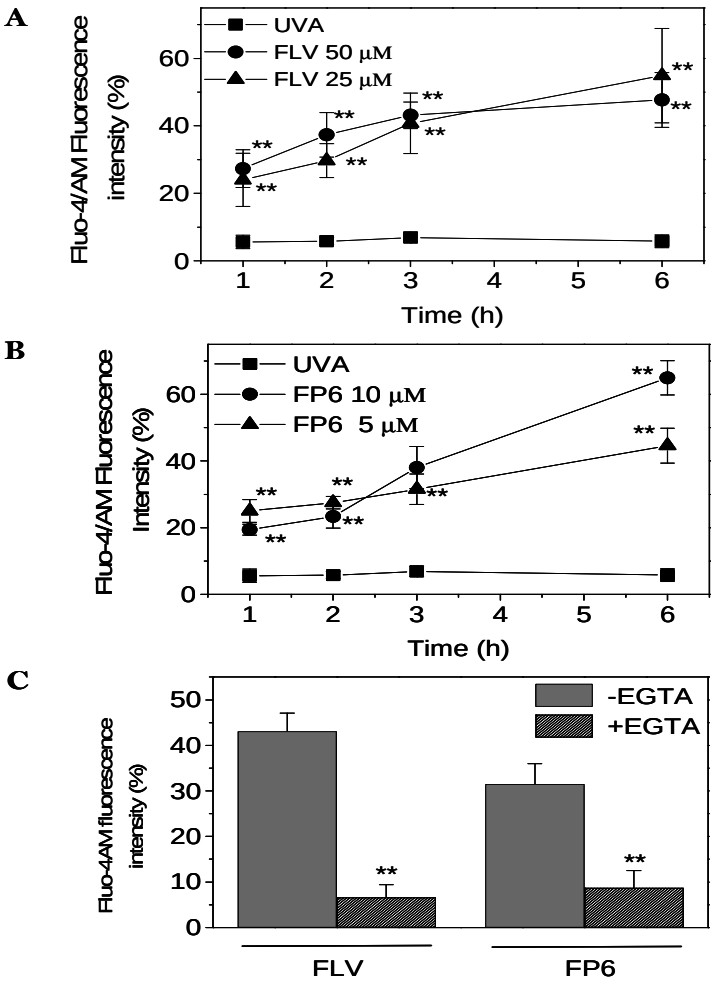

Figure 11. *Intracellular calcium measurement in NCTC-2544 cells after different times from the irradiation (3.75 J cm^{-2}) in the presence of FLV 50 and 25 μM (Panel A) and FP6 10 and 5 μM (Panel B). Ca^{2+} was measured by labeling the cells with 2.5 μM of Fluo-4/AM and examining the fluorescence by flow cytometry. Analogous experiments were performed in a calcium free medium containing 1mM EGTA (Panel C) and analyzed after 3h from the irradiation. Data represent mean of fluorescence intensity± S.E.M of four independent experiments. **p<0.01 vs UVA irradiated cells*

3.8 Lipid peroxidation and GSH content assay.

To gain insight into the photoinduced cell death mechanism activated by FLV and FP6, we investigated if these compounds cause lipid peroxidation by measuring the level of malonyldialdeide (MDA) bound to thiobarbituric acid (TBA) in treated and untreated NCTC. This assay is a measure of membrane injury as the cellular level of MDA correlates with lipid peroxidation. The results showed (Figure 12, panel A) that in untreated cells or in UVA irradiated cells the levels of TBARS were relatively low,

in contrast the levels of TBARS increased significantly just after 6h after the irradiation in the presence of FLV and then further augmented at later times. On the contrary, the effect of FP6 on lipid peroxidation became significant after 12 h from irradiation although less marked in comparison to the parent compound. Therefore, lipid peroxidation initiated by photoactivated FLV is well correlated with the increase of cell permeability to PI .

The photoinduced lipid peroxidation also occurred in a concentration dependent way as depicted in Figure 12 (panel B) after 24h from the irradiation the levels of TBARS increased of about ten times for FLV at the concentration of 50 μM and decrease proportionally with 25 μM and 12.5 μM. In the case of FP6, the increase of TBARS was about 3 times at the concentration of 10 μM and decreased at the concentration of 5 μM. Thus, the induced oxidative damage to membrane lipids is well correlated with the extent of cell death suggesting that an extensive lipid peroxidation could play a major role in the photokilling mechanism.

We investigated whether the induction of lipid peroxidation may be linked to a reduction of intracellular Glutathione (GSH) levels. GSH plays a central role in the defence of cells against ROS and is a potent factor in the control of lipid peroxidation (Higuchi 2004; Kim *et al.* 2005). Indeed, the depletion of GSH after irradiation became significant both for FLV and FP6 after 12 h from the irradiation (Figure 12 panel C), suggesting that a time lag exist between the photoinduction of membrane alteration, which is a rapid process, and the reduction of GSH levels. To confirm that the decrease of GSH may be the consequence of an oxidative stress and not to conjugation reaction with the drugs, we irradiated in aqueous buffered solution of FLV or FP6 and GSH at different molar ratio and the mixture analyzed by LC-MS-MS. The result (data not shown) have showed that the drugs are not able to form conjugates with GSH.

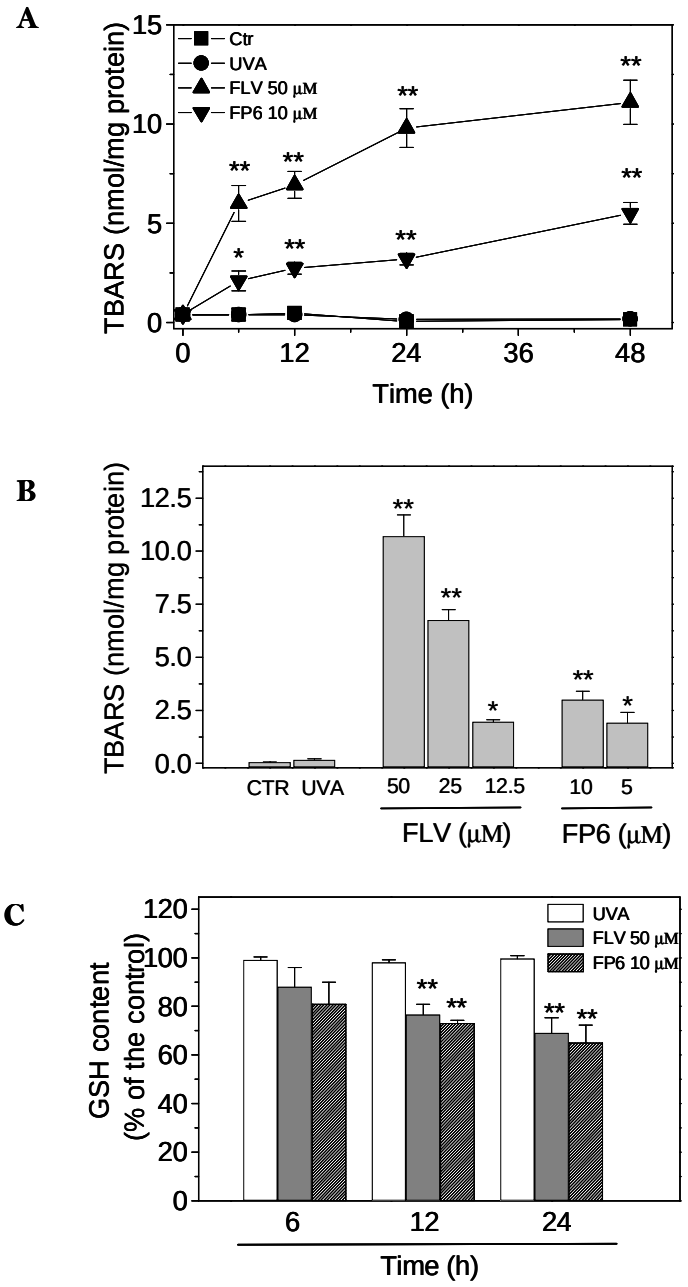

Figure 12. *Panel A. TBARS assay in NCTC-2544 cells after different times from the irradiation (3.75 J cm^{-2}) with FLV and FP6. Data are expressed as mean ± S.E.M. of three independent experiments. *<0.05 **p<0.01 vs UVA irradiated cells; Panel B. TBARS assay in NCTC-2544 cells after 24 h from the irradiation in the presence of different concentration of FLV and FP6. *<0.05 **p<0.01 vs UVA irradiated cells; Panel C. Relative depletion of GSH content after irradiation in the presence of FLV or FP6 Data are expressed as mean ± S.E.M. of three independent experiments.*p<0.05 ** p<0.01 vs UVA irradiated cells*

3.9 Protein photodamage.

To investigate more deeply the phosensitizing properties of FLV and FP6 toward other components of cellular membranes, such as proteins, aqueous buffered solutions of FLV and FP6 containing Bovine serum albumin (BSA), Human serum albumin (HSA) or Ribonuclease A (RNAse), as models, were irradiated for various times. The degree of oxidative modifications was measured by monitoring the carbonyl content, an index of oxidative damage of the proteins (Levine *et al.*, 1990). The results, reported in Figure 13, demonstrated that both FLV and FP6 significantly increased the carbonyl content of BSA and HSA after irradiation.

Irradiated BSA with FLV showed an increase in carbonyl content that is both concentration and UVA dose dependent. A similar picture was observed using HSA as a model protein.

RNAse was selected as a protein model because of the lack of Trp residues together with the presence of Tyr and Phe residues in its sequence. FP6 at the concentration of 10 μM did not significantly induce a high degree of protein oxidation using RNAse reaching at the highest UVA dose used (11 J cm^{-2}) an increase of the carbonyl content of about 10%. On the contrary, a remarkable increase of protein oxidation was observed with both HSA and BSA.

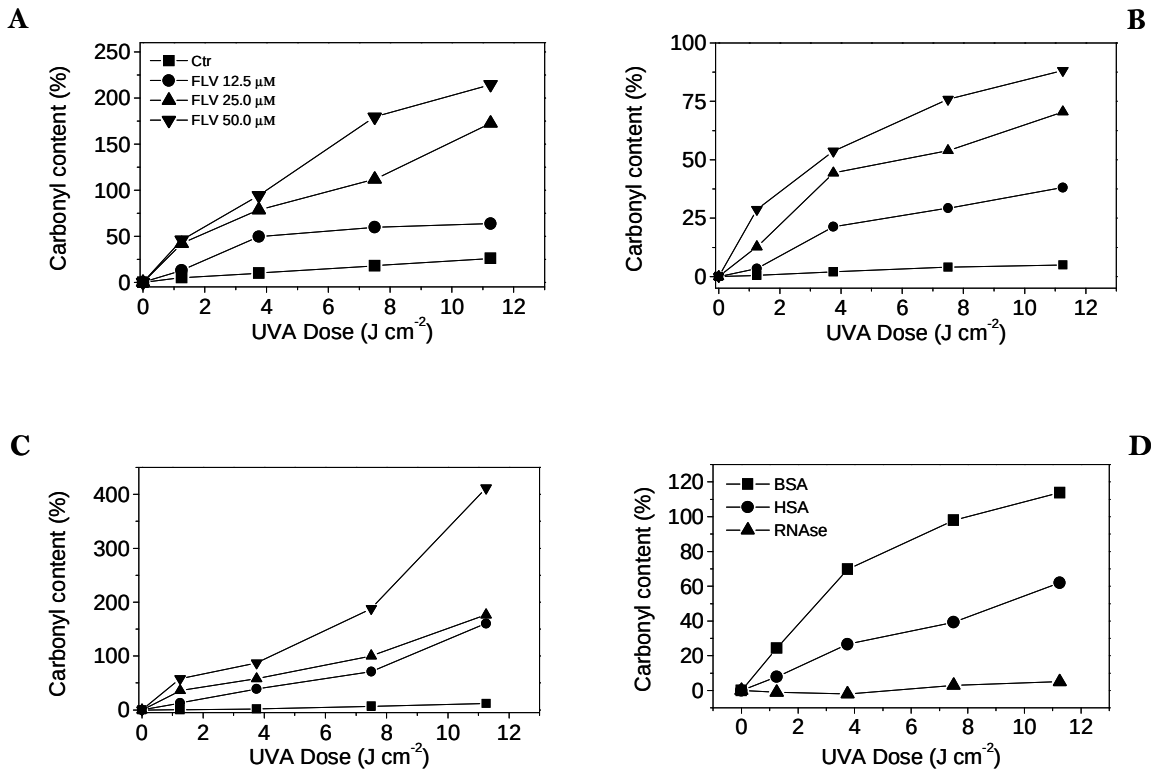

Figure 13. *Photosensitized protein oxidation by FLV and FP6. BSA (panel A), HSA (panel B) and RNAse (panel C), dissolved in phosphate buffer 10 mM pH=7.2, were irradiated at different UVA doses in the presence of FLV at the indicated concentrations and FP6 at the concentration of 10 µM, (panel D). Protein oxidation was evaluated spectrophometrically, by monitoring the carbonyl content after derivatization with 2,4-dinitrophenylhydrazine (DNPH).*

4 Discussion

In this work, we have examined the phototoxic effect of fluvastatin, a highly specific inhibitor of HMGCoA reductase. At the best of our knowledge, this is the first report in which the phototoxic effect of fluvastatin is demonstrated at cellular level. Previous reports (Mielcarek, *et al.*, 2005; Cermola *et al.*, 2007) have investigated the photostability of this drug and the characterization of its photoproducts after UV and solar irradiation. On the basis of these results, we evaluated the phototoxicity in a human cell line of keratinocytes. In our condition, the drug is completely degraded after a UVA dose of 7.5 J cm^{-2} and in agreement with Cermola *et al.* (2007), we were able to detect different photoproducts after HPLC analysis. We focused our attention on the isolation of a product of photocyclization (FP6) with the purpose to evaluate its phototoxicity, since it is well known that photochemical transformation of drugs leads

to different photoproducts that in some cases are more toxic than the parent compound (Beijersbergen van Henegouwen, 1997; Cosa, 2004).

Fluvastatin in combination with UVA light induced a reduction of the cell viability, but more importantly its photoproduct FP6 showed a remarkable increase of the phototoxicity at concentration ten times lower than the parent compound. It is interesting to note that the UVA doses used for the evaluation of phototoxicity are within the range of UVA doses sufficient to induce the photodegradation of the drug and its photocyclization. Thus, these results strongly suggest that the phototoxicity of FLV could be mediated by the formation of a benzocarbazole-like structure (FP6) that acts as a strong photosensitizers.

In our study, the treatment of keratynocytes with BHA, Mannitol and GSH significantly protects from the photoinduced cell death indicating the involvement of free radicals in the mechanism of action of both FLV and its photoproducts. Interestingly, the addition of an antioxidant enzyme such as SOD protects the cells against the loss of viability suggesting that $O^{\bullet -}$ is also involved .

Soon after irradiation with FLV, cells initiated a series of profound morphological alterations that affect subcellular organelles and the integrity of the plasma membrane. In contrast, the nuclear structure is preserved and no DNA degradation is detected. These features are typical necrotic cell death. Necrosis is associated with cell swelling, membrane rupture and release of cytosolic content to the external environment, whereby the loss of membrane integrity is considered an early event in the process.

To monitor the membrane integrity after irradiation with FLV, we used flow cytometry and double staining with Annexin-V and PI. Annexin-V staining precedes the loss of membrane integrity which accompanies the latest stages of cell death resulting from either apoptotic or necrotic processes. Considering that externalisation of PS occurs in the earlier stages of apoptosis, Annexin V staining identifies apoptosis at an earlier stage than sub-G_1 appearance, which represents a later stage of apoptosis being based on nuclear changes such as DNA fragmentation. On the contrary, PI is a plasma membrane impermeant dye. It should be noted that if plasma membrane is permeabilized, Annexin-V can bind to intracellular phosphatidylserine as well (Galluzzi *et al.*, 2009).

Our results showed a rapid increase in the PI positive cells whereas Annexin-V positive cells did not increase significantly at any time investigated. In excellent agreement with the MTT test, the photoproduct FP6 induced high amount of PI

positive cells but at lower concentration respect the parent compound indicating its involvement in the photoinduced cell death.

In this context, we observed a significant increase of intracellular Ca^{2+} concentration soon after the irradiation. Moreover, by depleting extracellular calcium with EGTA, we did not observe an increase of intracellular calcium after irradiation with FLV and FP6 suggesting that the increased intracellular Ca^{2+} was from extracellular sites probably due to a rapid loss of membrane integrity.

The subcellular localization of FLV is not well defined. The FLV molecules were readily detected into cell membranes and the partition coefficient is consistent with a hydrophobic character. However, FLV is also water soluble and would be expected to also reside in the cytoplasm. Accordingly, we have analysed the cellular disposition of FLV and FP6 by fluorescence confocal microscopy and the results did not show a distinct subcellular localization pattern but only a diffuse signal distributed in the cytoplasm. Further experiments revealed that mitochondria are not affected by the irradiation with FLV or FP6 but, on the contrary, lysosomes are damaged as demonstrated by the reduction of Lysotracker Red fluorescence in comparison to non irradiated cells. Since the acidic internal milieu of lysosomes is partly maintained by the action of an ATP driven proton pump, the lysosomal destabilization induced by FLV could be caused by damage to the ATP-dependent proton pump or the decrease of ATP levels.

In this context, Ollinger and Brunk (1995) have reported that oxidative stress induced by naphtazarin in human hepatocytes is preceded by lysosomal destabilization followed by lipid peroxidation and energy depletion. Moreover, it is interesting to note that in NCTC-2544 cell line addition of a cathepsin inhibitor prevent the cell death induced by UVA in cells treated with lovastatin suggesting that lysosomal damage is involved in the observed phenomenon (Quiec *et al.*, 1995).

The cell death induced by FLV and FP6 is accompanied by a reduction of ATP content but not by loss of mitochondrial membrane potential. Although the disruption of mitochondrial membrane potential plays an important role in necrotic and apoptotic processes, a lack of loss of mitochondrial membrane potential has been reported in non apoptotic cell death (Kim *et al.*, 2005). Given the rapid increase in cell membrane permeability after FLV or FP6 irradiation as evidenced by intracellular Ca^{2+} increase and PI permeability, it is more plausible that these compounds cause considerable damage to the cell membrane structure thereby promoting substantial ATP leakage into the extracellular spaces. As ATP depletion is thought to be the major cause of

necrotic cells death, such loss of the ATP pool may lead to necrosis. However, we cannot exclude the possibility that the drugs may inhibit oxidative phosphorylation without any changes in mitochondrial membrane potential or that the reduction in ATP concentration could be due to an increase in ATP consumption.

The assessment of GSH content and TBARS formation revealed a marked oxidative stress in cells irradiated in the presence of FLV and FP6. GSH is the main non-protein antioxidant in the cell and is able to clear away the superoxide anion and provides electrons for enzymes such as glutathione peroxidase, which reduces H_2O_2 to H_2O. Our results demonstrated that irradiation with FLV or FP6 depleted the intracellular GSH content in keratynocytes supporting the idea that intracellular GSH levels are related to the photoinduced cell death (Higuchi, and Yoshimoto, 2002). To sustain this hypothesis, we have observed an efficient protection from the cell death in the presence of exogenously GSH. Moreover, it also could possible that end-products of lipid peroxidation such as 4-hydroxy-2-nonenal (4-HNE) can react with the sulphydryl group of GSH and subsequently cause the reduction of GSH levels (Kinter and Roberts, 1996).

In summary, we have established for the first time that FLV is endowed with a clear phototoxic potential *in vitro* in a human keratinocyte cell line and also in 3T3 fibroblasts. Its phototoxicity could be mediated by the formation of a photoproduct endowed with high photosensitizing properties. We also identified plasma membrane as one of the major targets of the FLV action, which ultimately leads to necrosis as the principal mode of cell death. The photoproduct formation and the possible consequences on the biological effects of the photosensitization of cutaneous cells in patients treated with FLV deserve further studies.

5 Supplementary

5.1 Photodegradation spectra

Light absorption spectra were recorded with a Perkin-Elmer Lambda 15 spectrophotometer after irradiation with increasing doses of UVA ligth. The measurements were carried out with a quartz cuvette containing a solution of fluvastatin in phosphate buffer 10 mM, pH = 7.0.

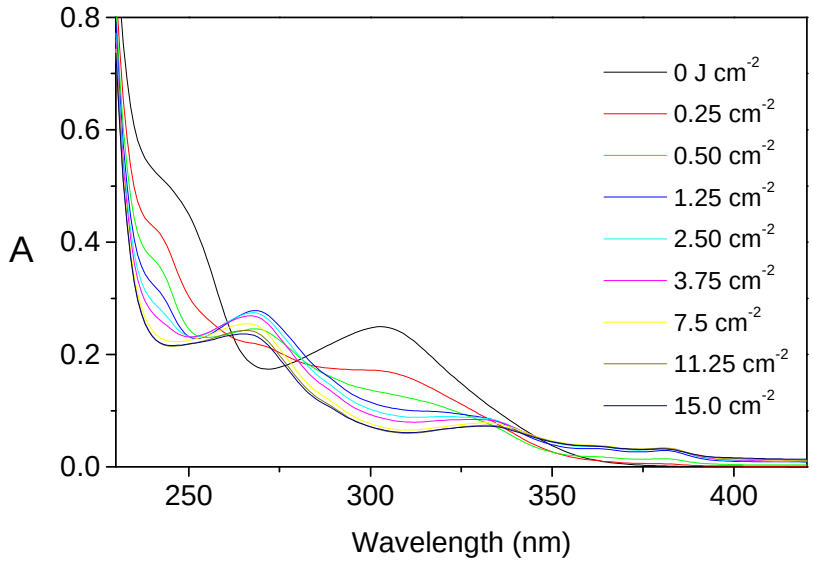

Figure S1 *Absorption spectra of Fluvastatin 10 μM in phosphate buffer 10 mM, pH=7.2 after irradiation with the indicated doses of UVA light*

^{1}H NMR analysis

Spectra were recorded in deuterated methanol with a Bruker AMX-600 spectrometer, operating at 600 MHz for ^{1}H.

Fluvastatin sodium: (600 MHz, d_4-methanol) 7.55 (1H, d, *J* 8.4 Hz), 7.40 (3H, m), 7.12 (3 H, m), 6.99 (1H, t, *J* 7.8 Hz), 6.68 (1 H, d, *J*=16.1 Hz), 5.72 (1 H, dd, J=6.4, 16.0 Hz), 4.92 (1 H, sept, *J* 7.0 Hz), 4.37 (1 H, dd, m), 3.97 (1 H, m), 2.33 (1 H, dd, *J* 4.6; 15.2 Hz), 2.26 (1 H, dd, *J* 7.9, 15.2 Hz), 1.69 (1 H, m), 1. 64 (6 H, d, *J* 7.0 Hz), 1.51 (1 H, m).

Photoproduct FP6: δ_H (600 MHz, d_4-methanol) 8.80 (1 H, dd, *J* 9.5, 5.5 Hz), 8.56 (1 H, d *J* 8.6 Hz), 7.95 (1 H, d, *J* 9.0 Hz), 7.85 (1 H, d, *J* 9.0 Hz), 7.66 (1 H, dd, *J* 8.3 Hz), 7.66 (1 H, dd, *J* 2.5, 10.0 Hz), 7.48 (2 H, m), 7.33 (1 H, t, *J* 7.5 Hz), 5.28 (1 H, sept, *J* 7.0 Hz), 1.77 (6 H, d, *J* 7.0 Hz).

5.2 Mass Spectrometry Analysis.

Mass spectra were obtained by means of a Mariner API-TOF spectrometer (PerSeptive Biosystems, Stafford, TX), by direct injection of the samples dissolved in methanol-formic acid (99:1, v/v). To obtain exact mass values, the instrument was

calibrated through an internal standard composed of 4,8-dimethyl-7-hydroxycoumarin, desipramine, and dansylglycyltryptophan.

Table S1. *Retention times, m/z values of fluvastatin photoproducts.*

Compound	Retention time (min)	Molecular ion	Mass	
			Measured	Calculated
FLV	14.4	$[C_{24}H_{26}FNO_4 + H]^+$	412.1916	412.1918
FP-1	5.3	$[C_{24}H_{26}FNO_6 + H]^+$	444.1681	444.1817
FP-2	5.7	$[C_{24}H_{26}FNO_6 + H]^+$	444.1579	444.1817
FP-3	13.4	$[C_{24}H_{26}FNO_4 + H]^+$	412.1850	412.1873
FP-4	15.1	$[C_{24}H_{26}FNO_4 + H]^+$	412.1780	412.1873
FP-5	16.6	$[C_{24}H_{26}FNO_4 + H]^+$	412.1880	412.1873
FP-6	22.1	$[C_{19}H_{16}NF + H]^+$	278.1167	278.1496

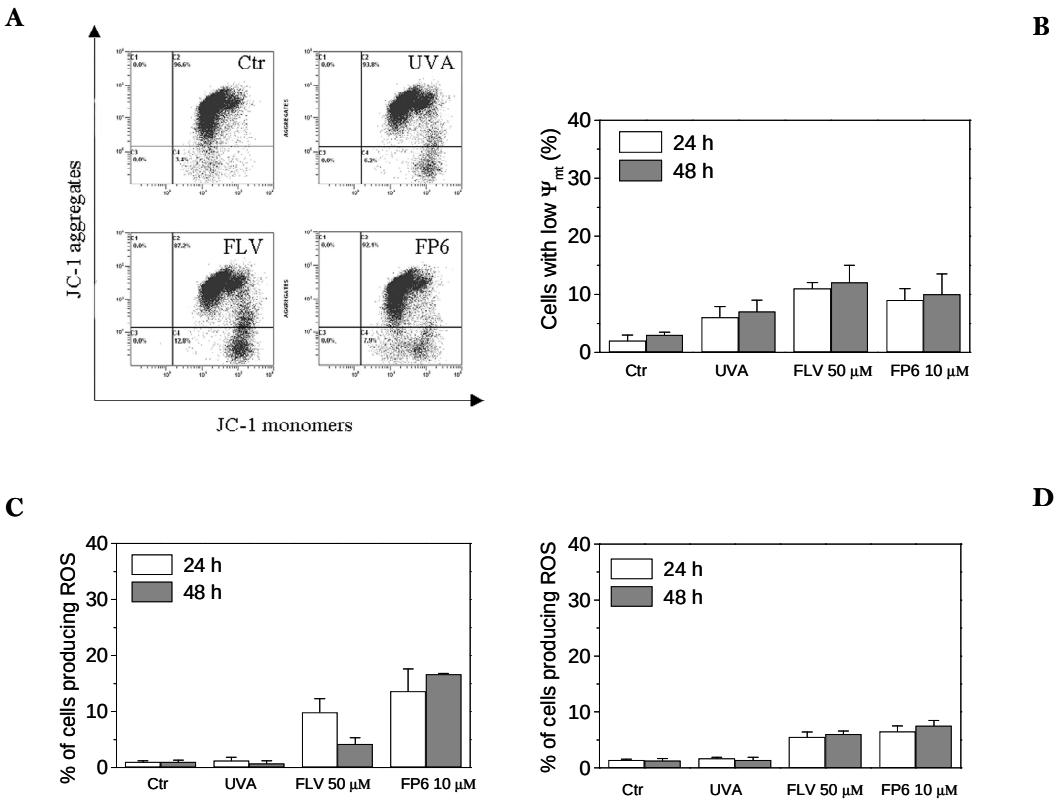

Figure S2. *Panel A shows representative histograms of cells irradiated in the presence of FLV at the concentration of 50 μM and stained with the fluorescent probe JC-1, after 24 h of incubation. Panel B shows the percentage of cell with low mitochondrial potential after 24 and 48 h from the irradiation (3.75 J cm^{-2}) in the presence of FLV and FP6. Panels C and D show the mitochondrial production of ROS evaluated by flow cytometry using the fluorescent probe HE (panel C) and H2DCFDA (Panel D). Data are expressed as mean ± S.E.M. of three independent experiments*

Funding

This work was partially supported by Polish State Committee on Science (KBN, project No. N N405 3478 33).

6 References

Alexander, K.P., Blazing, M.A., Rosenson, R.S., Hazard, E.; Aronow, W.S., Smith, S.C. Jr, and Ohman E.M. (2009.) Management of hyperlipidemia in older adults. *J Cardiovasc. Pharmacol. Ther.* **14,** 49-58.

Antunes, F., Cadenas E., and Brunk U.T. (2001) Apotosis induced by exposure to a low steady state concentration of H_2O_2 is a consequence of lysosomal rupture *Biochem J.* ***356***, 549-55.

Astarita, M., Della Greca, M., Iesce M.R., Montanaro S., Previtera L., and Temussi F. (2007) Polycyclic cobvmpounds by sunlight exposure of the drug rosuvastatin in water *J. Photochem. Photobiol. A* 187, 263–268.

Beijersbergen van Henegouwen, G.M.J. Medicinal Photochemistry (phototoxic and phototherapeutic aspect of drugs). In *Advances in Drug Research* (B. Testa, and U. Mayer eds.) *volume* 29, New York: Academic Press; 1997: 79-170

Buytaert E., Dewaele M., and Agostinis, P., (2007) Molecular effectors of multiple cell death pathways initiated by photodynamic therapy *Biochim.Biophys. Acta* **1776**, 86-107.

Cermola F., Della Greca M., Iesce M.R., Montanaro S., Previtera L., Temussi F., and Brigante, M. (2007) Irradiation of fluvastatin in water structure elucidation of photoproducts *J. Photochem. Photobiol. A: Chemistry* **189**: 264-271.

Cermola F., Della Greca M., Iesce M.R., Montanaro S., Previtera, L., and Temussi F. (2006) Photochemical behavior of the drug atorvastatin in water *Tetrahedron* 62, 7390–7395.

Cosa, G. (2004) Photodegradation and photosensitization in pharmaceutical products: assessing drug phototoxicity *Pure Appl. Chem.* **76**, 263-275.

Eguchi, Y., Shimizu, S., and Tsuijmoto, Y. (1997) Intracellular ATP levels determine the cell death fate by apoptosis or necrosis *Cancer Res.* **57**, 1835-1840

Elisei F., Aloisi G.G., Barbafina A., Dall'Acqua F., Mazzuccato U., Canton M., Facciolo L., Latterini L., and Viola G. (2004) Photophysical and photobiological behaviour of antimalarial drugs in aqueous solutions. *Photochem. Photobiol.* **79**, 248-258.

Ferguson, J. (2002) Photosensitivity due to drugs. *Photodermatol. Photoimmunol. Photomed.* **18**, 262-269.

Galluzzi, L., Aaronson, S.A., Abrams, J., Alnemri, E.S., Andrews, D.W., Baehrecke E.H., Bazan, N.G., Blagosklonny, M.V., Blomgren, K., Borner, C., Bredesen D.E., Brenner, C., Castedo, M., Cidlowski, J.A., Ciechanover A., Cohen G.M., De Laurenzi V., De Maria, R.,Deshmukh, M., Dynlacht, B.D., El-Deiry, W.S., Flavell, R.A., Fulda, S., Garrido, C., Golstein, P., Gougeon, M.L., Green, D.R., Gronemeyer, H., Hajnóczky, G., Hardwick J.M., Hengartner M.O., Ichijo H., Jäättelä M., Kepp O., Kimchi A., Klionsky, D.J., Knight, R.A., Kornbluth, S., Kumar, S., Levine, B., Lipton, S.A., Lugli, E., Madeo F.,Malomi W., Marine J.C., Martin S.J., Medema, J.P., Mehlen, P., Melino, G., Moll U.M., Morselli, E., Nagata, S., Nicholson, D.W., Nicotera, P., Nuñez G., Oren M., Penninger, J., Pervaiz S., Peter, M.E., Piacentini, M., Prehn, J.H., Puthalakath H., Rabinovich G.A., Rizzuto R., Rodrigues C.M., Rubinsztein, D.C., Rudel, T., Scorrano, L., Simon, H.U., Steller, H., Tschopp, J., Tsujimoto, Y., Vandenabeele, P., Vitale, I., Vousden, K.H., Youle, R.J., Yuan, J., Zhivotovsky, B., and Kroemer, G. (2009) Guidelines for the use and interpretation of assays for monitoring cell death in higher eukaryotes. *Cell Death Differ.* **16**, 1093-1107.

Girotti, A.W. (2001) Photosensitized oxidation of membrane lipids: reaction pathways, cytotoxic effects, and cytoprotective mechanisms. *J Photochem. Photobiol. B.* **63**,103-113.

Golstein P., and Kroemer G., (2007) Cell death by necrosis: toward a molecular definition. *Trends Biochem. Sci.* 32, 37-43.

Grobelny P., Viola G., Vedaldi D., Dall'Acqua F., Gliszczynska-Swiglo A., and Mielcarek J. (2009) Photostability of pitavastatin, a novel HMG-CoA reductase inhibitor *J. Pharm. Biomed. Anal.* **50**, 597-601.

Hedley, D.W., and Chow, S. (1994) Evaluation of methods for measuring cellular glutathione content using flow cytometry *Cytometry* **15**, 349-358.

Higuchi, Y. (2004) Glutathione depletion-induced chromosomal DNA fragmentation associated with apoptosis and necrosis *J. Cell. Mol. Med.* **8**, 455-464.

Higuchi, Y., and Yoshimoto, T. (2002) Arachidonic acid converts the glutathione depletion-induce apoptosis to necrosis by promoting lipid peroxidation and reducing caspase-3 activity in rat glioma cells. *Arch. Biochem. Biophys.* **400**,133-140.

Holme, S.A., Pearse, A.D., and Anstey, A.V. (2002) Chronic actinic dermatitis secondary to simvastatin *Photodermatol Photoimmunol Photomed.* **18**, 313-314.

Kessel, D., and Luo, Y. (2001) Intracellular sites of photodamage as a factor in apoptotic cell death. *J. Porphyrins Phthalocyanines* **5**, 181-184.

Kim, W.H., Choi C.H., Kang, S., Kwon, C.H., and Kim, Y.K. (2005) Ceramide induces non-apoptotic cell death in human glioma cells *Neurochem. Res.* **30**, 969-979.

Kinter, M. and Roberts, J.R., (1996) Glutathione consumption and glutathione peroxidase inactivation in fibroblast cell lines by 4-hydroxy-2-nonenal *Free Rad. Biol. Med.* **21**;457-462.

Kumar, S. (2007) Caspase function in programmed cell death. *Cell Death Differ.* **14**, 32-43.

Leist M., Single B., Castoldi, A.F., Kuhnle, S., Nicotera, P. (1997) Intracellular adenosine triphosphate (ATP) concentration: a switch in the decision between apoptosis and necrosis *J. Exp. Med.* **185**, 1481-1486.

Levine L.R.; D. Garland, C.N.; Oliver, A.; Amici, I.; Climent, A.G.; Lenz, B.G.; Ahn, S.; Shaltiel G.; and Stadtman E.R. (1990) Determination of carbonyl content in oxidatively modified proteins *Methods Enzymol.* **186**, 464-480.

Mielcarek J. ,Kula M., Zych R., Grobelny P. (2005) Kinetic studies on fluvastatin photodegradation in solutions *React. Kinet. Catal. Lett.* 86:119–126.

Montanaro S., Lhiaubet-Vallet V., Iesce M.R., Previtera L., and Miranda M.A. (2009) A mechanistic study on the phototoxicity of atorvastatin: singlet oxygen generation by a phenanthrene-like photoproduct *Chem. Res. Toxicol.* **22**, 173-78.

Morliére, P., Mysan, A., Santus, R., Huppe, R., Mazière, J.C., and Dubertret, L. (1991) UVA-induced lipid peroxidation in cultured human fibroblast. *Biochim. Biophys. Acta* 1084, 261-268.

Nohl, H., Gille, L., Staniek, K., (2005) Intracellular generation of reactive oxygen species by mitochondria, *Biochem. Pharmacol.* 69**,** 719–723.

Oleinick, N.L., Morris, R.L., Belichenko, I. (2002). The role of apoptosis in response to photodynamic therapy: what, where, why and how. *Photochem. Photobiol. Sci.*, **1**, 1-21.

Ollinger, K., and Brunk, U.T. (1995) Cellular injury induced by oxidative stress is mediated through lysosomal damage *Free Rad. Biol. Med.* **19**, 565-574.

Ouedraogo, G., Morliere, P., Bazin, M., Santus, R., Kratzer, B., Miranda, M.A, Castell, J.V. (1999) Lysosomes are sites of fluoroquinolone photosensitization in human skin fibroblasts: a microspettrofluorometric approach. *Photochem. Photobiol.* **70**, 123-129.

Porter, A.G., and Janicke, R.U. (1999) Emerging role of caspase-3 in apoptosis *Cell Death Differ.* **6,** 99-104.

Quiec, D., Mazière, C., Auclair, M., Santus, R., Gardette, J., Redziniak, G.,Franchi J., Dubertret L., Mazière, J.C. (1995) Lovastatin enhances the photocytotoxicity of UVA radiation towards cultured N.C.T.C. 2544 human keratinocytes: prevention by cholesterol supplementation and by a cathepsin inhibitor. *Biochem. J.* **310**, 305-309.

Rothe, G., and Valet, G. (1990) Flow cytometric analysis of respiratory burst activity in phagocytes with hydroethidine and 2',7'-dichlorofluorescein. *J. Leukoc. Biol.* **47**, 440-448.

Salvioli, S., Ardizzoni, A., Franceschi, C., and Cossarizza, A. (1997) JC-1 but not DiOC6(3) or rhodamine 123 is a reliable fluorescent probe to asses $\Delta\Psi$ changes in intact cells: implications for studies on mitochondrial functionality during apoptosis, *FEBS Lett.* **411**, 77-82.

Shaw S.M., Fildes J.E., Yonan N., Williams S.G. (2009) Pleiotropic effects and cholesterol-lowering therapy *Cardiology* **112**, 4-12.

Spielmann, H., Balls, M., Dupuis, J., Pape, W.J.W., Pechvith G., De Silva O. (1998) The international EU/COLIPA in vitro phototoxicity validation study: results of the Phase II (blind trial); part 1: the 3T3 NRU phototoxicity test *Toxicol. In Vitro* **12**, 305-27.

Stadtman, E.R. and Levine, R.L. (2003) Free radical-mediated oxidation of free amino acids and amino acid residues in proteins. *Amino Acids.* **25**, 207-218.

Stahlmann, R., and Lode H. (1999) Toxicity of quinolones. *Drugs* **9**, Suppl 2, 37-42.
Vermes, I., Haanen, C., Steffens-Nakken, H., and Reutelingsperger, C.P. (1995). A novel assay for apoptosis. Flow cytometric detection of phosphatidylserine expression on early apoptotic cells using fluorescein labelled Annexin V. *J. Immun. Method* **184**, 39-51.

Viola, G., and Dall'Acqua, F. (2006) Photosensitization of biomolecules by phenothiazine derivatives *Curr. Drug Targets* **7,** 1135-1154.

Viola, G., Salvador, A., Cecconet, L., Basso, G., Dall'Acqua, F., Vedaldi, D., Aloisi, G., Elisei, F., Latterini, L., and Barbafina, A. (2007) Photophysical properties and photobiological behaviour of amodiaquine, chloroquine and primaquine. *Photochem. Photobiol.* **83**:1415-1427.

Yuan, M.X., Li, W., Dalen, H., Lotem, J., Kama, R., Sachs, L., and Brunk, U.T. (2002) Lysosomal destabilization in p53 induced apoptosis. *Proc. Natl. Acad. Sci. USA* **99**, 6286-6291.

Pitavastatin, A New Hmg-Coa Reductase Inhibitor, Induces Phototoxicity In Human Keratinocytes Nctc-2544 Through The Formation Of Benzophenanthridine-Like Photoproducts

Giampietro Viola[†], Pawel Grobelny[§], Maria Antonella Linardi[†], Alessia Salvador[††], Stefano Dall'Acqua[††], Lukasz Sobotta[‡], Jadwiga Mielcarek[‡], Francesco Dall'Acqua[††] Daniela Vedaldi[††], and Giuseppe Basso[†]

[†]*Department of Pediatrics, Oncohematology Laboratory, University of Padova, Italy*

[§]*Department of Pharmaceutical Technology, Poznan University of Medical Sciences, Grunwaldzka 6, 60-780 Poznan, Poland*

[††]*Department of Pharmaceutical Sciences, University of Padova, Italy*

[‡]*Department of Inorganic and Analytical Chemistry, Poznan University of Medical Sciences, Grunwaldzka 6, 60-780 Poznan, Poland*

-------Archives of Toxicology 2011.. DOI: 10.1007/s00204-011-0772-4------

Abstract

This study reports the results of an investigation of the phototoxicity mechanism induced by pitavastatin and its photoproducts, namely 6-cyclopropyl-10-fluoro-7,8-dihydrobenzophenanthridine (PP3) and 6-cyclopropyl-10-fluorobenzophenanthridine (PP4). The phototoxicity wastested in human keratinocytes cell lines NCTC-2544, and the results proved that under the same conditions, all three compounds exhibited phototoxic effects in the model tested. The reduction in cell viability was found to be both concentrationand UVA dose-dependent. A point of note is that both the photoproducts produced a dramatic decrease in cell viability with GI50 values one order of magnitude lower compared to the parent compound. In particular, the fully aromatic derivative (PP4) showed the highest antiproliferative activity. Flow

cytometric analysis indicated that pitavastatin and the photoproduct PP4 principally induced necrosis, as revealed by the large appearance of propidium iodide-positive cells and also confirmed by the rapid drop in cellular ATP levels. Further studies committed to better understanding of photoinduced cell death mechanism(s) revealed that neither pitavastatin nor PP4 induced mitochondrial depolarization or lysosomal damage, but, interestingly, extensive cell lipid membrane peroxidation along with a significant oxidation of model proteins occurred, suggesting that pitavastatin and PP4 exert their phototoxic effect mainly in the cellular membranes. The present results suggest that the phototoxicity of pitavastatin may be mediated by the formation of benzophenanthridine-like photoproducts that appear to have high potential as photosensitizers.

Keywords Pitavastatin _ Phototoxicity _ Photoproduct _Necrosis _ Lipid peroxidation _ Protein oxidation.

Abbreviations:

BHA, 2,6-di-tert-butylhydroxyanisole; BSA, bovine serum albumin; DMTU, N-N'-dimethyl thiourea; DNPH, 2,4-dinitrophenyl hydrazine; GSH, glutathione reduced form; MDA, malonyl dialdheide; PIT, Pitavastatin; RNAse A, Ribonuclease A; SOD superoxide dismutase; TBA, Thiobarbituric acid; TOC, tocopherol acetate;

1 Introduction

Pitavastatin, NK-104, monocalcium bis(*3R,5S,6E*)-7-(2-cyclopropyl-4-[4-fluorophenyl]-3-quinolyl)-3,5-dihydroxy-6-heptenoate (PIT, Figure 1) is a totally synthetic HMG-CoA reductase inhibitor that significantly reduces serum total cholesterol, LDL cholesterol, and triglyceride levels while modestly raising HDL cholesterol (1,2).

The cellular mechanism of action is attributed to the inhibition of cholesterol biosynthesis in the liver and the drug is the first-line agent for lipid lowering in patients with atherosclerosis and cardiovascular disease (3). Additionally, recent reports have suggested that pitavastatin may exhibit pleiotropic effects and is now being tested for the treatment of other diseases, including Alzheimer's disease and osteoporosis (4,5). (Ose et al. 2009). Additionally, recent reports have suggested that pitavastatin may exhibit pleiotropic effects and is now being tested for the treatment for other diseases, including Alzheimer's disease and osteoporosis (Mundy 2001;

Caballero and Nahata 2004). Metabolism of pitavastatin by the cytochrome P450 system is minimal, principally through CYP 2C9, with little the involvement of the CYP 3A4 isoenzyme, potentially reducing the risk of drug–drug interactions (Fujino et al. 2003). Of great importance is a high systemic bioavailability resulting from a moderate first-pass metabolism, and the drug's long elimination half-life of approximately 11 h (Mukhtar et al. 2005).Currently, the photostability of active pharmaceutical ingredients (APIs) as well as final dosage forms is of great interest because the photodegradation process can result in a loss of the potency of the drug and also in adverse effects due to the formation of toxic degradation products. It is accepted that fraction of the optical radiation above 300 nm can penetrate sufficiently deep into skin to react with substances circulating in the bloodstream. In case of new chemical entities for both topical and systemic application, whichabsorb light in the range of 290–700 nm, the phototoxic potential must be assessed through the use of appropriate assays. Thus, the study of the photostability of pharmaceuticals and their formulations is of more than simple scientific interest but has implications for the market.

The literature survey shows that certain statins including cerivastatin, atorvastatin, fluvastatin, and rosuvastatin are highly photochemically reactive (Krol et al. 1993; Cermola et al. 2006, 2007; Astarita et al. 2007). Moreover, we have recently concluded that the phototoxic potential of fluvastatin may be attributed to the formation of a polycyclic product with strong photosensitizing activity (Viola et al. 2010). The photodegradation of atorvastatin to a highly reactive phenanthrene-like photoproduct also may contribute to the phototoxic activity of the compound (Montanaro et al. 2009). Our recent study (Grobelny et al. 2009) showed that pitavastatin exhibited susceptibility to degradation after exposure to UVA light, yielding polycyclic products. In particular, we noticed the formation of photoproducts after UVA exposure of the drug in aqueous media, indicating that photocyclization is the main reaction involved in the formation of the products observed. In this context, it would be of great importance to conduct experiments on the phototoxic potential of pitavastatin. Thus, the aim of this work is to evaluate the light-induced toxicity of pitavastatin and its main photoproducts in cultured NCTC-2544 human keratinocytes. In order to gain insight into the mechanism of phototoxicity, we have extended our studies to the photochemical damage on the protein model in vitro. To the best of our knowledge, this is the first report in which the phototoxic effects of pitavastatin are demonstrated at cellular level.

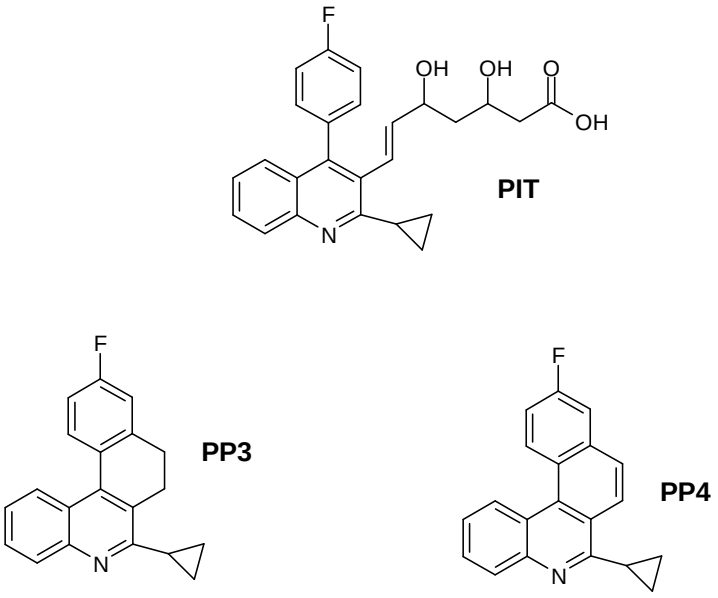

Figure 1 *Chemical structures of pitavastatin (PIT) and its main photoproducts PP3 and PP4.*

2 Experimental section

2.1 Chemicals. Pitavastatin calcium, monocalcium bis(3R,5S,6E)-7-(2-cyclopropyl-4-[4-fluorophenyl]3-quinolyl)-3,5-dihydroxy-6-heptenoate was obtained from Zydus Cadila, India.

Thiobarbituric acid (TBA), sodium azide (NaN_3), N-N'-dimethyl thiourea (DMTU), superoxide dismutase (SOD), bovine serum albumin (BSA), Ribonuclease A (RNAse A), 2,6-di-tert-butylhydroxyanisole (BHA), tocopherol acetate and glutathione reduced form (GSH) were purchased from Sigma-Aldrich (Milano, Italy).

2.2 HPLC analysis. Analytical HPLC was carried out on an Agilent 1200 instrument equipped with a UV-DAD detector. The chromatographic separation was achieved on an octadecylsilane-coated column, 150 mm × 4.6 mm, 5 μm (Gemini, Phenomenex), using ternary gradient elution conditions at a flow rate of 1.0 mL/min as follows: water, solvent A; acetonitrile, solvent B; methanol, solvent C. The gradient conditions were: (a) 75% of A and 25% of B for 0-6 min, (b) linear gradient from 75 to 40% of A, 25% to 40% of B and 0% to 20% of C for 6-7 min and continued till 25 min. Fractions

corresponding to PP3 and PP4 respectively, were collected and the solvent evaporated at room temperature using a rotary evaporator.

2.3 NMR analysis. The NMR spectra were recorded on a BrukerAvance II (400 MHz) NMR spectrometer, using MeOD as solvent and tetramethylsilane (TMS) as the internal standard.

2.4 Irradiation procedure. Two HPW 125 Philips lamps, mainly emitting at 365 nm, were used for irradiation experiments. The spectral irradiance of the source was 4.0 mW cm^{-2} as measured at the sample level by a Cole-Parmer Instrument Company radiometer (Niles, IL, USA) equipped with a 365-CX sensor.

2.5 Cellular phototoxicity. An immortalized, non-tumorigenic cell line of human keratinocytes (NCTC-2544) was grown in a DMEM medium (Sigma-Aldrich Milan, Italy), supplemented with 115 units/mL of penicillin G, 115 µg/ml streptomycin, and 10% fetal calf serum (Invitrogen, Milan, Italy). Individual wells of a 96-well tissue culture microtiter plate (Falcon, Becton-Dickinson) were inoculated with 100 µl of complete medium containing $8x10^3$ NCTC-2544. The plates were incubated at 37 °C in a humidified 5% CO_2 incubator for 18 hours prior to the experiments. After medium removal, 100 µl of the drug solution, dissolved in DMSO and diluted with Hank's Balanced Salt Solution (HBSS pH=7.2), were added to each well, incubated at 37 °C for 30 minutes and then irradiated. After irradiation, the solution was replaced with the medium, and the plates were further incubated for 72 hours. Cell viability was assayed by the MTT [(3-(4,5-dimethylthiazol-2-yl)-2,5 diphenyl tetrazolium bromide)] test as previously described (16).

2.6 Cell cycle analysis. For flow cytometric analysis of DNA content, $5x10^5$ cells in exponential growth were irradiated as described above. After specified time intervals, the cells were trypsinized and together with floating cells, centrifuged and fixed with ice-cold ethanol (70%). Subsequently, the keratinocytes were treated with a lysis buffer containing RNAse A and stained with propidium iodide. Samples were analyzed on a Beckman Coulter Cytomic FC500 flow cytometer. For cell cycle analysis, DNA histograms were analyzed using MultiCycle™ for Windows (Phoenix Flow Systems, CA, USA).

2.7 Externalization of phosphatidylserine. The surface exposure of phosphatidylserine (PS) by apoptotic cells was measured by flow cytometry with a Coulter Cytomics FC500 (Coulter) by adding Annexin V-FITC to cells according to the manufacturer's instructions (Roche Diagnostic, Monza, Italy). Simultaneously, the cells were stained with PI. Excitation was set at 488 nm and the emission filters were set at 525 nm and in the range of 560-680 nm for FITC and PI fluorescence, respectively.

2.8 Detection of DNA fragmentation by agarose gel. Total genomic DNA was extracted from irradiated keratinocytes by a commonly used salting out protocol. Afterwards, 1 □g of DNA obtained was subsequently loaded on a 1.5% agarose gel at 50 V for 6 h in TAE buffer. After staining in an ethidium bromide solution, the gel was washed with water and the DNA bands were detected under UV radiation with an ImageQuant 300 transilluminator (GE Health care) equipped with a CCD camera.

2.9 Intracellular calcium measurement. The intracellular calcium concentration in NCTC-2544 cells was measured by flow cytometry using the Ca^{2+}-sensitive fluorescent dye Fluo-4/AM (Molecular Probes). Briefly, after specified time intervals, irradiated cells were washed and incubated with 2.5 μM Fluo-4/AM in the complete medium for 30 minutes at 37 °C. The cells were then trypsinised, washed two times and then re-suspended in HBSS. The intracellular calcium level was analyzed immediately for Fluo-4/AM fluorescence intensity by flow cytometry.

2.10 ATP assay. Cells were irradiated in the presence of PIT or its photoproducts and from different times of irradiation, the cells were collected and counted. The ATP content per 100,000 cells was then determined using the CellTiter-Glo luminescent assay (Promega, Milano, Italy) according to the manufacturer's instructions, using a Victor^{3TM} luminometer (Perkin Elmer). Data are normalized to the ATP content in non-irradiated cells.

2.11 Caspase-3 assay. Caspase-3 activation in NCTC-2544 cells was evaluated by flow cytometry using a human active caspase-3 fragment antibody conjugated with FITC (BD Pharmingen). Briefly, after irradiation, the cells were collected by centrifugation and resuspended in Perm/Wash^{TM}(BD Pharmingen) buffer for 20

minutes, washed and then incubated for 30 minutes with the antibody. After this period, the cells were washed and analyzed by flow cytometry.

2.12 Lipid peroxidation. TBARS assay. Lipid peroxidation was measured using a thiobarbituric acid assay as described previously (16). A standard curve of 1,1,3,3 tetraethxoypropane was used to quantify the amount of malonaldehyde produced. Data are expressed in terms of nanomoles of TBARS normalized to the total protein content, measured in an aliquot of the cell extract.

2.13 Protein oxidation. Solutions of Bovine serum albumin (BSA) and Ribonuclease A (RNAse A), (0.5 mg/ml) in the phosphate buffer 10 mM were irradiated in the presence of the test compounds for various times in a quartz cuvette. At different times, an aliquot of the solution was taken and the degree of protein oxidation was monitored spectrophotometrically, as described previously (17) by derivatization with 2,4-dinitrophenylhydrazine (DNPH).

2.14 Statistical analysis. Unless otherwise indicated, the results are presented as mean ± S.E.M. The differences between the irradiated and non-irradiated sample were analysed using the two-sided Student's t test.

3 Results

3.1Photolysis and cellular phototoxicity.

Pitavastatin showed absorption maxima in the UVA range (320-400 nm) and underwent rapid photodegradation upon UVA irradiation in buffered aqueous solution, as previously reported (15). After irradiation, we were able to isolate by HPLC (Figure 2), and characterize two main photoproducts that were subjected to NMR analyses. The isolated compounds were pure, as was determined by analytical HPLC and NMR analysis. NMR spectra (Table 1), indicated structures consistent with tetracyclic compounds, namely 6-cyclopropyl-10-fluoro-7,8-dihydrobenzophenantridine (PP3) and (6-cyclopropyl-10-fluorobenzophenantridine (PP4) depicted in Figure 1, in strong agreement with our previous results (15).

Table 1. *Nuclear magnetic resonance data of photoproducts PP3 and PP4.*

	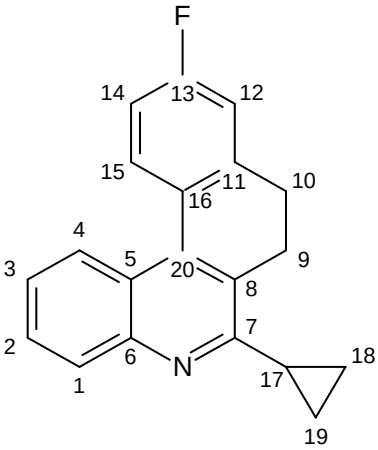 **PP3**		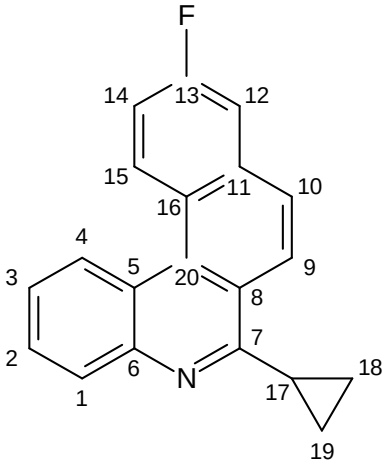 **PP4**	
	^{1}H (*J*)	^{13}C	^{1}H (*J*)	^{13}C
1	8.01 d (8.4)	128.36	8.11 d (1.2)	130.07
2	7.69 t (7.6)	130.23	7.75 m	129.59
3	7.53 t (7.6)	127.36	7.67 m	127.14
4	8.33 d (8.4)	126.49	8.91 d (8.4)	128.05
5	-	124.59	-	124.57
6	-	147.11	-	146.90
7	-	161.10	-	162.24
8	-	131.98	-	125.73
9	3.05 t (6.3)	25.44	8.62 (2.71)	125.00
10	2.89 d (6.3)	29.63	8.07 m	128.84
11	-	144.69	-	138.09
12	7.22 m	115.83	7.81 dd (9.4; 2.7)	113.14
13	-	163.17	-	162.24
14	7.14 m	114.11	7.57m	116.98
15	7.90 m	132.61	9.17 dd (9.4; 5.5)	132.50
16	-	129.30	-	127.14
17	2.40 m	15.59	2.89 tt (8.3; 5.0)	15.65
18	1.14 t (8.6)	9.03	1.31 m	9.19
19	1.19 t (7.7)	9.03	1.20 m	9.19
20	-	141.51	-	132.78

Chemical shift values are given in ppm, J expressed in Hz

The phototoxicity of PIT and its photoproducts PP3 and PP4 was evaluated in a cell line of immortalized human keratinocytes NCTC-2544 by use of an MTT assay

carried out 72 hours after irradiation. Figure 2 (panel A) shows the reduction in viability obtained in NCTC-2544 cells at different concentrations and different UVA doses. As can be observed, a concentration and UVA dose-dependent reduction in cell viability is induced by PIT. The calculated GI_{50} are shown in Table 2. In the same experimental conditions, but in the absence of irradiation, PIT did not show any decrease of viability.

Table 2. *GI_{50} of PIT, PP3 and PP4 after 72 h from the irradiation of NCTC-2544*

	GI_{50}[a](μM)		
UVA dose (J cm^{-2})	**PIT**	**PP3**	**PP4**
1.25	>100	24.7	21.7
2.5	>100	16.4	11.1
3.75	78.1	8.2	2.8
7.5	8.7	n.d	n.d

[a] *Drug concentration, expressed in μM, which reduces the cell proliferation by 50%*

In the same model, the photoproducts PP3 and PP4 were tested. The two photoproducts did not affect cell viability without irradiation but on the contrary, after irradiation, a reduction in cell viability can be observed for both compounds in comparison to the parent one, as showed in Figure 3 (panels B and C). In particular, a remarkable decrease in cell viability was observed with the fully aromatic PP4 in comparison to the dihydro derivative PP3. Altogether, these data suggest that the phototoxicity of PIT could be mediated by the formation of these photoproducts.

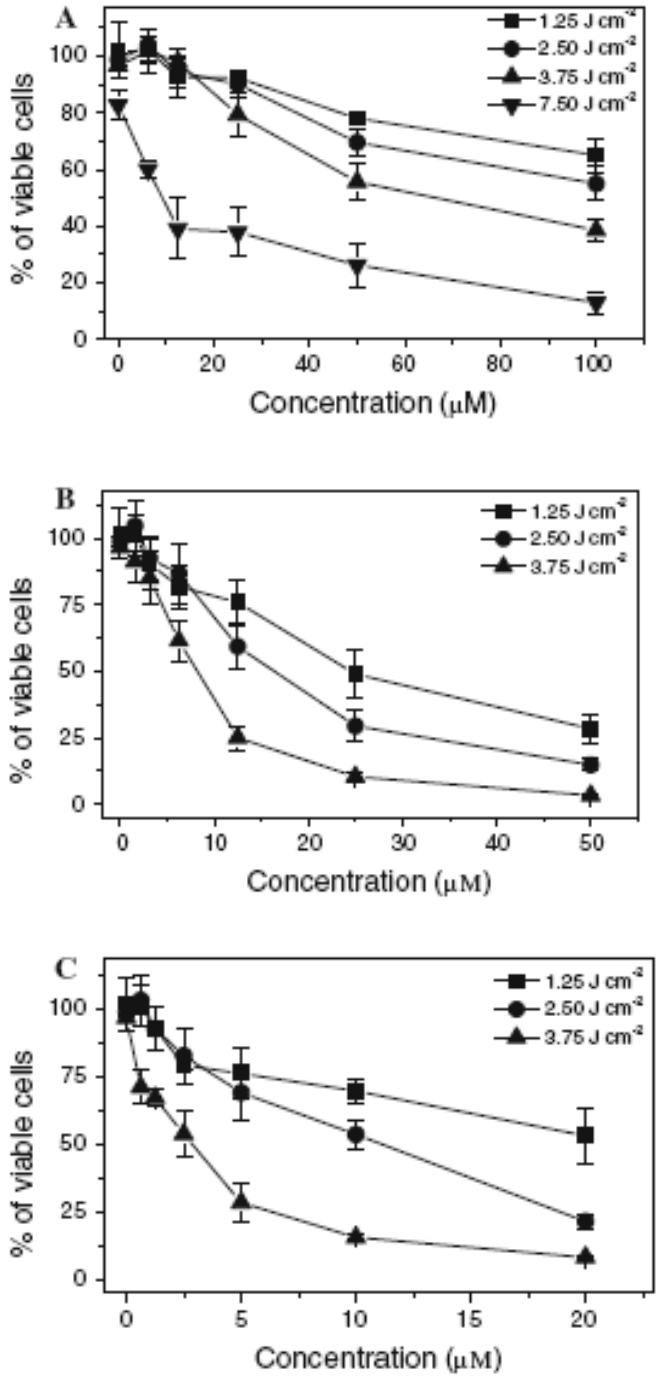

Figure 2. *Percentage of viability of human keratinocytes NCTC-2544 after UVA irradiation in the presence of PIT (panel A), photoproduct PP3 (panel B) and photoproduct PP4. Cells were irradiated at the different UVA doses indicated and at different concentrations of compounds. Cell viability was measured by MTT test after 72 h after irradiation. Data represent mean ± S.E.M for at least four independent experiments.*

3.2 UVA radiation induced photoproducts formation in NCTC-2544 keratinocytes

To evaluate whether PIT is converted to PP3 and/or PP4 in the cellular system, NCTC-2544 cells were irradiated in the presence of 100 lM PIT with the same UVA doses that induce cell killing and the cellular extracts were analyzed by LC–MS. As shown in Fig. 3 (panel a), after 2.5 J cm-2, we were able to observe the appearance of two peaks corresponding to PP3 and PP4 indicating that the build up of the two photoproduct is effective also in a cellular system. Moreover, we analyzed the uptake of PIT and its photoproducts in NCTC-2544 cells utilizing their intrinsic fluorescence. As shown in Fig. 3 Panel b, we can observe an efficient incorporation of the drugs inside the cells after 2 h of incubation without a particular disposition suggesting that both PIT and its photoproducts are able to bind and to penetrate inside the cells.

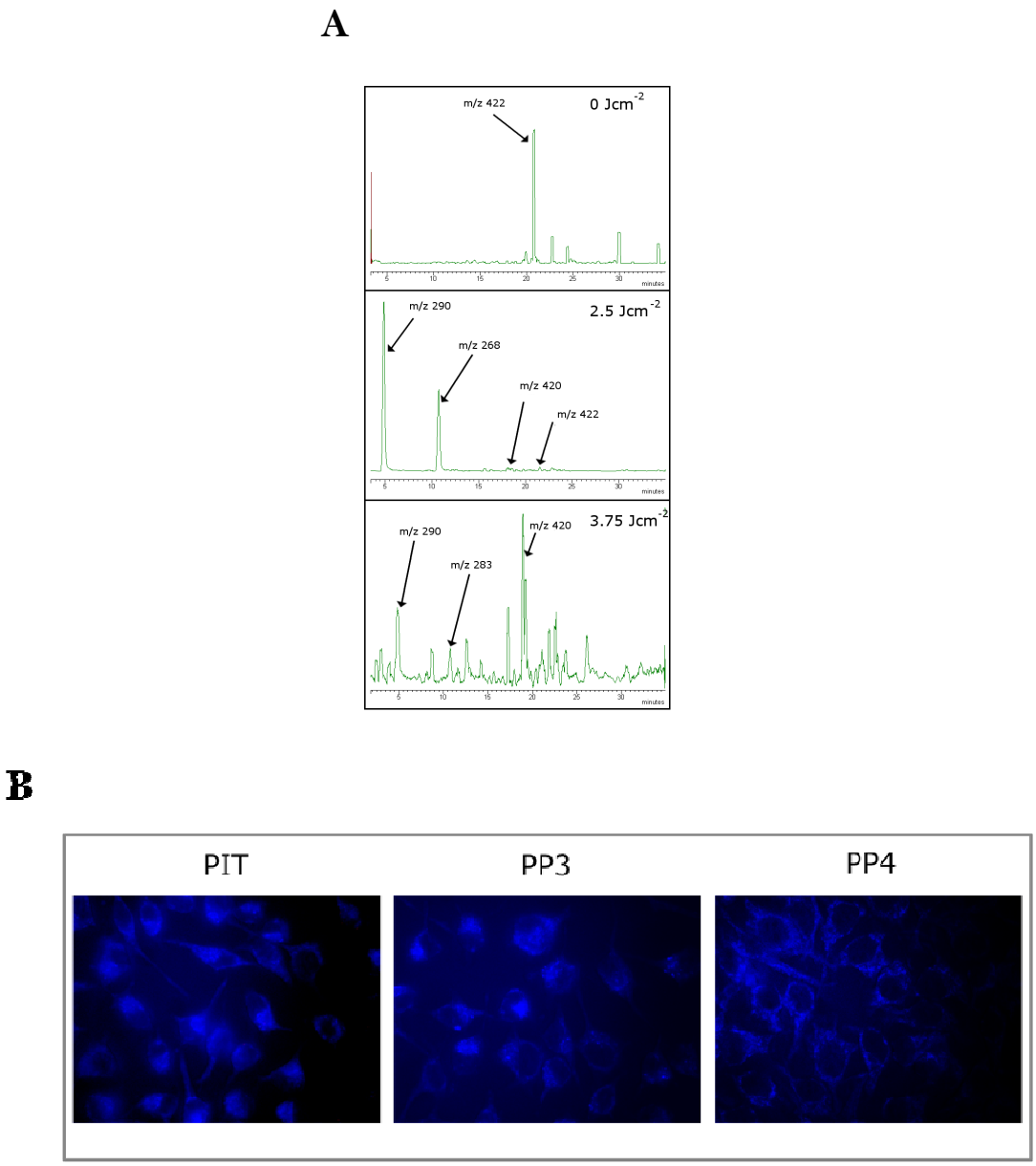

Figure. 3. *Panel a LC–MS profile of NCTC cells after irradiation with PIT (100 lM) with the indicated UVA doses. Panel b Fluorescence microphotographs showing the intracellular localization of PIT, PP3, and PP4 in NCTC-2544 cells after 24 h of incubation at the concentration of 100 lM and 20 (PP3 and PP4), respectively.*

3.3 Assessment of the mode of cell death

To characterize the mode of cell death (necrosis or apoptosis) photoinduced by PIT and its photoproduct PP4, a biparametric cytofluorimetric analysis was performed in order to quantify the precise extent of apoptosis versus necrosis using propidium iodide, which stains DNA and is permeable only to dead cells, and the protein Annexin-V, conjugated with Fluorescein isothiocyanate (FITC), which binds to phosphatidylserine in a highly selective manner (18). This phospholipid flips from the

inner to the outer leaflet of the plasma membrane during apoptosis. Positive staining with Annexin-V correlates with the loss of plasma membrane polarity but precedes the complete loss of membrane integrity that accompanies the later stages of cell death resulting from either apoptosis or necrosis. In contrast, PI can only enter cells after the loss of their membrane integrity. Thus dual staining with Annexin-V and PI allows clearly to discriminate between unaffected cells (Annexin-V^-/PI^-), early apoptotic cells (Annexin-V^+/PI^-), late apoptotic cells (Annexin-V^+/PI^+) and necrotic cells (Annexin-V^-/PI^+) (19).

Figure 4 shows six biparametric histograms as representative, in which the effect of PIT and PP4 at 24 and 48 h from the irradiation is depicted. It is quite evident that PIT and PP4 early induced an accumulation of PI positive cells in comparison to the irradiated control.

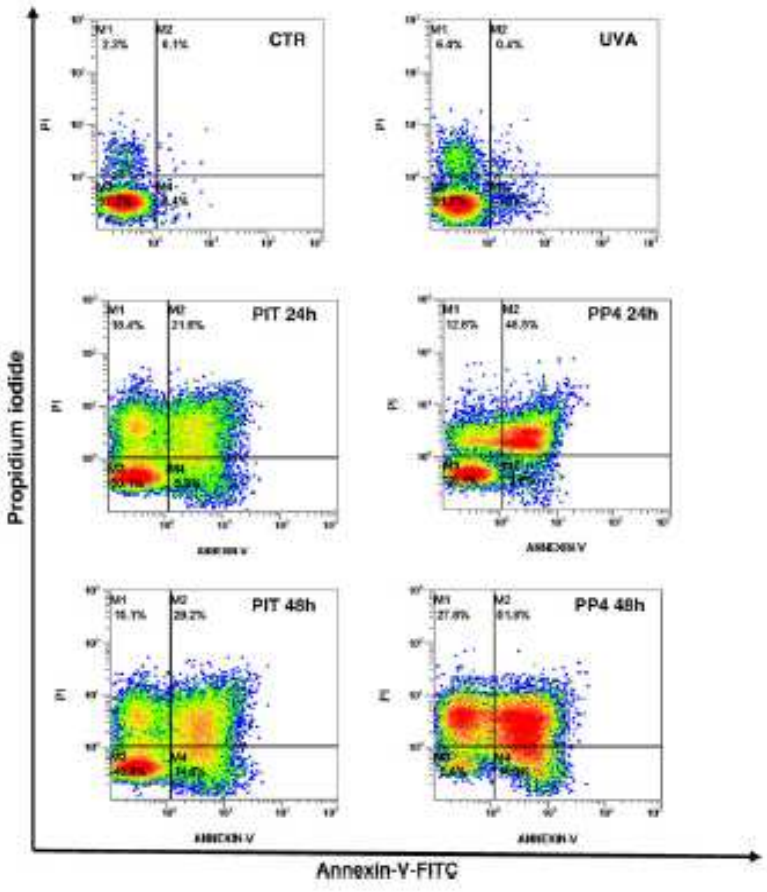

Figure 4. *Determination of the mode of cell death using Annexin-V and PI staining and flow cytometric analysis.Representative biparametric histograms obtained after 24 and 48 h after the irradiation (3.75 J cm-2) of human keratinocytes NCTC-2544 in the presence of PIT 100 and PP4 20 μM*

A complete picture of the results is presented in Figure 5 for PIT at the concentration of 100 and 50 μM and in Figure 6 for PP4 at the concentration of 20 and 10 μM. We did not observe a significant amount of A^+/PI^- cells at any time point investigated but, on the contrary, a large percentage of PI positive cells was found, suggesting a rapid permeabilization of the cell plasma membrane that leads to necrotic cell death.

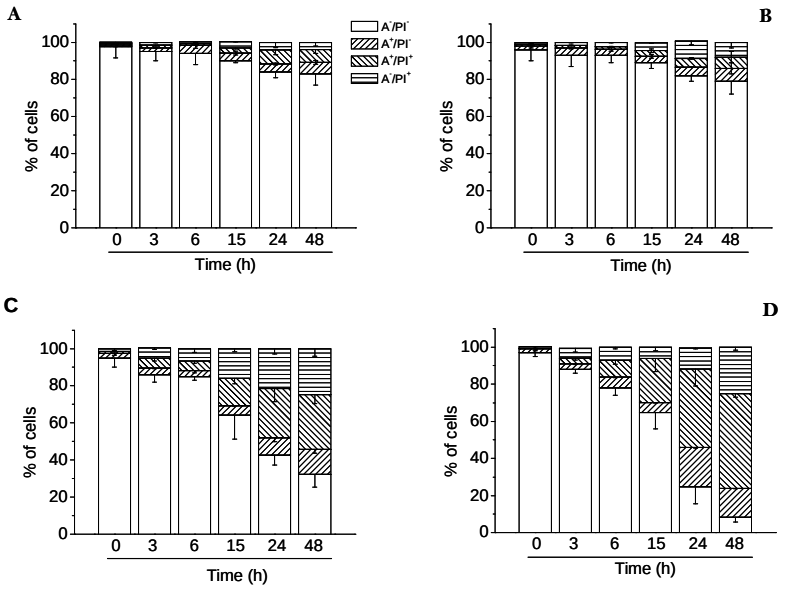

Figure 5. *Keratinocytes NCTC-2544 were irradiated in the presence of PIT at the concentration indicated, and after different times, the cells were collected, stained with Annexin-V-FITC and Propidium iodide (PI), and analyzed by flow cytometry. The results are expressed as a percentage of cells found in the different regions of the biparametric histograms showed in Fig. 4. Panel a Non-irradiated cells; Panel b UVA alone; Panel c: PIT 100 μM; Panel d 20 μM. Data represent the mean ± S.E.M of three independent experiments*

The mode of cell death was also followed by two most common endpoint analyses, such as morphological changes and analysis of DNA fragmentation (20). As shown in Figure 6 (panel A), visual inspection by contrast phase microscopy of the morphology of NCTC-2544 cells irradiated in the presence of PIT (100 μM) or PP4 (20 μM) revealed the presence of cellular swelling and rupture of the plasma membrane which are typical signs of necrotic type of cell death. Furthermore, agarose gel electrophoresis of DNA extracted after 24 and 48 h from keratinocytes irradiated in the presence of PIT and PP4 (Figure 6, panel B) showed a non-specific degradation resulting in a "smear" of randomly degraded DNA in the samples treated, which is indicative of necrotic cell death. In addition, we evaluated the activity of caspase-3, since this enzyme is essential to the propagation of the apoptotic signal after exposure

to many DNA-damaging agents and anti cancer drugs, and it is activated in most cases of photodynamic therapy with a number of different photosensitizers (21-23). As depicted in figure 6 (panel C), flow cytometric analysis of NCTC-2544 irradiated in the presence of PIT and PP4 did not show any activation of caspase-3.

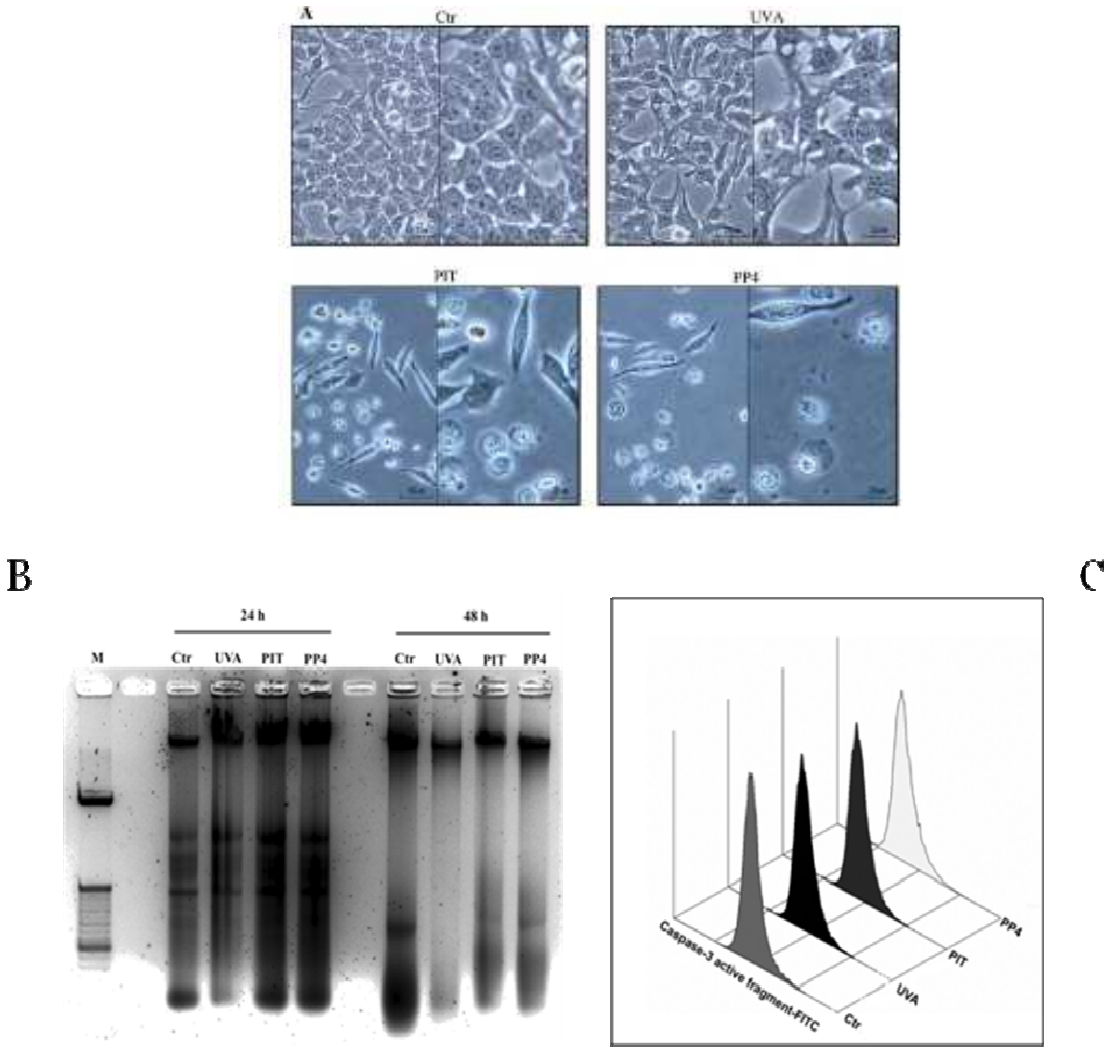

Figure 6. *Panel A. Cell micrographs taken after 24 h from the irradiation (3.75 J cm^{-2}) in the presence of PIT and PP4 at the concentrations of 100 μM and 20 μM, respectively. Magnifications 20x and 40x*
Panel B. Agarose gel electrophoresis of chromosomal DNA extracted from NCTC-2544 cells 24 h and 48 h after the irradiation (3.75 J cm^{-2}) in the presence of PIT (100 μM) and PP4 (20 μM). Lane M indicated size marker DNAs; Panel C. Flow cytometric analysis of Caspase-3 activity after irradiation in the presence of PIT (100 μM) and PP4 (20 μM). After 24 h of treatment, cells were harvested, and stained with an anti-human active Caspase-3 fragment monoclonal antibody conjugated with FITC. Representative histograms of three different experiments are shown.

3.4 Effect of antioxidant compounds

With the purpose of evaluating which reactive species are involved in the mechanism(s) of photoinduced cell toxicity, experiments were performed, which involved irradiating NCTC-2544 cells with PIT and PP4 in the presence of different scavengers as previously reported (24,16). The cell death was evaluated by flow cytometric analysis, by double staining of the cells with Annexin-V and PI. The additives used were NaN_3 (a singlet oxygen scavenger), superoxide dismutase (SOD, scavenger of $O^{\bullet-}$), DMTU (scavenger of $^{\bullet}OH$) and 2,6-di-tert-butylhydroxyanisole (BHA), tocopherol acetate and GSH, (free radical scavengers). It can be observed from Figure 7 that the photoinduced cell death by PIT and PP4 is efficiently counteracted by GSH, BHA and DMTU, which indicates that free and hydroxyl radicals may be involved in the mechanism of action.

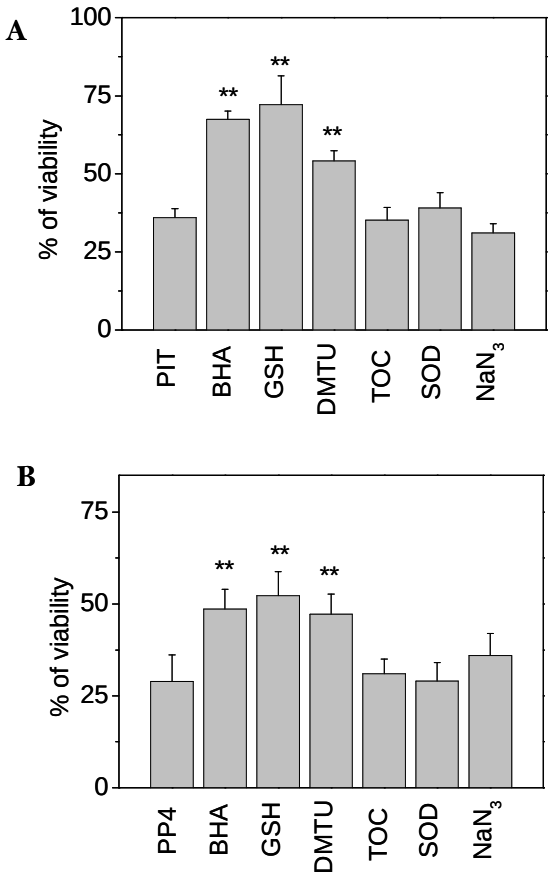

Figure 7.: *Cell viability measured by flow cytometry by double staining of the cells with Annexin-V and PI, 24 h after irradiation in the presence of PIT 100μM (panel A) and PP4 20 μM (panel B) in the presence of BHA 10μM, GSH 1mM, DMTU 1mM, SOD 2000 U.I., Tocopherol acetate 200 μM and NaN_3 10 mM. Data represent the mean ± S.E.M of three independent experiments. **p<0.01 vs PIT or PP4 irradiated cells.*

3.5 ATP assay.

Apoptosis is an energy-dependent process in which the decrease of ATP below critical levels may impede the execution of apoptosis and promote necrosis (25,26). In fact, necrosis is characterized by a rapid drop in ATP and given the potentially pivotal role attributed to ATP in the necrosis, we measured cellular ATP levels following irradiation with PIT and PP4. Using a luciferase-based assay for cellular ATP content, a dramatic depletion of ATP levels was detected in keratinocyte-irradiated cells in the presence of 100 μM PIT (Figure 8). Similarly, the irradiation with 20 μM PP4 dramatically decreases ATP levels in comparison to non-irradiated cells: this was already seen after 6 h from irradiation and a further reduction was detected at 24 h, reaching levels of around 10%. Taken together, these data suggested that the rapid and pronounced ATP depletion was a concurrent event that accompanied the loss of cell viability.

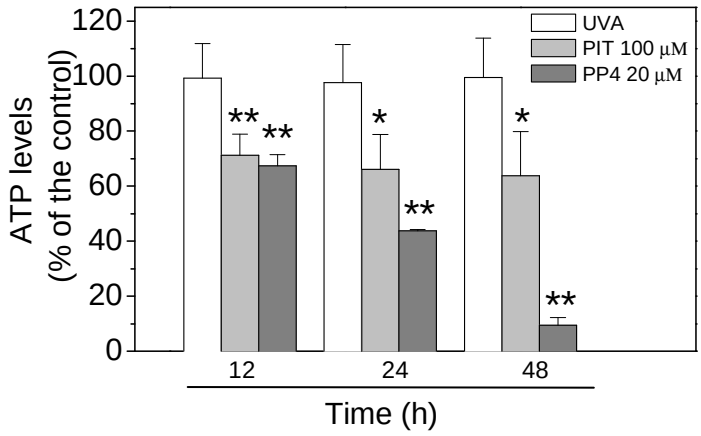

Figure 8. *ATP content was measured in NCTC-2544 cells after different times from the irradiation (3.75 J cm^{-2}) in the presence of PIT (100 μM) and PP4 (20 μM). Cells were collected and then counted, after which the ATP content per 100000 cells was determined using the CellTiter-Glo luminescent assay (Promega, Milano, Italy) according to the manufacturer's instructions, using a Victor^{3TM} luminometer (Perkin Elmer). Data are normalized to ATP content in non-irradiated cells. Data represent the mean ± S.E.M of three independent experiments. **p<0.01 vs UVA irradiated cells*

3.6 Analysis of Cell cycle.

To investigate the effects of PIT and PP4 upon UVA irradiation on the cell cycle, NCTC-2544 cells were treated with the test compounds at different concentrations and at the light dose of 3.75 J cm^{-2}. After 12, 24 and 48 h from the irradiation, the cells

were fixed and labelled with propidium iodide. The different phases of the cell cycle were analysed by flow cytometry.

Irradiation of keratinocytes with PIT induced an increase of the G2/M and S phase along with a reduction of the G1 phase (Table 3), in particular at 12 and 24 hours after the treatment. On the contrary, at 24 h PP4 induced an arrest of the cycle in the S phase. These data suggest that in response to phototoxic stress induced by the drugs, the progress of the cell cycle can be arrested at certain checkpoints that serve to maintain genomic integrity.

More importantly, it is interesting to note that the percentage of the cell population with a hypodiploid DNA content peak (subG1), representing those cells with a DNA content less than G1, which are usually considered as apoptotic cells, amounts to 10-20% at 24 h after treatment with PP4. Although statistically significant in respect to both control and UVA-treated cells, this represents a low amount in comparison to the large percentage of dead cells (70%) as depicted in Figure 6 and measured at the same time point.

Table 3. Effect of PIT and PP4 on the cell cycle of NCTC-2544 after UVA irradiation (3.75 J cm-2)

	% G1[a]	G2/M	S	Apoptotic Cells[b] (Sub-G1)
Ctr 12 h	65.1±2.0	11.0 ±1.9	25.6±1.7	1.8 ±0.1
UVA alone 12 h	64.6 ±3.0	10.0±1.7	25.4±3.5	1.3 ±0.2
PIT 12 h **100 μM** **50 μM**	37.3 ±3.1* 41.5±6.0*	25.6 ±3.5* 25.4±1.0*	37.1 ±2.5 33.0±7.1	3.4 ±1.5 2.2±0.9
PP4 12 h **20 μM** **10 μM**	44.6±2.8* 33.7±4.6*	18.5±1.5* 29.1±3.4*	36.7 ±4.1 37.2±4.8	4.2±1.2 0.7±0.1
Ctr 24 h	63.2±3.4	11.6±1.2	25.2±2.8	1.0 ±0.3
UVA alone 24 h	66.9±3.5	14.1 ±3.1	19.0 ±1.5	5.4 ±1.9
PIT 24 h **100 μM** **50 μM**	39.5 ±5.1* 45.5±5.6*	25.9±3.1* 21.9±1.7*	34.5±8.1 32.6±5.8	2.2±0.5 7.1±2.2
PP4 24 h **20 μM** **10 μM**	43.5±6.0 40.2±5.5	18.7±1.9 19.3±2.0	43.6±1.9* 40.5±7.5*	24.8±4.5* 13.8±1.4*
Ctr 48 h	62.8 ±1.2	10.4 ±2.9	26.8 ±1.6	5.0±1.5
UVA alone 48 h	63.4 ±2.7	9.8 ± 0.5	26.6 ±2.3	5.2±1.0
PIT 48 h **100 μM** **50 μM**	58.2±3.9 66.7±3.2	14.6 ±2.0 17.6±6.8	27.3±2.3 15.6±3.5	7.7±1.4 9.5±0.9

aThe percentage of each phase on the cell cycle was calculate on living cell
b Percentage of the cell population with hypodiploid DNA content peak (apoptotic cells).
Data expressed as the mean ± SEM of three experiments *$p<0.05$

3.7 Mitochondrial and lysosomal integrity assessment.

To investigate which cellular sites are involved in the phototoxicity induced by PIT and its photoproduct PP4, we focused our attention on mitochondria and lysosomes. It has been shown previously that mitochondrial and/or lysosomial alterations are involved in cell death caused by many photosensitisers including fluoroquinolones, phenothiazines, antimalarial drugs and porphyrins (16,27-29).

Further experiments to assess changes in mitochondrial functions after irradiation in the presence of PIT and PP4 were performed measuring the mitochondrial potential ($\Delta\Psi_{mt}$) by flow cytometry and using the JC-1 dye, which is considered a reliable probe to assess such events (30). Flow cytometric analysis of NCTC-2544 cells after 12, 24 or 48 h from the irradiation in the presence of the compounds showed no significant variations (Figure S1, Supporting information) of $\Delta\Psi_{mt}$ in comparison to the irradiated control, indicating the non-involvement of this organelle in photoinduced cell death. To confirm that mitochondria were not involved in the photokilling mechanism, we also evaluated the mitochondrial production of ROS by two fluorescent probes, hydroethidine (HE) and 2',7'-dichlorodihydrofluorescein diacetate (H_2DCFDA) by flow cytometry (31,32). In agreement, only a slight increase of ROS production was observed for cells irradiated with PIT and PP4 (Figure S1, Supporting information).

In order to investigate the integrity of lysosomes after irradiation with the test compounds, flow cytometric analysis was performed using the fluorescent acidotropic dye LysoTracker Red. The results (Figure S2, Supporting information) indicate only a slight reduction in fluorescence intensity, suggesting that lysosomes also do not represent a major target of the phototoxic action of the drugs.

3.8 Intracellular Ca^{2+} Measurement.

It has been demonstrated that the overload of intracellular Ca^{2+} is associated with the necrotic cell pathway (33). To verify whether a calcium signal is involved in the photoinduced cell death mechanism activated by PIT and PP4, we used the Ca^{2+}-sensitive dye Fluo-4/AM. The cells displayed an increase in Fluo-4/AM fluorescence intensity after just one hour from irradiation and the intensity was two-three times greater than the irradiated controls for both PIT and its photoproduct PP4 (Figure 9, panels A and B).

To verify the source of calcium, we performed a similar experiments using a calcium-free medium containing 1 mM EGTA. The results showed (Figure 9 panel C) that in these experimental conditions, a significant decrease of fluorescence occurred,

indicating that the increased intracellular calcium is due to a calcium influx from the extracellular sites without calcium release from internal stores.

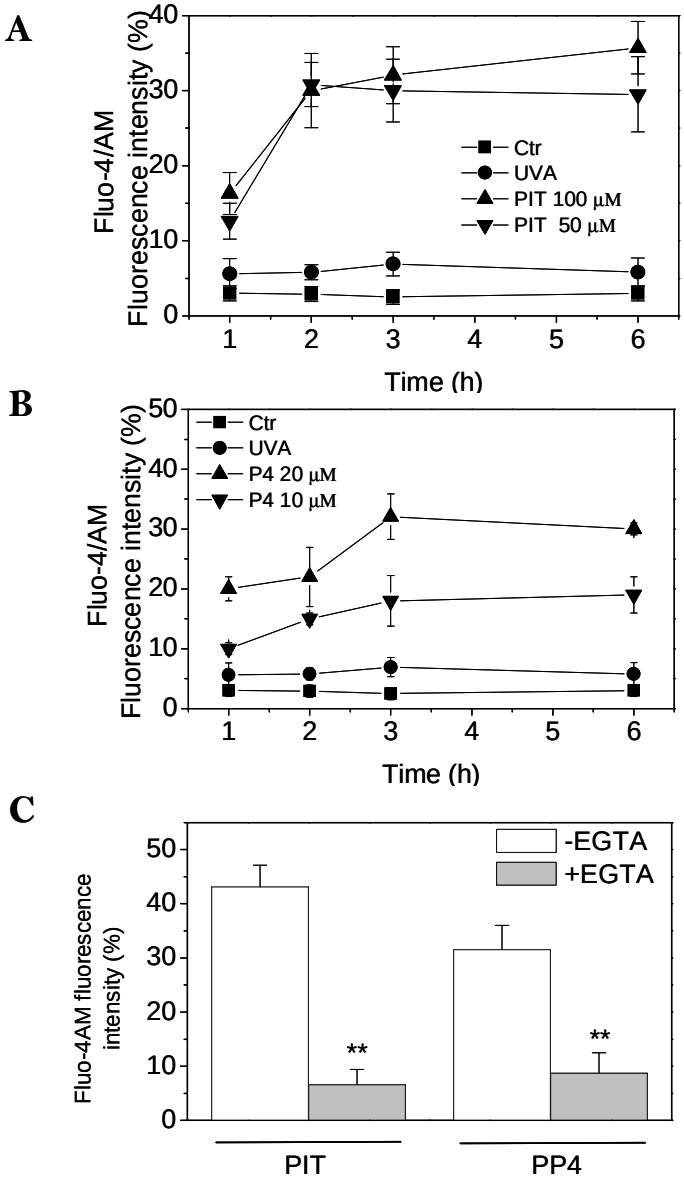

Figure 9. *Intracellular calcium measurement in NCTC-2544 cells after different times from the irradiation (3.75 J cm^{-2}) in the presence of PIT 100 and 50 µM (Panel A) and PP4 20 and 10 µM (Panel B). Ca^{2+} was measured by labeling the cells with 2.5 µM of Fluo-4/AM and examining the fluorescence by flow cytometry. Analogous experiments were performed in a calcium-free medium containing 1 mM EGTA (Panel C) and analyzed after 3h from irradiation. Data represent the mean of fluorescence intensity.□ S.E.M of four independent experiments. **p<0.01 vs UVA irradiated cells.*

3.9 Lipid peroxidation.

To gain insight into the photoinduced cell death mechanism activated by PIT and PP4, we investigated whether these compounds cause lipid peroxidation by measuring the level of malonyldialdeide (MDA) bound to thiobarbituric acid (TBA) in treated and untreated NCTC-2544 cells. This assay is a measure of membrane injury as the cellular level of MDA correlates with lipid peroxidation (34). The results showed (Figure 10), that in untreated cells or in UVA-irradiated cells the levels of TBARS were relatively low. In contrast, the levels of TBARS increased significantly after 12 h after irradiation in the presence of PIT and PP4 and then they further augmented at later times. Therefore, lipid peroxidation initiated by photoactivated PIT is well correlated with the increase of cell permeability measured with propidium iodide.

Thus the induced oxidative damage to membrane lipids is well correlated with the extent of cell death suggesting that an extensive lipid peroxidation could play a major role in the photokilling mechanism.

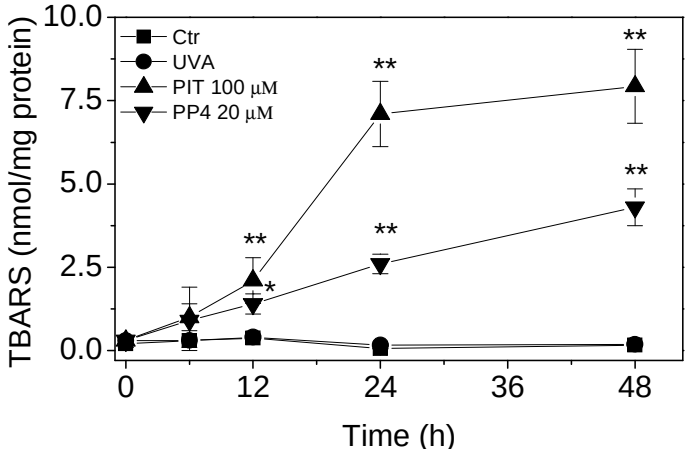

Figure 11. *TBARS assay in NCTC-2544 cells after different times from the irradiation (3.75 J cm^{-2}) with PIT and PP4 at the indicated concentrations. Data are expressed as the mean ± S.E.M. of three independent experiments. p*<0.05 **p<0.01 vs UVA irradiated cells.*

3.10 Protein photodamage.

To investigate more deeply the phosensitizing properties of PIT and PP4 toward other components of cellular membranes, such as proteins, aqueous buffered solutions of PIT and PP4 containing Bovine serum albumin (BSA) or Ribonuclease A (RNAse

A) as models (35) were irradiated for various times. The degree of oxidative modifications was measured by monitoring the carbonyl content, an index of oxidative damage of the proteins (17). RNAse A was selected as a protein model because of the lack of Trp residues, together with the presence of Tyr and Phe residues in its sequence. The results, reported in Figure 12, demonstrated that PIT significantly increased the carbonyl content of BSA and RNAse A after irradiation and this effect is both concentration- and UVA-dose dependent. On the contrary, PP4 only induced a slight increase in the carbonyl content for both BSA and RNAse A. This could be due to a lower binding of PP4 to the protein.

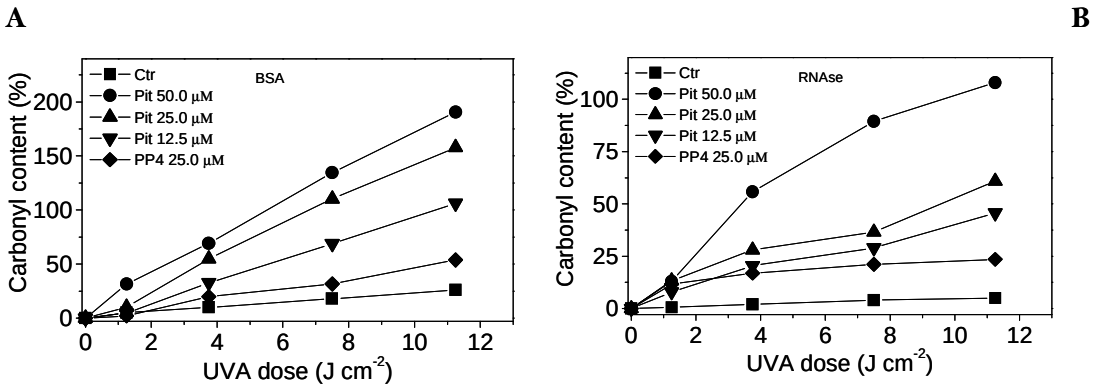

Figure 12. *Photosensitized protein oxidation by PIT and PP4. BSA (panel A), and RNAse A (panel B), dissolved in phosphate buffer 10 mM, pH=7.2, were irradiated at different UVA doses in the presence of PIT and PP4 at the indicated concentrations. Protein oxidation was evaluated spectrophometrically by monitoring the carbonyl content after derivatization with 2,4-dinitrophenylhydrazine (DNPH).*

4 Discussion

As a continuation of our research into molecular mechanisms of the light-induced reactivity of drugs, we have examined the phototoxic effect of pitavastatin, a highly specific inhibitor of HMG-CoA reductase inhibitor. PIT fulfill the criteria for photosafety testing, including (1) high systemic bioavailability and long half-time; (2) administration over a long period of time; (3) degradation in solution during photoirradiation; (4) presence of essential chemical functionalities (aromatic moiety, double bond, luorine atom); and (5) significant absorbance above 290 nm. Pitavastatin, in combination with UVA light, induced a reduction in the cell viability, but more importantly, its photoproducts PP3 and PP4 showed a remarkable increase in the

phototoxicity at a concentration ten times lower than the parent compound. It is interesting to note that the UVA doses used for the evaluation of phototoxicity are within the range of UVA doses sufficient to induce the photocyclization reaction resulting in efficient formation of photoproducts in vitro as demonstrated by LC–MS. Therefore, these results strongly suggest that the phototoxicity of PIT could be mediated by the formation of benzophenanthridine-like structures (PP3 and PP4) that act as strong photosensitizers Soon after irradiation with PIT, cells initiated a series of remarkable morphological alterations that affect the integrity of the plasma membrane. In contrast, the nuclear structure is preserved and no DNA degradation is detected as also demonstrated by the analysis of DNA extracted from irradiated cells. These features are typical for necrotic cell death. Necrosis is associated with cell swelling, membrane rupture, and the release of cytosolic content to the external environment, whereby the loss ofmembrane integrity is considered an early event in this process. In order to monitor the membrane integrity after irradiation with PIT, we used flow cytometry and double staining with Annexin-V and PI. Annexin-V staining precedes the loss of membrane integrity, which accompaniesthe latest stages of cell death resulting from either apoptotic or necrotic processes. It should be noted that if the plasma membrane is permeabilized, Annexin-V can bind to intracellular phosphatidylserine as well (Galluzzi et al.2009). Our results showed a rapid increase in the PI-positive cells, whereas Annexin-V-positive cells did not increase significantly at any time investigated, suggesting that necrosis and not apoptosis is the major pathway of cell death. In excellent agreement with the MTT test, the photoproduct PP4 induced a high amount of PI-positive cells but at lower concentrations with respect to the parent compound indicating its involvement in the photoinduced cell death. In this context, we observed a significant increase in intracellular Ca^{2+}concentration soon after the irradiation. Moreover, by depleting extracellular calcium with EGTA, we did not observe an increase in intracellular calcium after irradiation with PIT and PP4, which suggests that the increased intracellular $Ca^{2+}$was from extracellular sites and probably due to a rapid loss of membrane integrity resulting from lipid peroxidation as demonstrated byTBARS formation and protein oxidation.The cell death induced by PIT and PP4 is accompanied by a reduction in the ATP content but not by the loss of mitochondrial membrane potential. Although the disruption of mitochondrial membrane potential plays an important role in necrotic and apoptotic processes, a lack of loss of mitochondrial membrane potential has been reported in non-apoptotic cell death (Kim et al. 2005). Given the rapid increase in cell membrane permeability after PIT or PP4 irradiation, as evidenced by intracellular Ca^{2+}increase and PI permeability,

it is more plausible that these compounds cause considerable damage to the cell membrane structure, thereby promoting substantial ATP leakage into the extracellular spaces. As ATP depletion is considered to be the major cause of necrotic cell death, such a loss of the ATP pool may lead to necrosis. However, we cannot exclude the possibility that the drug may inhibit oxidative phosphorylation without any changes in mitochondrial membrane potential or that the reduction in ATP concentration could be due to an increase in ATP consumption. Preliminary experiments devoted to evaluate which reactive species could be involved in the photoinduced cell death showed that the irradiation of keratinocytes in the presence of BHA, DMTU, and GSH significantly protects against cell death, indicating the involvement of free and/or hydroxyl radicals in the mechanism of action of both PIT and its photoproducts. Certainly, a detailed photophysical determination of the excited states generated after UVA absorption as well as reactive oxygen species is required for a better understanding of the mechanism of action.

In summary, we have established for the first time that PIT is endowed with a clear phototoxic potential in vitro in a human keratinocyte cell line. Its phototoxicity could be mediated by the formation of photoproducts endowed with high photosensitizing properties. Moreover, we identified plasma membrane as one of the major targets of the PIT action, which ultimately leads to necrosis as the principal mode of cell death. The photoproduct formation and the possible onsequences on the biological effects of the photosensitization of cutaneous cells in patients treated with PIT deserve further studies.

5 Supplementary

5.1 Methods:

Photodegradation spectra. Light absorption spectra were recorded with a Perkin-Elmer Lambda 15 spectrophotometer after irradiation with increasing doses of UVA light. The measurements were carried out with a quartz cuvette containing a solution of pitavastatin in phosphate **b**uffer 10 mM, pH = 7.0.

HPLC analysis. Analytical HPLC was carried out on an Agilent 1200 instrument equipped with a UV-DAD detector. The chromatographic separation was achieved on an octadecylsilane-coated column, 150 mm × 4.6 mm, 5 μm (Gemini, Phenomenex), using ternary gradient elution conditions at a flow rate of 1.0 mL/min as follows: water, solvent A; acetonitrile, solvent B; methanol, solvent C. The gradient conditions

were: (a) 75% of A and 25% of B for 0-6 min, (b) linear gradient from 75 to 40% of A, 25% to 40% of B and 0% to 20% of C for 6-7 min and continued till 25 min. Fractions corresponding to PP3 and PP4 respectively, were collected and the solvent evaporated at room temperature using a rotary evaporator.

NMR analysis. The NMR spectra were recorded on a Bruker Avance II (400 MHz) NMR spectrometer, using MeOD as solvent and tetramethylsilane (TMS) as the internal standard.

Assessment of mitochondrial changes and production of reactive oxygen species. The mitochondrial membrane potential was measured with the lipophilic cation 5,5',6,6' tetrachlo-1,1',3,3'-tetraethylbenzimidazol-carbocyanine (JC-1, Molecular Probes Eugene, OR, USA). Briefly, after different times from the irradiation, the cells were collected by centrifugation and resuspended in HBSS containing the JC-1 at a concentration of 2.5 μM. The cells were then incubated for 10 min at 37 °C, centrifuged and resuspended again in HBSS. The fluorescence was directly recorded with the flow cytometer (Coulter Cytomics FC500).

The production of Reactive oxygen species (ROS) by flow cytometry using Hydrohethidine (HE) and 2',7'-dichlorodihydrofluorescein diacetate (H_2DCFDA). All of these fluorescent probes were purchased from Molecular Probes (Eugene, OR, USA). After 24 and 48 h from the irradiation, the cells were trypsinized and collected by centrifugation and resuspended in HBSS containing the fluorescence probes HE, or H_2DCFDA at the concentration of 2.5 μM, and 100nM respectively. As above, the cells were then incubated for 30 min at 37 °C, centrifuged and resuspended again in HBSS. The fluorescence was directly recorded with the flow cytometer using as excitation wavelength 488 nm and emission at 585 nm for HE and at 525 nm for H_2DCFDA.

Lysosomal integrity assay. Cells were irradiated in the presence of pitavastatin or the photoproduct and after different times the cells were collected by centrifugation and resuspended in DMEM containing the fluorescent probe LysoTracker RED DND-99 (Molecular Probes) at the concentration of 50 nM and incubated for 30 min at 37 °C. After this period the cells were washed and analyzed by flow cytometry.

5.2 Results

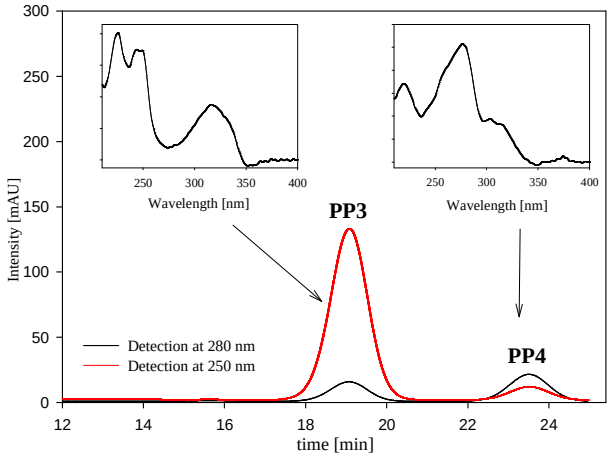

Figure S1. *HPLC analysis of the crude mixture after the photodegradation of pitavastatin in aqueous solution showing the separation of investigated photoproducts. The elution profile was monitored at 250 (red line) and 280 nm (black line). The inset in the chromatogram represents absorption spectra.*

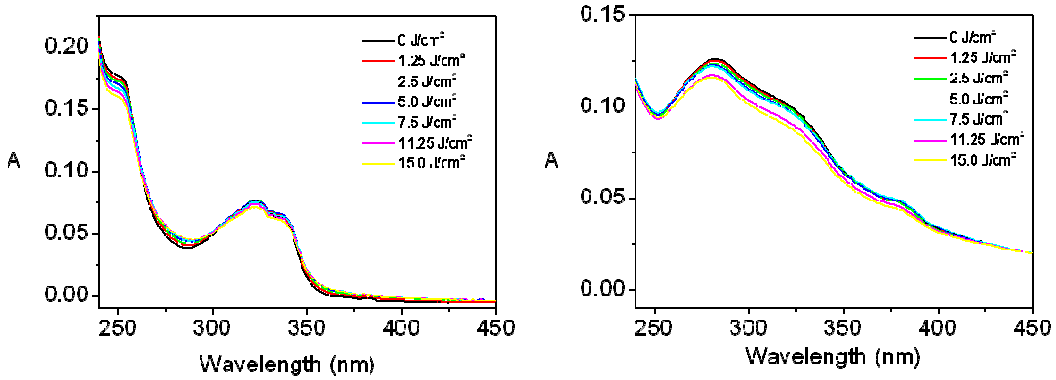

Figure S2 Photodegradation spectra of PP3 and PP4

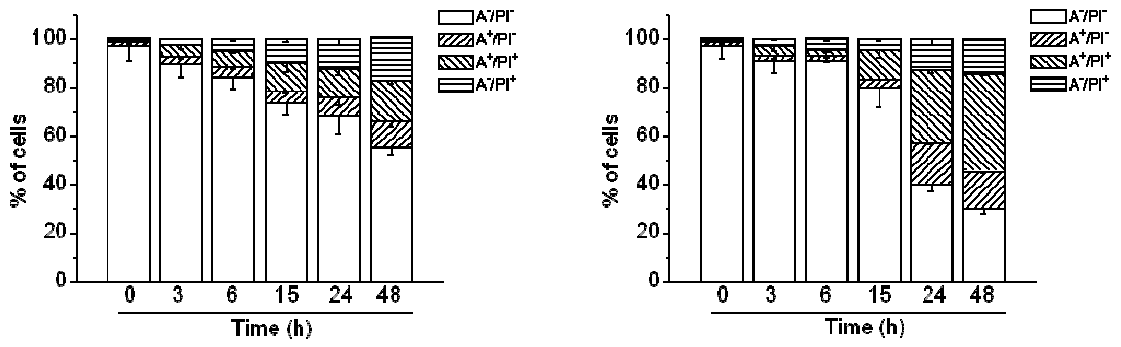

Figure S3. *Determination of the mode of cell death using Annexin-V and PI staining and flow cytometric analysis. Representative biparametric histograms obtained after 24 and 48 h after the irradiation (3.75 J cm⁻²) of human keratinocytes NCTC-2544 in the presence of PIT 50 and PP4 10 μM.*

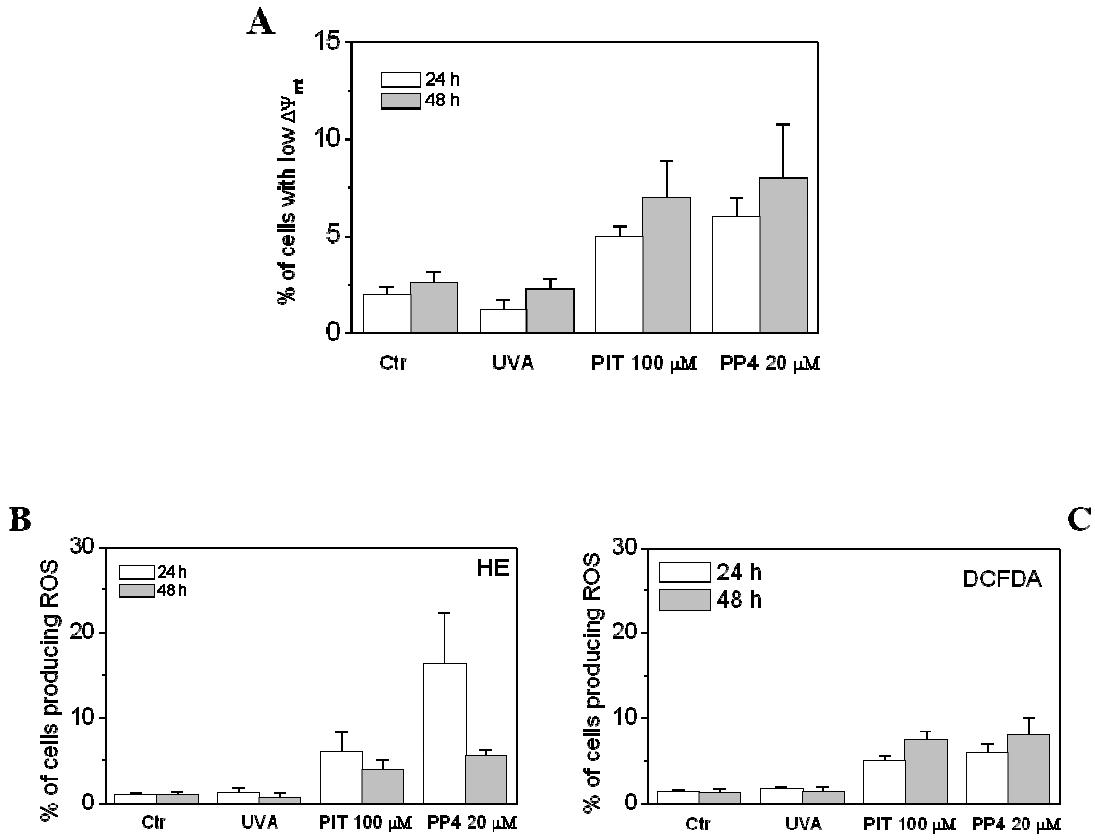

Figure S4. *Panel A shows the percentage of cell with low mitochondrial potential after 24 and 48 h from the irradiation (3.75 J cm⁻²) in the presence of PIT and PP4. Panels B and C show the mitochondrial production of ROS evaluated by flow cytometry using the fluorescent probe HE (panel B) and H₂DCFDA (Panel C). Data are expressed as mean ± S.E.M. of three independent experiments.*

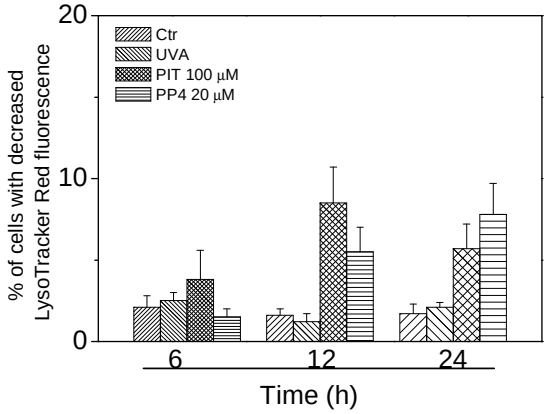

Figure S5. *Percentage of cells with reduced Lysotracker fluorescence. NCTC-2544 cells were irradiated in the presence of PIT or PP4 and after the indicated times stained with LysoTracker RED and analyzed by flow cytometry, Data are expressed as mean ± S.E.M. of three independent experiments*

Acknowledgments This work was supported by University of Padova and partially supported by Polish State Committee on Science (KBN, project No. NN405 3478 33).

5 References

1. Kajinami, K., Mabuchi, H., and Saito, Y. (2000) NK-104: a novel synthetic HMG-CoA reductase inhibitor. *Expert Opin. Investig. Drugs* **9**, 2653-2661.

2. Kajinami, K., Takekoshi, N., and Saito, Y. (2003) Pitavastatin: efficacy and safety profiles of a novel synthetic HMG-CoA reductase inhibitor. *Cardiovasc. Drug Rev.* **21**, 199-215.

3. Ose, L., Budinski, D., Hounslow, N., and Arneson, V. (2009) Comparison of pitavastatin with simvastatin in primary hypercholesterolaemia or combined dyslipidaemia. *Curr. Med. Res. Opin.* **25**, 2755-2764.

4. Mundy, G.R., (2001) Statins and their potential for osteoporosis. *Bone* ***29***, 495-497.

5. Caballero, J. and Nahata, M. (2004) Do statins slow down Alzheimer's disease? A review. *J. Clin. Pharm. Ther.* 29, 209-213.

6. Fujino, H., Yamada, I., Shimada, S., Yoneda, M., and Kojima, J. (2003) Metabolic fate of pitavastatin, a new inhibitor of HMG-CoA reductase: human UDP-glucuronosyltransferase enzymes involved in lactonization. *Xenobiotica* ***33***, 27-41.

7. Mukhtar, R.Y., Reid, J., and Reckless, J.P. (2005) Pitavastatin. *Int. J. Clin. Pract. 59*, 239-252.

8. Beijersbergen van Henegouwen, G.M.J., (1997) Medicinal photochemistry: phototoxic and phototherapeutic aspect of drugs In: *Advances in Drug Research* (Testa, B., Mayer, U.A. Eds.), Volume 29, pp.79-170 Academic Press, New York and London.

9. Cosa, G. (2004) Photodegradation and photosensitization in pharmaceutical products: assessing drug phototoxicity. *Pure Appl. Chem.* **76**, 263-275.

10. Krol, G.J. Beck, G.W., Ritter, W., and Lettieri, J.T. (1993) LC separation and induced fluorometric detection of rivastatin in blood plasma. *J. Pharm Biomed. Anal.* **11**, 1269-1275.

11. Cermola, F., Della Greca, M., Iesce, M.R., Montanaro, S., Previtera, L., and Temussi, F. (2006) Photochemical behavior of the drug atorvastatin in water. *Tetrahedron* 62, 7390-7395.

12. Cermola, F., Della Greca, M., Iesce, M.R., Montanaro, S., Previtera, L., Temussi, F., and Brigante, M. (2007) Irradiation of fluvastatin in water structure elucidation of photoproducts. *J. Photochem. Photobiol. A: Chemistry* **189**, 264-271.

13. Astarita, M., Della Greca, M., Iesce, M.R., Montanaro, S., Previtera, L., and Temussi, F., (2007) Polycyclic compounds by sunlight exposure of the drug rosuvastatin in water. *J. Photochem. Photobiol. A* 187, 263-268.

14. Viola, G., Grobelny, P., Linardi, M.A., Salvador, A., Basso, G., Mielcarek, J., Dall'Acqua, S., Vedaldi, D., and Dall'Acqua F. (2010) The phototoxicity of fluvastatin an HMG-CoA reductase inhibitor is mediated by the formation of a benzocarbazol-like photoproduct. *Toxicol. Sci.* **118**, 236-250.

15. Montanaro, S., Lhiaubet-Vallet, V., Iesce, M.R., Previtera, L., and Miranda, M.A., (2009) A mechanistic study on the phototoxicity of atorvastatin: singlet oxygen generation by a phenanthrene-like photoproduct *Chem. Res. Toxicol.* **22**, 173-178.

16. Grobelny, P., Viola, G., Vedaldi, D., Dall'Acqua, F., Gliszczynska-Swiglo, A., and Mielcarek, J. (2009). Photostability of pitavastatin - a novel HMG-CoA reductase inhibitor. *J. Pharm. Biomed. Anal.* **50**, 597-601.

17. Viola, G., Salvador, A., Cecconet, L., Basso, G., Dall'Acqua, F., Vedaldi, D., Aloisi, G., Elisei, F., Latterini, L., and Barbafina, A., (2007) Photophysical properties and photobiological behaviour of amodiaquine, chloroquine and primaquine. *Photochem. Photobiol.* **83**, 1415-1427.

18. Levine L.R., Garland D., Oliver C.N., Amici A., Climent I., Lenz A.G., Ahn B.G., Shaltiel S., and Stadtman E.R. (1990) Determination of carbonyl content in oxidatively modified proteins *Methods Enzymol.* **186**, 464-480.

19. Martin S. J., Reutelingsperger C. P., McGahon A. J., Rader J. A., van Schie R. C., Laface D. M., and Green D. R. (1995). Early redistribution of plasma membrane phosphatidylserine is a general feature of apoptosis regardless of the initiating stimulus: Inhibition by overexpression of Bcl-2 and Abl. *J. Exp. Med.* **182**,1545-1556.

20. Vermes, I., Haanen, C., Steffens-Nakken, H., and Reutelingsperger, C.P. (1995) A novel assay for apoptosis. Flow cytometric detection of phosphatidylserine expression

on early apoptotic cells using fluorescein labelled Annexin V. *J. Immun. Method* **184**, 39-51.

21. Galluzzi, L., Aaronson, S.A., Abrams, J., Alnemri, E.S., Andrews, D.W., Baehrecke, E.H., Bazan, N.G., Blagosklonny, M.V., Blomgren, K., Borner, C., et al. 2009) Guidelines for the use and interpretation of assays for monitoring cell death in higher eukaryotes. *Cell Death Differ.* **16**, 1093-1107.

22. Porter, A.G., and Janicke, R.U. (1999) Emerging role of caspase-3 in apoptosis. *Cell Death Differ.* **6**, 99-104.

23. Kumar, S. (2007) Caspase function in programmed cell death. *Cell Death Differ.* ***14,*** 32-43.

24. Oleinick, N.L. Morris, R.L. and Belichenko, I. (2002) The role of apoptosis in response to photodynamic therapy: what, where, why and how. *Photochem. Photobiol. Sci.* **1**, 1-21.

25. Elisei, F., Aloisi, G.G., Barbafina, A., Dall'Acqua, F., Mazzuccato, U., Canton, M., Facciolo, L., Latterini, L., and Viola, G. (2004) Photophysical and photobiological behaviour of antimalarial drugs in aqueous solutions. *Photochem. Photobiol.* **79**, 248-258.

26. Eguchi, Y., Shimizu, S., and Tsuijmoto, Y. (1997) Intracellular ATP levels determine the cell death fate by apoptosis or necrosis. *Cancer Res.* **57**, 1835-1840.

27. Leist, M., Single, B., Castoldi, A.F., Kuhnle, S., and Nicotera, P. (1997) Intracellular adenosine triphosphate (ATP) concentration: a switch in the decision between apoptosis and necrosis *J. Exp. Med.* **185**, 1481-1486.

28. Ouedraogo, G., Morliere, P., Bazin, M., Santus, R., Kratzer, B., Miranda, M.A, and Castell, J.V. (1999) Lysosomes are sites of fluoroquinolone photosensitization in human skin fibroblasts: a microspectrofluorometric approach. *Photochem. Photobiol.* **70**, 123-129.

29. Viola, G., and Dall'Acqua, F. (2006) Photosensitization of biomolecules by phenothiazine derivatives *Curr. Drug Targets* **7**, 1135-1154.

30. Kessel, D., and Luo, Y., (2001) Intracellular sites of photodamage as a factor in apoptotic cell death. *J Porphyr. Phthalocyanines* ***5,*** 181-184.

31. Salvioli S., Ardizzoni A., Franceschi C., and Cossarizza A. (1997) JC-1 but not DiOC6(3) or rhodamine 123 is a reliable fluorescent probe to asses $\Delta\Psi$ changes in intact cells: implications for studies on mitochondrial functionality during apoptosis. *FEBS Lett.*, **411**, 77-82

32. Rothe, G., and Valet, G. (1990) Flow cytometric analysis of respiratory burst activity in phagocytes with hydroethidine and 2',7'-dichlorofluorescein. *J. Leukoc. Biol.* **47**, 440-448.

33. Nohl, H., Gille, L., and Staniek, K. (2005) Intracellular generation of reactive oxygen species by mitochondria. *Biochem. Pharmacol.* **69,** 719-723.

34. Golstein, P.,and Kroemer, G. (2007) Cell death by necrosis: toward a molecular definition. *Trends Biochem. Sci.* **32**, 37-43

35. Girotti, A.W. (2001) Photosensitized oxidation of membrane lipids: reaction pathways, cytotoxic effects, and cytoprotective mechanisms. *J. Photochem. Photobiol. B.* **63**, 103-113.

36. Stadtman, E.R, and Levine, R.L. (2003) Free radical-mediated oxidation of free amino acids and amino acid residues in proteins. *Amino Acids* **25**, 207-218.

37. Kim, W.H., Choi C.H., Kang, S., Kwon, C.H., and Kim, Y.K. (2005) Ceramide induces non-apoptotic cell death in human glioma cells *Neurochem. Res.* **30**, 969-979.

38. Alexander, K.P., Blazing, M.A., Rosenson, R.S., Hazard, E.; Aronow, W.S., Smith, S.C. Jr, and Ohman E.M. (2009.) Management of hyperlipidemia in older adults. J Cardiovasc. Pharmacol. Ther. **14**, 49-58

PART2: NATURAL COMPOUNDS AS POTENTIAL ANTITUMORAL DRUGS

Introduction

Nature has an enormous wealth of therapeutic resources, in fact, there are more 300.000 plant species with an enormous biodiversity and adaptability. They also have undergone a natural evolution under selective pressure present a structural variety and are bioactive.

Since old time was known to use natural compounds such as drugs: in fact since prehistoric times man has learned to distinguish between the beneficial and toxic of the plants. *(Bruni A. 1999)*

At the period from 4000 BC to 500 BC back the first written documents of the plants used as cure.

- 4000 BC : The Treaty of Imotep.
- 3000 BC: the Sumerians on clay tablets imprinted the first texts written on herbal medicine.
- 2800 BC: The Chinese herbals the emperor Shennung (considered the father of chinese medicine) by a treaty indicates the plants useful for treating various diseases.
- 1550 BC: Egypt; Ebers Papyrus.
- 200 BC in Greece some doctors created the first antidotes at the poisons. the most famous is the triaca used since XIX sec like stomach sedative.
- In the Middle Ages the Arab school brought to Europe new drug and complex medication that required appropriate places for the preparation.
- In Renaissance are important the works of Paracelso that shows the presence of the fifth essence that is the bioactive compounds
- 1700 AC: the first treated where the was descriptions of the treatment with extracts from plants.
- 1800 AC are identify and isolated many active principle. Es morphine, atropine, digitalis, quinine and caffeine. Hereafter began manufacturing the industry and the drugs was replaced of the bioactive compound. (*Shoeb M. 2006*).

Suddenly the natural compund were replaced but in the last year their used are returned high.

In the past the use of natural substances such as flowers, leaves, and bark are used in form of herbal tea infusions and medical ointments, has been the main source cure of many diseases. Nowadays the natural product have an important role in the discovery and development of drugs (*Newman et al 2007*), in fact many drugs were created basing on of traditional remedies at vegetal base.

Today more than 40% of drugs in current use are natural compounds or substances derived from them.

The natural compound are classified in:

- Primary metabolites essential for their life such as lipids and proteins. They are produced from primary metabolism and they partecipate at the energy production and cell division. These are not specific species since that they are ubiquitous.
- Secondary metabolites, which are not essential for life.They derived from primary metabolites and are produced from secondary metabolism They are produced and accumulated in the organ.

These extracts are highlighted by chemical screening and they have these requirements:

simple, rapid, selective, sensitive.

These metabolites are very important for plants because they act like messenger for the interaction with the external ambient, for protection, and for mechanical support. *(Bruni A. 1999).* Example of these metabolites are:

Alkaloids: they are organic heterocyclic compound that have N in reducted oxidation state. They are biologically active , and very eterogenic; an example is morphine.

Papaverum sunniferum

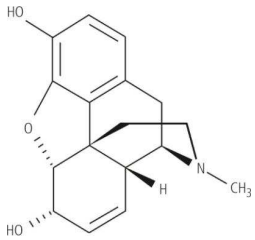

Morphine

Terpenes and steroids : They have different structures but have a link of five atoms of carbon, that name is isoprene units.: for example monoterpenes protect the plant from the attack of the microorganisms, and Artesimine is an important antimalarian.

Lemon

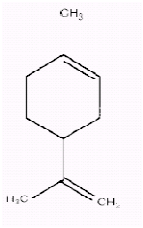

limonene

Phenols and polyphenols: they have many different structures and activity but all of them have one or more hydroxyl condensed groups, for example, flavonoids and the tannins.

Aegopodium (Apiacea)

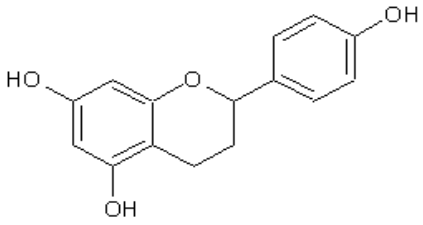

Flavon

Natural compounds allow to screen different biological targets. thanks to their diversity and their features. The peculiarity, of these compounds is the richness and structural complexity in their functional groups which make them ideal for modulation of their activity. In addition, many natural substances have a biological target, and also a good pharmacokinetic (*Newmann et al 2007)*. Sometimes the natural compounds are modified by proteins and they have an interaction with proteins, so they also must be able to bind them, but sometimes is necessary to change the structure to improve the characteristics of affinity and selectivity. These compounds also have some problems because the content of the drugs depends on the individual condition of the plant, of growth environment, of the collection, of the conservation and the extraction. Moreover there are also problems of costs and material supply. *(Bruni A. 1999).* Many natural compounds have been studied for their benefits in different types of tumor as prevention and as therapy for kill cancer cells. Many of these compounds are obtained from terrestrial plants, microorganisms,

marine organisms, and aquatic plants, in fact over of the 60% of anticancer drugs are derived from natural compounds. (*Banerrjee S. 2008).*

ANTICANCER DRUGS FROM NATURAL SOURCES

Taxol: The Taxus *brevifolia* is a tree that is located in the northwest Pacific and has a very slow growing. In recent years Taxol, one of its derivates, has been discovered as an effective antitumor agent. Taxol is a diterpen that is in the bark of tree. Taxol (palitaxel) is an antimitotic that binds to B-tubulin of microtubules inhibiting the depolymerization resulting in an accumulation which leads to cell death.

For its use there are many problems because the tree should be felled and the amount obtained was not high, so today taxol is obtained from alternative sources like 10-desacetilbaccatin wich is present in the leaves and in different species of fraxinus. Taxol are most used for the ovarian and breast cancer, and also small and non small cell lung cancer. *(Itokawa H. et al 2008), (Da Rocha et al 2001).*

Taxus brevifolia

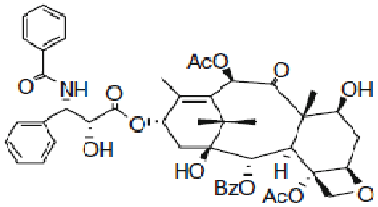

Taxol

Vincristine and Vinblastine derive from a plant the *Catharanthus roseus (*periwinkle of the Madagascar). They were the first agents used in clinical for the anticancer treatment.

They their target is cell mitosis, in fact for example vincristine induce block of mitotic spindle , inducing cell death. Vincristine was resulted efficacy in combination with other antiblastic drugs for leukemias and limphomas, and with other chemotherapeutic drugs for advanced testicular cancer,brest cancer and lung cancer.

periwinkle of the Madagascar

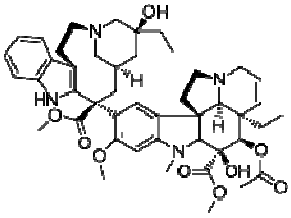

vinblastine

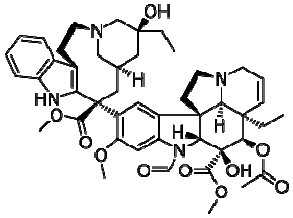

vincristine

Camptothecin is a potent antitumoral, extract from Tawainese or Chinese Camptotheca acuminata. This compound is a pentacyclic alkaloid; its use requires its extraction and a chemical modification. Camptothecin and semi-synthetic derivatives, topotecan and irinotecan, interact with the enzyme DNA polymerase I, stabilize the DNA binding with subsequent break of the replication fork. These compounds are used in ovarian and metastatic colon rectal cancer. *(Itokawa et al 2008).*

Camptotheca acuminata

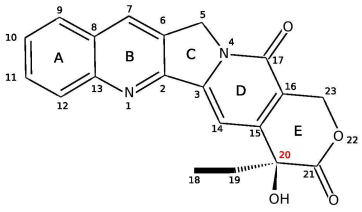

Camtothecin

Etoposide derived from the mandrake plant Podophyllum peltaum and the wild chervil Podophyllum emodi. This compound is an epipodophyllotoxin. Etoposide is a inhibitor of the enzyme Topoisomerasi II, that induce the stabilization of the enzyme-DNA complex witch leads to the DNA breakage. It is used in testicular cancer in combination with the chemotherapic bleomycin, and also in small cell lung cancer.*(Da Rocha et al 2001).*

Podophyllum peltaum

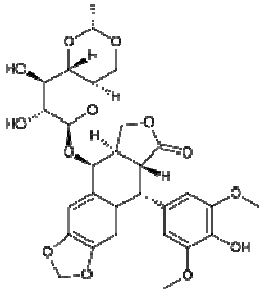

etoposide

Homoharringtonine derived from the Chinese tree Cephalotaxux harringonia drupacea. A racemic mixture of this bioactive compound was used in China for the treatment of acute myelogenous leukemia and cronic myogenous leukemia. *(Shoeb M. 2006).*

Cephalotaxux harringonia drupacea

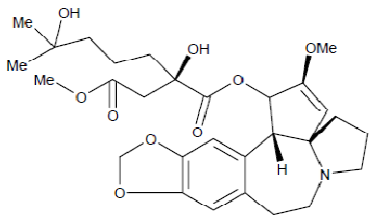

Homoharringtonine

References

Banerrjee S., Wang Z., Mohammad M., Sarkar F.H., and Mohammad R.M. Efficacy *of Selected Natural Products as Theraperutic Agents agains Cancer* 2008 J.Natural Product

Bruni A. *Farmacognosia generale e applicata: i farmaci naturali* Piccin editore 1999.

Da Rocha AB, Lopes RM, Schwartsmann G *Natural products in anticancer therapy.* Curr Opin Pharmacol. 2001 Aug;1(4):364-9.

Itokawa H, Morris-Natschke SL, Akiyama T, Lee KH. Plant-*derived natural product research aimed at new drug discovery* J Nat Med. 2008 Jul;62(3):263-80.

Newmann D.J. and Gordon M. Cragg *Natural Products as Sources of New Drugs over the last 25 Years.* J Natural Product 2007,70,461-477

Shoeb M. *Anticancer agents from medicinal plants* Bangladesh J Pharmacol 2006; 1: 35-41

Natural daucane sesquiterpenes with antiproliferative and proapoptotic activity against human tumor cells

Stefano Dall'Acqua[a], Maria Antonella Linardi[b], Filippo Maggi[c], Marcello Nicoletti[d], Valentina Petitto[d], Gabbriella Innocenti[a], Giuseppe Basso[b], Giampietro Viola[b]*.

[a]*Dipartimento di Scienze Farmaceutiche, Università di Padova, Padova, Italy*

[b]*Dipartimento di Pediatria, Laboratorio di Oncoematologia, Università di Padova, Padova, Italy*

[c]*School of Pharmacy, University of Camerino, Camerino, Italy*

[d]*Dipartimento di Biologia Ambientale, Università "La Sapienza" Roma, Italy*

----------Bioorganic & Medicinal Chemistry 2011 **19(19):5876-85**---------

Keywords: *Ferula communis*; *Ferula glauca*; *Ferulago campestris*; Coumarins; Daucane sesquiterpenes; Cytotoxicity; Apoptosis;

Abstract

Plants of the genera *Ferula* and *Ferulago* are known for their complex content in bioactive secondary metabolites such as coumarins, phenylpropanoids, and sesquiterpenes. We used the ground parts of *Ferula communis* subsp. *communis*, *F. glauca* subsp. *glauca* and *Ferulago campestris* as natural sources for the isolation of four coumarins (**CU-1-CU-4**), two phenylpropanoids (**PE-1** and **PE-2**), one polyacetylene (**PA-1**) and sixteen daucane esters (**DE-1-DE-16**). The cytotoxic activity of the isolated compounds was evaluated against a panel of seven human tumor cell lines. Fourteen of the daucane derivatives showed antiproliferative activity at least against one of the human tumor cell lines tested, four compounds (**DE-5, DE-8, DE-11** and

DE-16) were active against all the tested cell lines. Among them **DE-11** was the most cytotoxic compound against HeLa (4.4 ± 0.7 μM), A549 (2.8 ± 1.4 μM), HL-60 (2.6 ± 0.4 μM), K562 (26.5 ± 6.0 μM) RS 4;11 (1.7 ± 0.3 μM) and SEM (2.4 ± 0.1 μM) cell lines, while **DE-8** was the most active against Jurkat (3.3 ± 0.8 μM). Preliminary structure activity relationship suggests that the most active compounds in the daucane series present the *trans* fusion of the penta- and hepta- atomic cycles, and lipophylic ester groups linked to position 6. Isomeric derivatives such as **DE-8** and **DE-9** or **DE-3**, **DE-4** and **DE-5** exhibited significant differences in their IC_{50} supporting that the β orientation for the ester group in the position 2 enhances the cytotoxic activity. Furthermore, the pro-apoptotic effect of the most active compounds evaluated in Jurkat cell line showed that these compounds are able to induce apoptosis in a time and concentration-dependent manner. Our findings suggest the potential role of daucane derivatives as models for the development of proapoptotic compounds.

Abbreviations

Ferula communis, FCO; *Ferula glauca*, FGL; *Ferulago campestris* (Besser) Grecescu, FGO

1. Introduction

The plants of the genus *Ferula* (Apiaceae) are well known for the production of sesquiterpene and coumarin derivatives.[1-11] Morphologically and phytochemically related to the *Ferula* species are the plants belonging to the genus *Ferulago.* [12]

Ferula and *Ferulago* coumarins have been evaluated for antimicrobial[13,14], *in vitro* antileismanial [15] and cancer chemiopreventive activities.[16,17] Essential oils from *Ferula communis* (FCO), *Ferula glauca* L. (FGL) and *Ferulago campestris* (Besser) Grecescu (FGO) have been studied for their antimicrobial activity[18-20] and non alkaloidal acetylcholinesterase inhibitors were reported from FGO roots.[12] The daucane ester ferutinin and some related compounds, isolated from different *Ferula* species, possess estrogenic activity.[21] Furthermore, some of the *Ferula* sesquiterpenes have been studied for their antiviral, cytotoxic and proapoptotic properties.[22,23] Ionophoretic and apoptotic properties of the daucane ferutinin and related derivatives were studied and showed that ferutinin-induced DNA fragmentation was mediated by a caspase-3-dependent pathway.[24] Further studies about antiproliferative activity of daucane derivatives were reported on MCF-7 [25] and colon cancer cells.[11] Suzuki *et al.* reported that sesquiterpene lactones from *F. varia* act as cytotoxic agents against KB (human epidermoid carcinoma of the nasopharynx), KB-C2 (multidrug-resistant KB), K562

(leukemia) and K562/Adr (multidrug-resistant K562) cells.[26] Alkhatib *et al.* showed an inhibitory effect against two chronic myeloid leukemia (CML) cell lines,[27] by sesquiterpene esters isolated from *F. Elaeochytris* Korovin and recently humulane and germacrane sesquiterpene from *F. lycia* Boiss. have been studied for their activity against tyrosine kinase inhibitor-resistant cell lines, K562R and DA1-3b/M2BCR-ABL.[28] Therefore, among the various isolated *Ferula* sesquiterpenes, the daucane derivatives can be considered as attractive molecules especially as potential antiproliferative and anticancer compounds. In the continuation of our work on cytotoxic natural products[29-32] we have selected FCO, FGL and FGO from Italian populations as sources of bioactive natural products. In this paper we describe the isolation of two new daucane derivatives (**DE-4** and **DE-3**) together with twenty-one known compounds. The structures of all the isolated compounds were obtained on the basis of 1D and 2D NMR techniques as well as MS spectrometry. Moreover, the cytotoxic activity of all the isolated compounds was measured against seven different human tumor cell lines and a preliminary investigation on the mode of cell death was also carried out.

2. Experimental

2.1 Plant material. Roots of FGL and FGO were collected during the vegetative rest in November 2010 in rocky places sited in Madonna di Val Povera (Camerino, Marche, Central Italy, 900 m above sea level, N 43°06'33" E 13°00'06"), while FCO was collected in the same period along a speedway in Foligno (Umbria, central Italy, 240 m above sea level, N 42°58'13" E 12°42'59"). Botanical identification of the plants was confirmed by Dr Maggi. Voucher specimens were deposited in the Herbarium Camerinensis (included in the online edition of Index Herbariorum: http://sweetgum.nybg.org/ih/) of the School of Environmental Sciences, University of Camerino, Italy, under Accession Nos. CAME 25671 (FGL), CAME 13399 (FGO), and CAME 25672(FCO); they are also available at the following website: http://erbariitaliani.unipg.it.

2.2 Extraction and isolation of phytoconstituents. Silica gel plates (cod 5171 Merck) and silica gel (60 mesh) were from Sigma (Milan, Italy). Solvents from Carlo Erba (Milan). Varian Intelliflash flash chromatograph was used for preparative chromatography. NMR (1D and 2D) spectra were obtained on a Bruker AMX 300 spectrometer; optical rotation power was recorded on a Yasco 2000 digital

polarimeter. ESI-MS measurements were obtained on a Varian 500 MS ion trap spectrometer. HR-MS were measured on an API-TOF spectrometer (Mariner Biosystems). Samples were diluted in a mixture of 1:1 H_2O–AcCN with and directly injected at a flow rate of 10 μL/min.

HPLC-DAD-ELSD was obtained on a Agilent 1100 chromatographic system with Diode Array (1100 series) and a Sedex 60 LT evaporative light scattering detector. Agilent C-8 Zorbax 4.6 x 150 (5μ) was used as stationary phase. HPLC conditions for FCO and FGL extracts were as follows: acetonitrile (A) and water 0.1% formic acid (B) as eluents; gradient elution started from 50% (A), then in 35 min 75 % (A); the flow rate was 1 mL/min and the injection volume was 20 μL. For FGO extracts the HPLC conditions were the following: gradient elution started from 10% (A), then in 2 min 30% (A), and in 25 min 75 % (A); the flow rate was 1 mL/min and the injection volume was 20 μL.

Roots of FCO (450 g fresh material) were cleaned, chopped and extracted with methanol (200 mL) at room temperature for 10 min in a Ultrasound bath (ME-extract). Extraction was repeated twice. Solvent was removed *under vacuum* yielding a semi solid brown residue (12 % yield). A part of the solid residue (15 g) was dissolved in a mixture methanol/water (400 mL) and extracted with dichloromethane (DM-extract). The organic layer was anhydrified with sodium sulfate and solvent was removed under vacuum yielding a residue (FCDM-extract, 2.9 g).

FCDM extract (2.9 g) was applied to a silica gel column (500 mL) and eluted with, dichloromethane 1% of methanol (750 mL), dichloromethane 3% of methanol (800 mL), dichloromethane 5 % of methanol (240 mL), and then dichloromethane 20 % of methanol (400 mL). Seventy five fractions were collected and pooled on the basis of their chromatographic behavior in seven different fractions: A (320 mg), B (220 mg), C (190 mg), D (200 mg), E (250 mg), F (250 mg) and G (300 mg). The purification of fraction A and B by PTLC using cyclohexane ethyl acetate 6:1 yielded compounds DE-7 (116.7 mg), DE-1 (75.9 mg); from fraction C by PTLC using cyclohexane ethyl acetate 2:1 the compound DE-8 (60.7 mg) was isolated. The purification of fraction D and E by PTLC using cyclohexane ethyl acetate 6:1 and then cyclohexane ethyl acetate 2:1 yielded compounds DE-9 (13.2 mg), DE-3 (20.1 mg) and DE-2 (6.7 mg). From fraction F, using PTLC with dichloromethane/ methanol 97:3, the compounds DE-4 (30.1 mg), DE-5 (21.4 mg), DE-12 (8.2 mg) were obtained.

Roots of FGL (300 g fresh material) were chopped with methanol (200 mL) and extracted at room temperature for 10 min in a Ultrasound bath (ME-extract).

Extraction was repeated twice. Solvent was removed under vacuum yielding a semi solid brown residue (8 % yield). A part of the solid residue (9 g) was dissolved in a mixture of methanol/water (250 mL) and extracted with dichloromethane (DM-extract). The organic layer was anhydrified with sodium sulfate and solvent was removed under vacuum yielding a residue (FCDM-extract, 1.2 g). FGDM extract was applied to a silica gel column (200 mL) and eluted with dichloromethane (200 mL), dichloromethane 1% of methanol (300 mL), dichloromethane 5% of methanol (300mL), and then dichloromethane 10 % of methanol (300 mL). Fifty fractions were collected and pooled on the basis of their chromatographic behavior in four different fractions A (380 mg), B (430 mg), C (450 mg) and D (150 mg). Further purifications were obtained with semipreparative HPLC on a Licrosphere 100 C-18 (9,6 x 300 mm) using as mobile phase methanol water (60:40) at a flow of 2.5 ml/min. Compounds were obtained from fraction A DE-11 (8.0 mg), DE-16 (10.4mg), from fraction B DE-6 (15.5mg), DE-14 (4.7mg) respectively.

Cleaned roots of FGO (350 g fresh material) were chopped with methanol (200 mL) and extracted at room temperature for 10 min in a Ultrasound bath (ME-extract). Extraction was repeated twice. Solvent was removed *under vacuum* yielding a semi solid brown residue (9 % yield). A part of the solid residue (12 g) was dissolved in a mixture methanol/water (400 mL) and extracted with dichloromethane (DM-extract). The organic layer was anhydrified with sodium sulfate and solvent was removed *under vacuum* yielding a residue (FRDM-extract, 1.6 g). FRDM extract (1.5 g) was applied to a silica gel column (350 mL) and eluted with dichloromethane (350 mL), dichloromethane 1% of methanol (430 mL), dichloromethane 5% of methanol (250 mL), dichloromethane 10 % of methanol (640 mL), and then dichloromethane 15 % of methanol (300 mL). Eighty fractions were collected and pooled on the basis of their chromatographic behavior in five different fractions A (245 mg), B (330 mg) C (450 mg) and D (500 mg) E (250mg).

The purification of fraction A and B by repeated PTLC using cyclohexane ethyl acetate 2:1, and chloroform/methanol 95:5 yielded compounds CU-1 (40.0 mg), DE-7 (21.0 mg). Further purification of fraction C by PTLC using cyclohexane ethyl acetate 2:1 afforded PR-2 (10.4 mg), CU-2 (29.8 mg), DE-6 (14.4 mg), DE-10 (6.1 mg). From the fraction E further purifications were obtained by PTLC using chloroform-methanol (95:5) as eluents, and finally by HPLC using as methanol/water 60/40 yielding PR-1 (20.5 mg), CU-4 (21.7mg) and PA-1 (13.0 mg). Purity of isolated compounds was checked by HPLC analysis and was >97% by software integration.

2.3 Antiproliferative assays. Human T-leukemia (Jurkat), human promyelocytic leukemia (HL-60), human chronic myelogenous leukemia (K562), acute B-lymphoblastic leukemia SEM and RS 4;11 cells, the latter with a t(4;11) translocation cells were grown in RPMI-1640 medium, (Gibco Milano Italy). Human non-small lung carcinoma (A549) and human cervix carcinoma (HeLa) cells were grown in DMEM medium (Gibco, Milano, Italy), all supplemented with 115 units/mL of penicillin G (Gibco, Milano, Italy), 115 μg/mL streptomycin (Invitrogen, Milano, Italy) and 10% fetal bovine serum (Invitrogen, Milano, Italy). Individual wells of a 96-well tissue culture microtiter plate were inoculated with 100 μL of complete medium containing 8 x 10^3 cells. The plates were incubated at 37 °C in a humidified 5% CO_2 incubator for 18 h prior to the experiments. After medium removal, 100 μL of the drug solution, dissolved in complete medium at different concentrations, was added to each well and incubated at 37 °C for 72 h. Cell viability was assayed by the (3-(4,5-dimethylthiazol-2-yl)-2,5-diphenyl tetrazolium bromide (MTT) test as previously described.[47] The IC_{50} was defined as the compound concentration required to inhibit cell proliferation by 50%.

Analogous experiments were performed in the presence of the pancaspase inhibitor z-VAD.fmk (Sigma-Aldrich Milano, Italy).

Peripheral blood lymphocytes (PBL) from healthy donors were obtained by separation on Lymphoprep (Fresenius KABI Norge AS) gradient. After extensive washings, cells were resuspended (1.0 x 10^6 cells/mL) in RPMI-1640 with 10% FCS and incubated overnight. For cytotoxicity evaluations in proliferating PBL cultures, non-adherent cells were resuspended at 5 x 10^5 cells/mL in growth medium, containing 2.5 μg/mL phytohematoagglutinin (PHA, Irvine Scientific). Different concentrations of the test compounds were added and viability was determined 72 h later by MTT test. For cytotoxicity evaluations in resting PBL cultures, non-adherent cells were resuspended (5 x 10^5 cells/mL) and treated for 72 h with the test compounds, as described above.

2.4 Annexin-V assay. Surface exposure of phosphatidylserine on apoptotic cells was measured by flow cytometry with a Coulter Cytomics FC500 (Beckman Coulter) by adding Annexin-V-FITC to cells according to the manufacturer's instructions (Annexin-V Fluos, Roche Diagnostic). Simultaneously the cells were stained with PI. Excitation was set at 488 nm, and the emission filters were set at 525 nm and 585 nm, respectively.

2.5 Detection of DNA fragmentation by Agarose Gel. Total genomic DNA was extracted from treated Jurkat cells by a commonly used salting out protocol. One μg of DNA obtained was subsequently loaded on a 1.5% agarose gel at 50V for 6h in TAE buffer. After staining in ethidium bromide solution, the gel was washed with water and the DNA bands were detected under UV radiation with a ImageQuant 300 transilluminator (GE Healthcare) equipped with a CCD camera.

2.6 Flow cytometric analysis of cell cycle distribution. For flow cytometric analysis of DNA content, 2.5 x 10^5 Jurkat cells in exponential growth were treated with different concentrations of the test compounds for 24 and 48 h. After an incubation period, the cells were collected, centrifuged and fixed with ice-cold ethanol (70%). The cells were then treated with lysis buffer containing RNAse A and 0.1% Triton X-100, and then stained with PI. Samples were analyzed on a Cytomic FC500 flow cytometer (Beckman Coulter). DNA histograms were analyzed using MultiCycle for Windows (Phoenix Flow Systems).
with an ImageQuant 300 transilluminator (GE Health care) equipped with a CCD camera.

2.7 Intracellular calcium measurement. The intracellular calcium concentration in Jurkat cells was measured by flow cytometry using the Ca^{2+}-sensitive fluorescent dye Fluo-4/AM (Molecular Probes). Briefly, the cells were washed and incubated with 2.5 μM Fluo-4/AM in the complete medium for 30 minutes at 37 °C. The cells were washed and then re-suspended in medium RPMI. The intracellular calcium level was analyzed immediately for Fluo-4/AM fluorescence intensity by flow cytometry and then at the same time is treated with DE 8 at the 50 μM.

2.8 Assessment of mitochondrial potential and ROS production. The mitochondrial membrane potential was measured with the lipophilic cation 5,5',6,6'-tetrachlo-1,1',3,3'-tetraethylbenzimidazolcarbocyanine (JC-1, Molecular Probes), as described.[19,30] Briefly, after different times of treatment, the cells were collected by centrifugation and resuspended in Hank's Balanced Salt Solution (HBSS) containing 1 μM JC-1. The cells were then incubated for 10 min at 37 °C, centrifuged and resuspended in HBSS. The production of ROS was measured by flow cytometry using either HE (Molecular Probes) or H_2DCFDA (Molecular Probes).

After different times of treatment, cells were collected by centrifugation and resuspended in HBSS containing the fluorescence probes HE or H_2DCFDA at the concentrations of 2.5 and 0.1 μM, respectively. The cells were then incubated for 30 min at 37 °C, centrifuged and resuspended in HBSS. The fluorescence was directly recorded with the flow cytometer, using as excitation wavelength 488 nm and emission at 585 nm and 530 nm for HE and H_2DCFDA, respectively.

2.10 Statistical analysis. Unless indicated differently, the results are presented as mean ± S.E.M. The differences between control and treated were analysed, using the two-sided Student's *t* test.

3. Results and Discussion

The isolated compounds were obtained from the dichloromethane soluble fractions of FCO, FGL, and FGO on the basis of extensive chromatographic separations, as described in Experimental section. Namely compounds **CU-4**, **DE-1-DE-5**, **DE-7-DE-9**, **DE-11-DE-12** were isolated from FCO, **DE-11**, **DE-13**: **DE-16** were isolated from FGL, while compounds **CU-1**,**CU-2**,**CU-3**, **PR-1**, **PR-2**, **PA-1**, **DE-6 DE-7** and **DE-10** were isolated from FGO. Structures of isolated compounds were determined on the basis of 1D and 2D NMR (HMQC, HMBC, COSY, NOESY) experiments as well as on MS experiments (see supporting information).

Compound **DE-4** was isolated as clear amorphous solid. The HR-MS spectrum showed a pseudomolecular ion $[M+Na]^+$ at *m/z* 469.2120 (calculated 469.2202 for $C_{25}H_{34}NaO_7$). The ^{1}H-NMR spectrum showed signals due to a *p*-anysate group namely two *ortho* coupled doublets at δ 7.96 (H 2'-6') and 6.93 (H 3'-5') (J=7.8 Hz) integrating two proton each, and a singlet at δ 3.87 (H-7) integrating for three protons. Signals ascribable to oxymethyne were detected at δ 4.96 (H-2) (dd 1.1; 6.4), at δ 5.52 (H-6) (J=10.2; 6.00; 3.70) and a doublet at δ 4.10 (H-10) (J=7.2) integrating one proton each. Doublets at δ 0.79 (H-12) (J=6.7) and 0.94 (H-13) (J=6.5) integrating for three proton each, suggest the presence of an isopropyl group while the three singlets at δ 1.11 (H-15), 1.82 (H-14) and 2.12 (3H, each) support the presence of two different quaternary methyl groups and one acetyl residue, respectively. The structure of **DE-4** was established mainly on the basis of 2D NMR experiments. Three oxygenated non quaternary positions were detected in the HMQC spectrum with δ_H 5.52 (ddd, J= 10.2; 6.0; 3.7) and δ_C 70.4, δ_H 4.96 (dd, J= 6.4; 1.1),δ_C 84.6 and δ_H 4.10 (d J= 7.2) δ_C

71.8. Diagnostic HMBC correlations were observed from the methyl group 15 (δ 1.11) with carbon resonances at δ 52.0 (C-1), 71.8 (C-10), 84.6 (C-2) and 47.8 (C-5), from the methyl group 14 (δ 1.82) and the carbon resonances at δ 136.9 (C-8), 126.5 (C-9) and 39.2 (C-7), and from the methyne proton signal at δ 3.20 (H-5) with carbons C-7, C-10, C-1, C-3 and C-2. The comparison with the literature[5,33,34] allows to establish the presence of a daucane derivative formerly related to a *trans* fused dauc-8-ene as 10-hydroxy-jaeschkeanadiol.[5] HMBC correlations allowed also to establish the esterification position due to the HMBC correlation observed from H-6 to C-1' (δ 167.0) and due to the HMBC correlation observed from H-2 (δ 5.52) and C-1'' (δ 170.0). The comparison of coupling constants of H-2 (J= 6.4, 1.1), H-6 (J=10.5, 6.0, 3.7,) and H-10 (J=7.10) with literature[5]} and the data obtained with NOESY spectrum allowed to establish the orientation of proton 2, 6 and 10 as β. Thus it has been determined as 2α-acetoxy-6α-*p*-methoxybenzoyl-10α-hydroxy-jaeschkeanadiol. NMR data and assignments are reported in Table 1. This derivative was not previously isolated from natural sources, albeit the epimer derivative 2α-acetoxy-6α-*p*-methoxybenzoyl-10β-hydroxy-jaeschkeanadiol was previously isolated from *F. communis* subsp. *communis*.[5]

Compound **DE-3** was isolated as clear amorphous solid. The HR-MS spectrum showed a pseudomolecular ion $[M+Na]^+$ at *m/z* 469.2165 (calculated 469.2202 for $C_{25}H_{34}NaO_7$), accounting for an isomer of **DE-4**. The ^{1}H-NMR spectrum appears similar to that of **DE-4** except for the chemical shift of a oxymethine at δ 3.88 (m) and the broad singlet at δ 5.57. Careful reading of HMQC, HMBC and COSY spectra and comparison with literature[5] allowed to establish the structure of 10-hydroxy-jaeschkeanadiol for the terpene nucleus and to determinate the esterification position as 10-acetyl and 6-p-methoxybenzoyl. The comparison of the coupling constants for H-2 (J= 6.1, 1.1), H-6 (J=10.2, 6.0, 3.3) and H-10 (brs) and literature data[5] as well as the NOESY correlations observed from methyl group 15 (δ 1.18) with proton signals at δ 3.88 (H-2) and 5.31 (H-6) and the NOESY correlations from proton signal at δ 2.74 (H-5) with proton at δ 5.57 (H-10) allow to establish the relative orientation of the H-2 and H-6 as β while H-5 and H-10 as α.

Thus, the structure **DE-3** was established as 2α-hydroxy-6α-*p*-methoxybenzoyl-10β-acetoxy-jaeschkeanadiol. NMR data and assignments are reported in Table 1. This compound was not previously isolated from natural source; the similar derivative 2α-

acetoxy-6α-*p*-methoxybenzoyl-10β-hydroxy-jaeschkeanadiol was isolated from *F. communis* subsp. *communis*[5] and also in this work as **DE-5**.

Table 1. *NMR data for compounds DE-3 and DE-4. Spectra were recorded in $CDCl_3$ at 300MHz for ^1H and 75 MHZ for ^{13}C. Coupling constant are reported in Hz.*

	DE-3		**DE-4**	
Position	δH (mult, *J*, int)	δC	δH (mult, *J*, int)	δC
1	-	52.3	-	52.0
2	3.88 (dd, 6.1, 1.1, 1H)	79.0	4.96 (dd 6.4, 1.1, 1H)	84.6
3	1.92-2.23 (m, 2H)	21.1	2.14 (m, 2H)	20.0
4	-	85.2	-	84.8
5	2.74 (d, 10.5, 1H)	53.1	3.20 (d, 10.5, 1H)	47.8
6	5.31 (ddd,10.2, 6.0, 3.3, 1H)	69.9	5.52 (ddd, 10.5, 6.0, 3.7, 1H)	70.4
7	2.53-2.10 (m, 2H)	40.8	3.87-2.10 (m, 2H)	39.2
8	-	132.2	-	136.9
9	5.26 (brs, 1H)	128.2	5.69 (brd, 7.10, 1H)	126.5
10	5.57 (brs, 1H)	76.3	4.10 (d, 7.10, 1H)	71.8
11	1.81 (m, 1H)	37.9	1.77 (m, 1H)	37.2
12	0.87 (d, 6.5, 3H)	17.3	0.79 (d, 6.6, 3H)	17.8
13	1.02 (d, 6.9, 3H)	18.2	0.94 (d, 6.9, 3H)	18.6
14	1.87 (brs, 3H)	26.7	1.82 (brs, 3H)	27.4
15	1.18 (s, 3H)	15.2	1.11 (s, 3H)	20.8
1'	-	122.6	-	122.8
2'-6'	8.00 (d, 7.9, 2H)	131.8	7.97 (d, 8.3, 2H)	131.9
3'-5'	6.97 (d, 7.9, 2H)	114.1	6.93 (d, 8.3, 2H)	114.0
4'	-	165.5	-	164.5
7'	-	168.1	-	167.1
OCH_3	3.91 (s, 3H)	55.8	3.87 (s, 3H)	55.6
CH_3-	2.16 (s, 3H)	21.2	2.10 (s, 3H)	21.8
CH_3C=O	-	171.4	-	170.0

Structure of compound **DE-12** was established as 8,9-dihydro-8,14-dehydro-9-hydroxyferutinin; obtained by semisinthesys,[35] but never isolated in natural sources.

The comparison of the obtained spectral data with the literature allows to establish the following structures for the other constituents: **DE-1** 14-*p*-methoxybenzoyl-dauc-4,8-diene,[36] **DE-2** 14-*p*- methoxybenzoyl-4,5epoxy-dauc-8-ene,[5] **DE-5** 2α-acetoxy-6α-*p*-methoxybenzoyl-10β-hydroxy-jaeschkeanadiol,[5] **DE-6** lapiferin or 6α-angeloyl-10α-acetyl-8,9-epoxy-jaeschkeanadiol,[37] **DE-7** ferutinin,[21,25] **DE-8** 2α-acetoxy-6α-*p*-methoxybenzoyl-10β-acetoxy–jaeschkeanadiol,[5] **DE-9** 2α-acetoxy-6α-*p*-methoxybenzoyl-10α-acetoxy–jaeschkeanadiol,[5] **DE-10** siol anisate,[5] **DE-11** pallinin or 6α,10α-diangeloyl-jaeschkeanadiol,[38] **DE-12** 8,9-dihydro-8,14-dehydro-9-

hydroxyferutinin [35], **DE-13** ferutidin,[39] **DE-14** lancerodiol *p*-methoxybenzoate,[4] **DE-15** lancerodiol *p*-hydroxybenzoate [4] **DE-16** 2α-hydroxy ferutinin,[40] **CU-1,**[12] **CU-2,**[12] **CU-3,**[41] **CU-4**, **PR-1,**[42] **PR-2,**[43] **PA-1**.[44] Structures of the isolated daucane are reported in Chart 1, while structures of other isolated compounds are reported in Chart 2.

3.1 Structures of the isolated compounds.

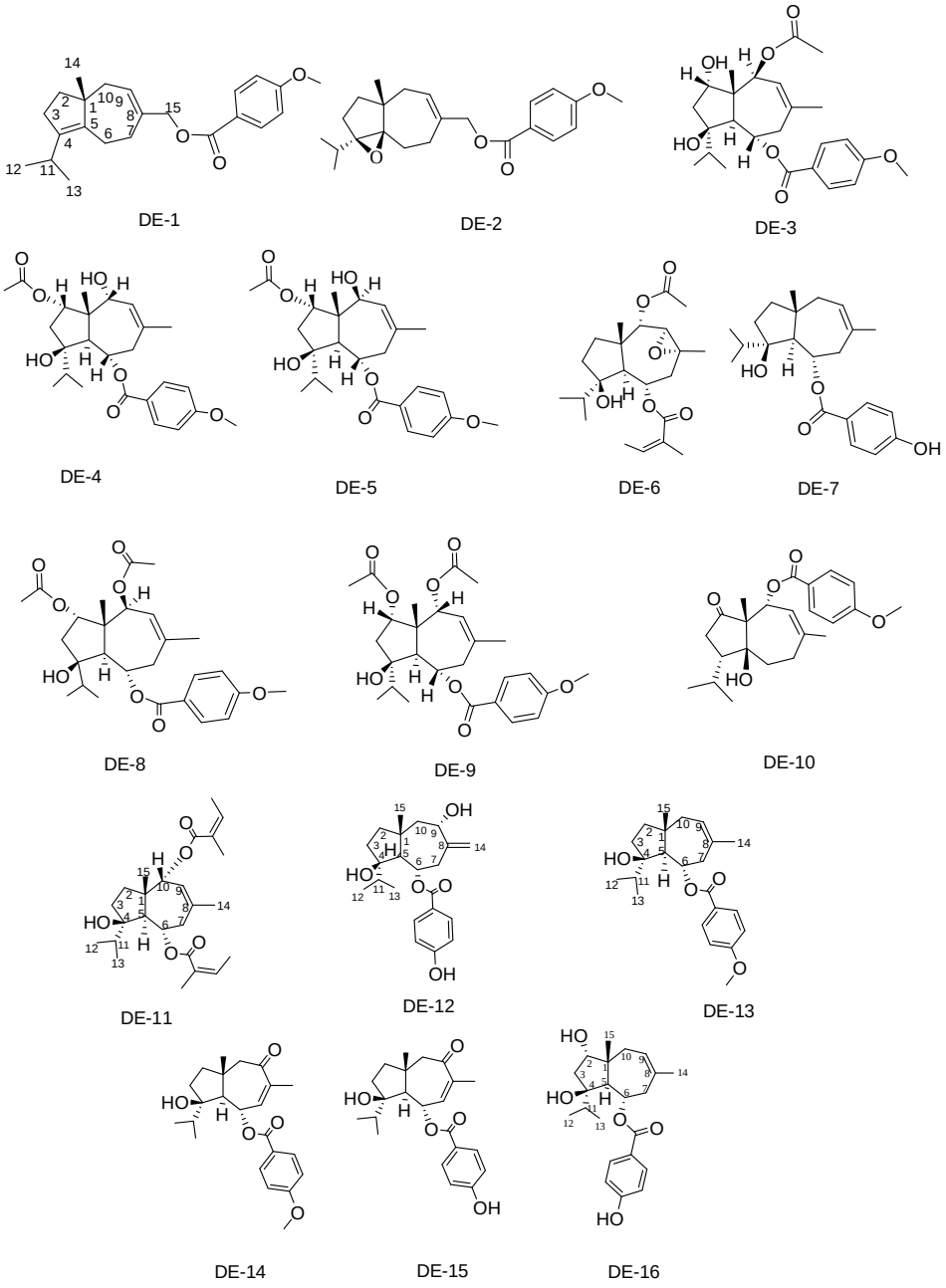

Chart 1: structures of isolated daucane derivatives

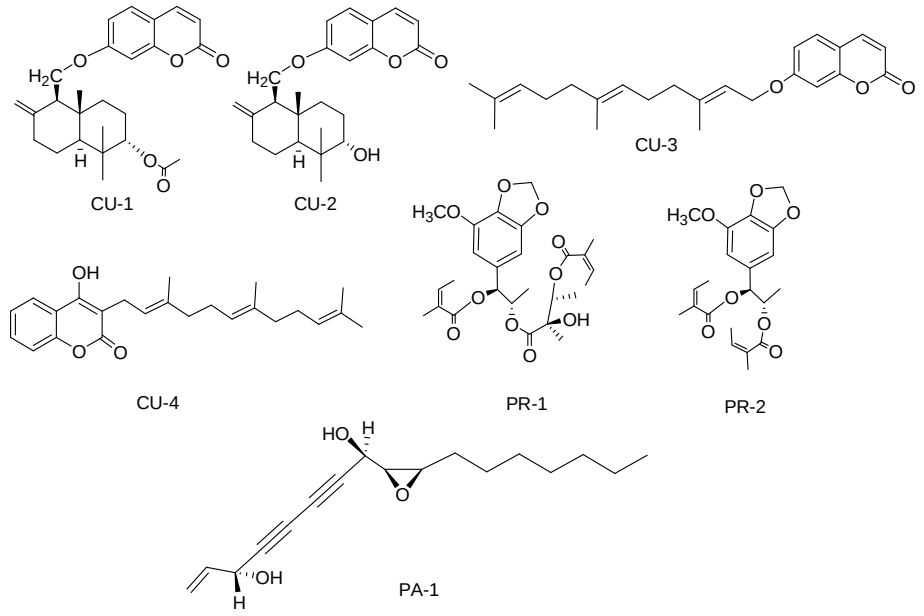

Chart 2: structures of coumarins, phenylpropanoids and polyacetilene isolated compounds

3.2 Antiproliferative activity of isolated compounds.

The cytotoxic activity of all the isolated compounds was evaluated against seven different human tumour cell lines, namely HeLa, A549, HL-60, Jurkat, K562, RS 4;11 and SEM.

The four coumarines (**CU-1-CU-4**), the phenylpropanoid derivatives (**PR-1-PR-2**) and the polyacetilene derivatives (**PA-1**) were inactive (IC_{50} > 100μM) in all the cell lines.

Compounds **DE-5**, **DE-8**, **DE-11** and **DE-16** exhibit cytotoxic effects against all the considered cell lines and the results are reported in Table 2. Compound **DE-8** was the most active against Jurkat (IC_{50} 3.3 μM) while **DE-11** showed the highest activity against all the other tested cell lines.

Some preliminary evaluation of structure activity relationships can be traced considering the measured IC_{50} values.

Structurally, the daucane derivatives are based on a central bicycle hydrocarbon skeleton, whose geometry depends by the junction stereochemistry influencing the flatness of the molecule, more or less surrounded by a crown of oxygenated functions and a series of acylating moieties, responsible of the differences in polarity of the products.

Table 2. Antiproliferative activity of Daucane esters in human tumor cells

Compd	IC_{50} [a] (μM)						
	HeLa	A549	HL-60	Jurkat	K562	RS 4;11	SEM
DE-1	>100	>100	30.7±6.2	25.6±7.4	67.0±6.5	44.1±4.0	25.5±1.6
DE-2	>100	>100	>100	>100	>100	60.9±1.8	84.0±9.5
DE-3	52.6±1.8	>100	14.9±5.0	9.1±4.1	70.4±6.2	26.8±4.4	26.5±1.9
DE-4	>100	>100	24.0±4.2	33.6±5.5	85.2±7.9	70.4±4.3	>100
DE-5	52.9±2.6	79.6±0.7	23.0±0.9	5.9±3.4	48.2±7.7	34.4±2.1	18.1±3.0
DE-6	>100	>100	>100	>100	>100	>100	>100
DE-7	>100	>100	>100	>100	>100	>100	>100
DE-8	14.5±3.9	23.3±1.7	11.3±2.4	3.3±0.8	39.6±3.9	2.8±0.2	15.0±1.3
DE-9	>100	>100	83.5±9.8	62.2±8.8	>100	42.9±1.2	32.9±2.5
DE-10	>100	>100	>100	>100	>100	>100	23.9±2.4
DE-11	4.4±0.7	2.8±1.4	2.6±0.4	7.7±1.4	26.5±6.0	1.7±0.3	2.4±0.1
DE-12	>100	>100	43.4±2.8	55.0±12.8	>100	29.0±3.5	34.7±1.8
DE-13	>100	31.9±2.7	20.1±1.8	30.5±7.2	67.8±13.7	17.6±1.4	18.2±2.9
DE-14	29.7±6.8	31.8±4.4	38.9±6.0	40.5±6.5	>100	28.6±3.0	28.4±1.6
DE-15	26.1±3.3	14.5±8.8	82.5±7.5	40.5±12.1	>100	28.2±2.2	24.4±2.0
DE-16	56.5±15.5	83.7±10.2	3.5±6.5	40.3±4.7	95.0±0.7	33.4±1.8	22.4±1.8

[a] Compound concentration required to reduce cell growth inhibition by 50%.
Values are the mean ± SEM for four separate experiments.

All the most active compounds possess ring fusion with *trans* geometry and the 6(α)-ester linked group (*p*-methoxy benzyl or angeloyl), compounds possessing *cis* geometry (**DE-1** and **DE-10**) or epoxy group in 4-5 (**DE-2**) have poor activity. Also the double bond in the hepta-atomic ring appears critical; active compounds present the 8,9 or the 7,8 (**DE-14** and **DE-15**) double bond while the 8,9 epoxy derivative (**DE-6**) is inactive.

Furthermore, significant changes in the cytotoxic effects against all the considered cell lines have been observed for the compounds with different stereochemistry of position 10 (**DE-8** and **DE-9** and **DE-4** and **DE-5**) suggesting that the 10β-hydroxy function or the 10β-acetoxy substituent is important for the cytotoxic activity of these compounds. Notably, for the two isomers **DE-4** and **DE-5** the IC_{50} is lower or at least the same (for HL-60) in all the cell lines for the compound bearing the 10β-hydroxy group (**DE-5**). This is also observed for the two 10-acetyl derivatives **DE-8** and **DE-9**

(see table 2). The 2α-acetyl or 2α-hydroxy group and 10β-hydroxy or acetoxy function as **DE-5** and **DE-8** all present significant cytotoxic activity suggesting that the preferred orientation for hydroxyl or acetoxy functions in such positions are 2α and 10β.

3.3 Cytotoxicity for normal cells.

To obtain more insights into the cytotoxic potential of test compounds for normal human cells, the most active compounds were assayed *in vitro* against peripheral blood lymphocytes (PBL) from healthy donors (Table 3).

Compounds **DE-3**, **DE-5** and **DE-8** proved cytotoxic for both PHA-stimulated and resting PBL, but at concentrations higher than those active against the lymphoblastoid cell line Jurkat. Instead, compound **DE-11** is more cytotoxic in PHA-stimulated PBL respect to the unstimulated lymphocytes indicating that this derivative acts preferentially on proliferating cells. Anyway, also in this case it works at concentrations higher respect to Jurkat cells.

Table 3. Cytotoxicity of Daucane Esters for Human Peripheral Blood Lymphocytes (PBL)

Cell line	IC_{50} (μM) [a]			
	DE-3	**DE-5**	**DE-8**	**DE-11**
$PBL_{resting}$ [b]	30.3±3.0	20.5±1.5	6.6±1.4	22.6± 2.3
PBL_{PHA} [c]	33.7±1.6	27.2±2.3	9.4±1.0	13.7±1.2

[a] Compound concentration required to reduce cell growth inhibition by 50%.
[b] PBL not stimulated with PHA
[c] PBL stimulated with PHA.
Values are the mean ± SEM for three separate experiments.

3.4 Determination of the mode of cell death.

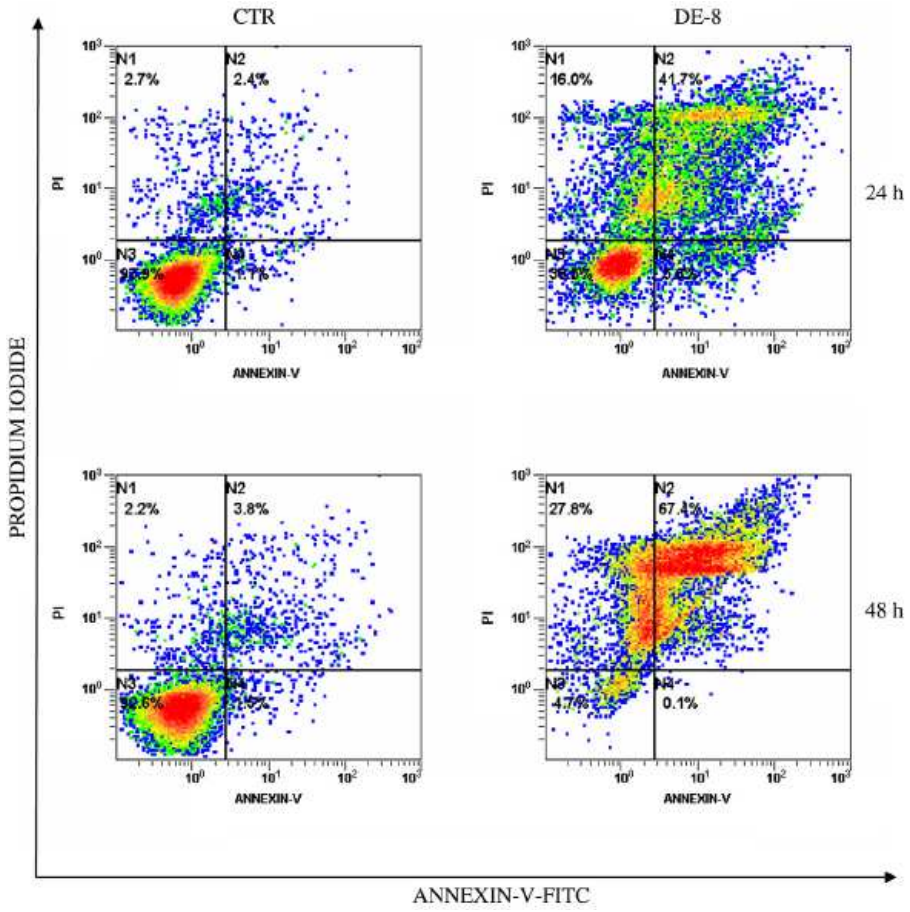

Figure 1. *Representative biparametric histograms obtained by flow cytometric analysis. Jurkat cells after 24 and 48 h after incubation in the presence of DE-8 50 μM, were collected and stained with Annexin-V-FITC and Propidium iodide (PI) and analysed by flow cytometry.*

To characterize the mode of cell death, we performed a biparametric cytofluorimetric analysis using propidium iodide (PI) and AnnexinV-FITC which stain DNA and phosphatidylserine (PS) residues, respectively.[45] Because externalization of PS occurs in the earlier stages of apoptosis, Annexin V staining identifies apoptosis at an earlier stage than sub-G_1 appearance which represents a later stage of apoptosis being based on nuclear changes such as DNA fragmentation.

After drug treatment for 24 and 48 h, Jurkat cells were labelled with the two dyes, washed and the resulting red (PI) and green (FITC) fluorescence was monitored by flow cytometry.

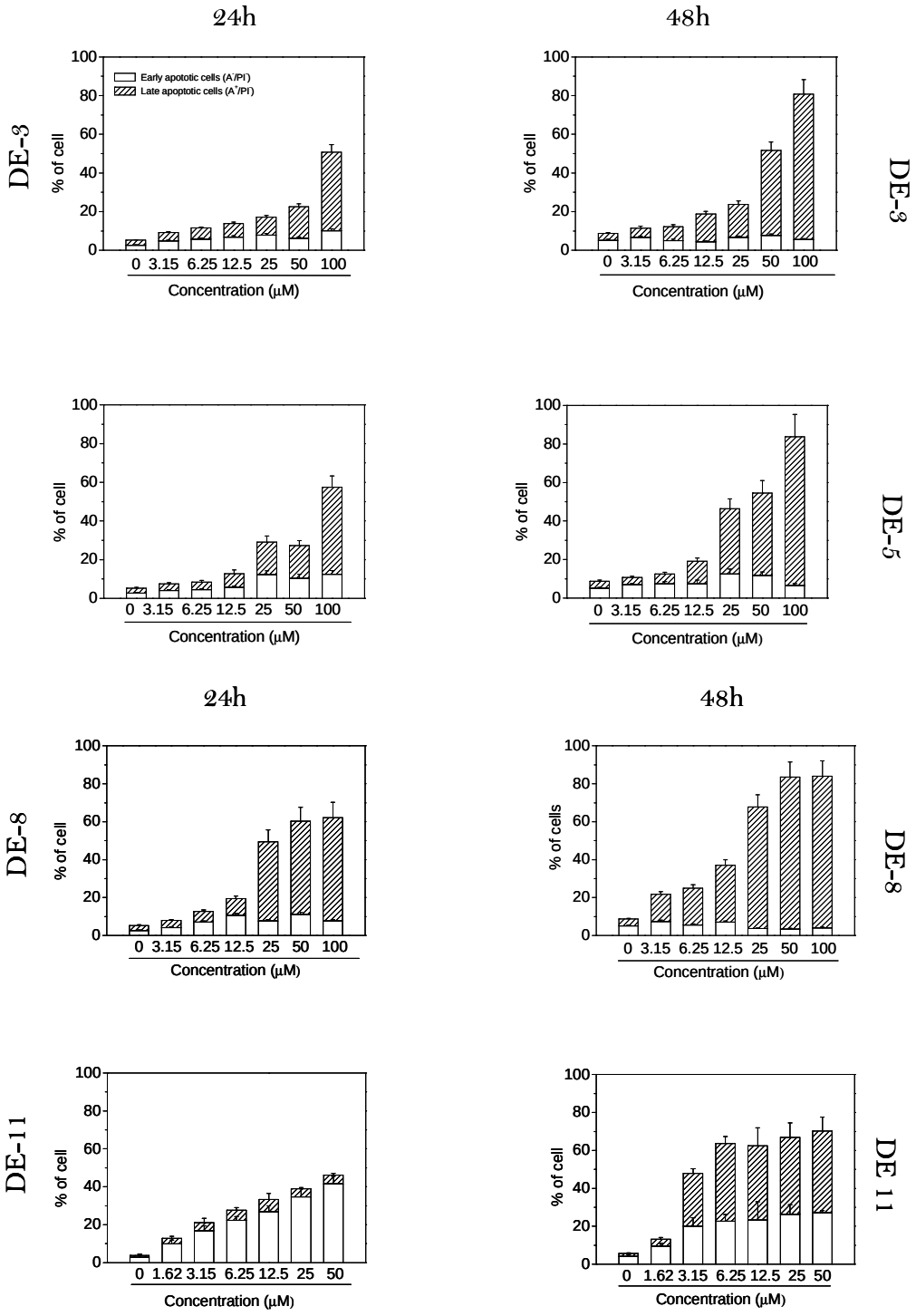

Figure 2. *Determination of the mode of cell death using Annexin-V and PI staining and flow cytometric analysis. Jurkat cells were incubated in the presence of DE-3, DE-5, DE-8 and DE-11 at the indicated concentrations and after 24 and 48 h the cells were collected and stained with Annexin-V-FITC and propidium iodide (PI) and analysed by flow cytometry. The results are expressed as percentage of early apoptotic cells (Annexin-V$^+$/PI) and late apoptotic cells (Annexin-V$^+$/PI$^+$) as found in the different region of the biparametric histograms showed in Figure 1. Data represent mean ± S.E.M. of three independent experiments.*

A complete picture of the results is presented in Figure 2 for **DE-3**, **DE-5**, **DE-8** and **DE-11** evaluated at different concentrations ranging from 1.25 to 100 μM and after 24 and 48h of incubation. It can be observed an increase of late apoptotic cells(A^+/PI^+) for compounds **DE-3**, **DE-5** and **DE-8** while for compound **DE-11** we observed the formation of early apoptotic cells (A^+/PI^-) in a concentration-dependent manner at 24 h followed at later times (48 h) by the appearance of A^+/PI^+ cells suggesting that this last derivative may have delayed effect on the induction of apoptosis.

The mode of cell death was also followed by a common endpoint analysis such as analysis of DNA fragmentation.[46] As shown in Figure 3 (panel A), agarose gel electrophoresis of DNA extracted from Jurkat cells treated with the two most active compounds (**DE-8** and **DE-11**) showed a massive DNA fragmentation after 48 h of incubation for **DE-11** while with **DE-8**, we did not observed a clear fragmentation, but only a "smear" of degraded DNA.

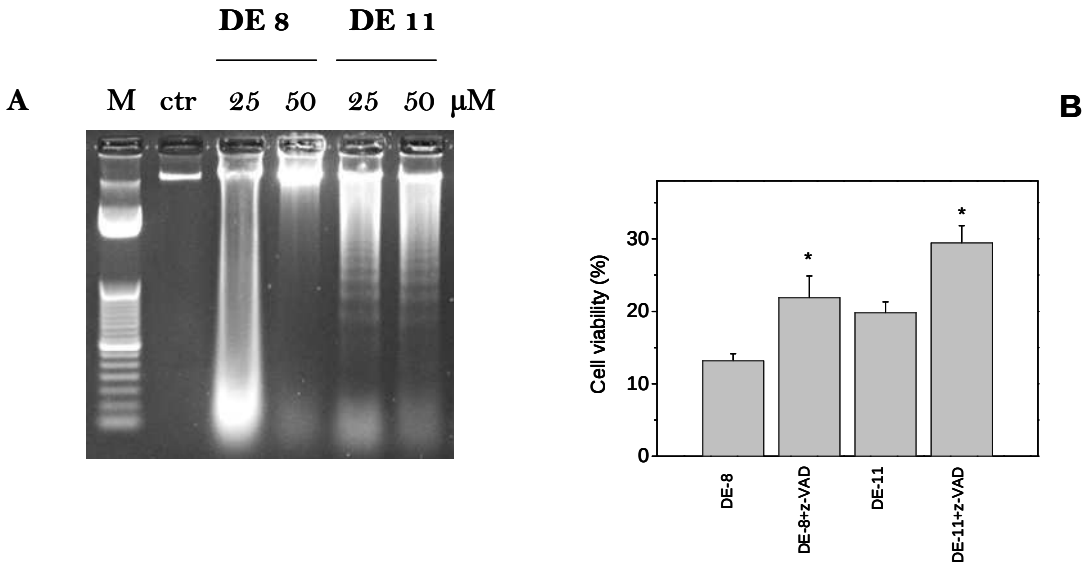

Figure 3. *Agarose gel electrophoresis of chromosomal DNA extracted from Jurkat cells after 48 h of incubation in the presence of DE-8 (50 and 25μM) and DE-11 (25 and 12.5 μM) Lane 1: Ctr; lane 2. UVA; Lane 3: FLV 50 μM; Lane 4: FP6 (10 μM) Lane M indicated size marker DNAs. Panel B Percentage of cell viability, determined by MTT test, after 48 h of incubation of Jurkat cells with DE-8 (50 μM) or DE-11 (25 μM) in the presence or in the absence of z-VAD.fmk (100 μM). Mean ± SEM of three independent experiments. *p<0.01 vs. treated cells in the absence of inhibitor.*

To evaluate if the cell death induced by **DE-8** and **DE-11** is caspase-dependent, Jurkat cells were treated with the two compounds in the absence or presence of the pan-caspase inhibitor z-VAD Inhibition of caspases significantly increased cell viability (Figure 3, panel B), but this caspase inhibition had only a partial impact on the induced cell death. The caspase inhibitor increased cell survival from about 13% to 21%, and from 19% to 29% for DE-8 and DE-**11** respectively, suggesting that other mechanism(s) may lead to cell death following treatment with daucane esters.

3.5 Analysis of the cell cycle.

To investigate the effects of daucane esters on the cell cycle, Jurkat cells were treated with the test compounds at different concentrations, and after 48 h incubation, the cells were fixed and labelled with propidium iodide. The different phases of the cell cycle were analysed by flow cytometry. Figure 4 (panel A), show the results obtained for compounds DE-3, DE5, DE-8 and DE-11. The four compounds showed a different behaviour; while DE-5 and DE-11 induce, in a concentration–dependent manner, a G2/M arrest along with a decrease of all the other phases of the cell cycle, the other two compounds DE-3 and DE-**8** induce a slight accumulation of the cells in G1 phase that disappear at higher concentrations (50 μM).

This effect is accompanied by a reduction of the S phase whereas the G2/M remain practically unchanged. It is worthwhile to note the appearance of a remarkable hypodiploid peak (Sub-G1) indicative of apoptosis (Figure 4, panel B) in well agreement with the above results.

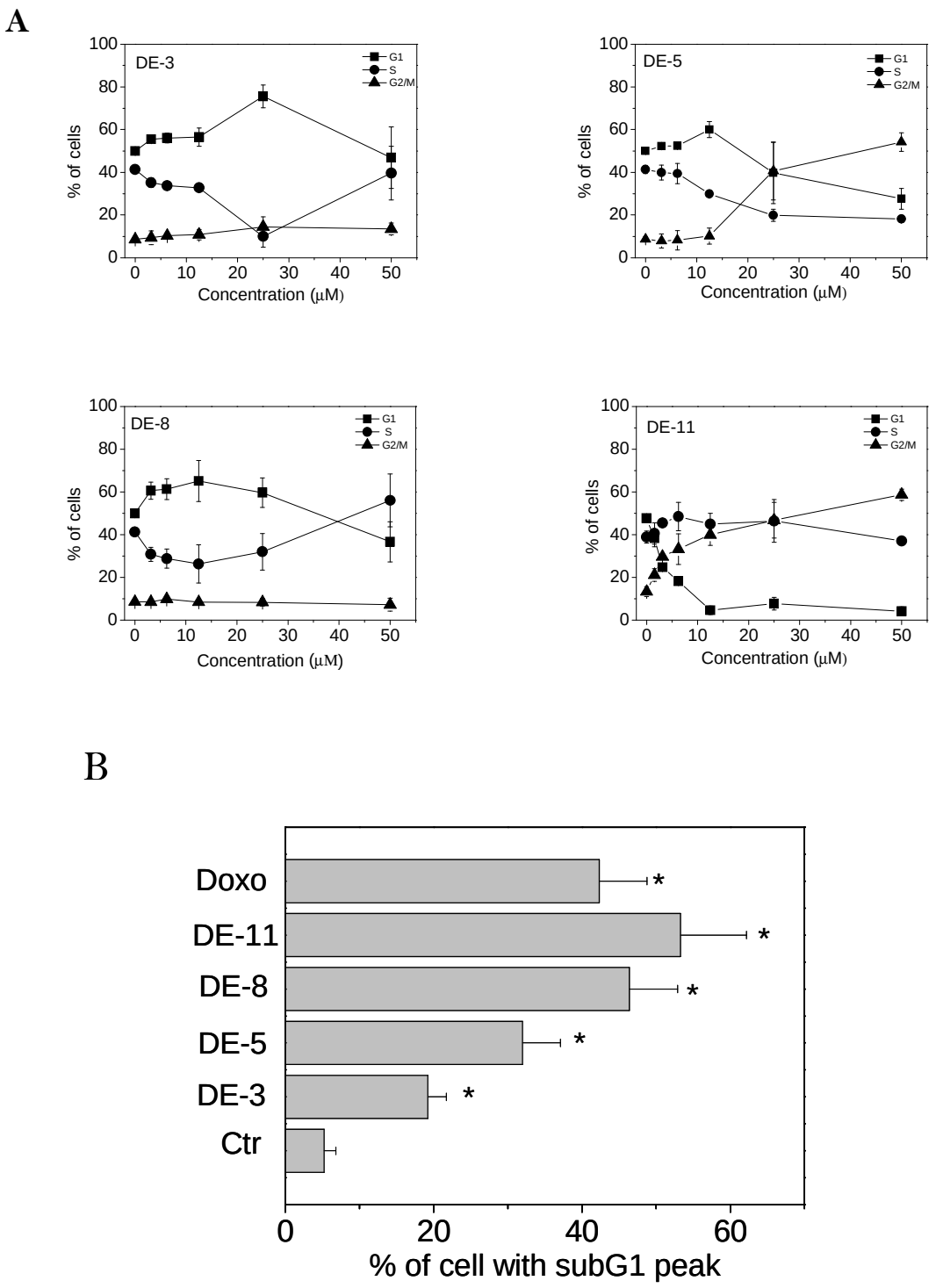

Figure 4. *Effects of DE-3, DE-5 DE-8 and DE-11 on the cell cycle in Jurkat cells (panel A). Cells were treated with different concentrations ranging from 1.25 to 100 μM for 48 h. Then the cells were fixed and stained with PI to analyze DNA content by flow cytometry. Data are presented as mean ± SEM of three independent experiments. Panel B. Percentage of cells presenting a hypodipolid peak (SubG1) after treatment of cells with the indicated compounds at the concentration of 50 μM. Doxorubicin (Doxo) was used as positive control at the concentration of 1 μM. Data are presented as mean ± SEM of three independent experiments. *p<0.01 vs control cells.*

3.6 Detection of the release of calcium in DE 8.

We have analyzed the release of calcium through the fluorescent probe Fluo 3 AM. We incubated the cells with the probe but without the compound, after a period of stabilization in which we observed a stable baseline we added to the cell suspension compound DE 8 at 50 μM, and we recorded the fluorescence signal for one hour. As shown in Figure 5, it can be observed that immediately after the introduction of the compound in the reading start a release of calcium.

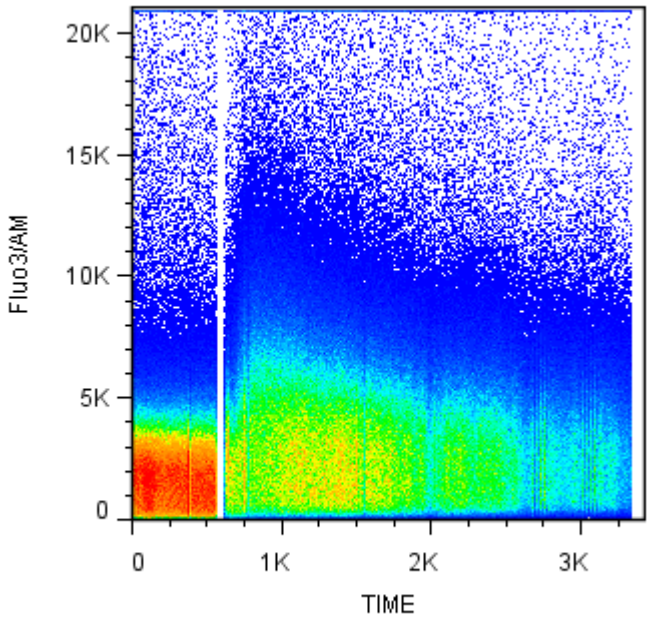

Figure 5: *Increasing of intracellular calcium after additionof DE8 (50 μM) to a suspension of Jurkat cells stained with the Ca^{2+} sensitive fluorescent probe Fluo3-AM*

Measurement of ROS production mitochondrial potential.

We analyzed the production of ROS by compound DE 8 in Jurkat cells. using two different fluorescent probes2',7'-dichlorodihydrofluorescein diacetate (H_2-DCFDA) and hydroethidine (HE). The results depicted in figure 6 show that there is a high ROS production, detected with both fluorescent probes, at a short times (1-3 h) after the incubation, that increase further at longer times (12h). Interestingly analysis of the mitochondrial potential carried out with the fluorescent probe JC1 showed that cells treated with DE8 present an evident mitochondrial depolarization only after 12-24 incubation, suggesting that initial production of ROS is not a merely consequence of the

mitochondrial depolarization but is due to interaction of the compound with some unknown system able to produce ROS

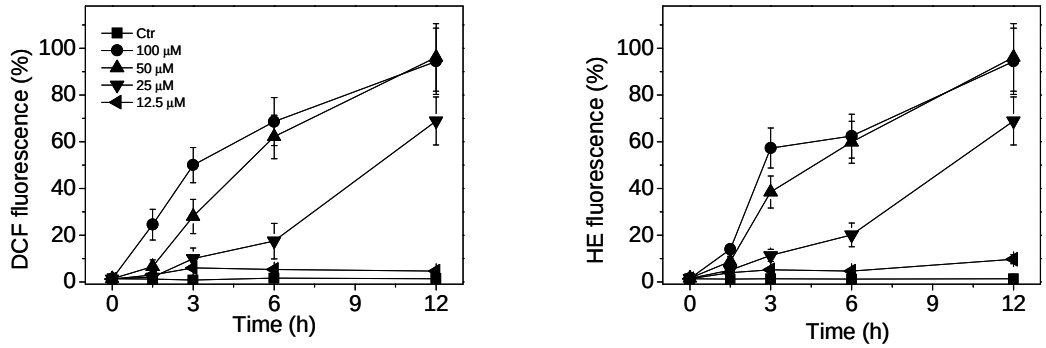

Figure 6. *DE-8 induce ROS production. Time course of ROS production in Jurkat cell treated with the indicated concentrations of DE-8. ROs production was detected by flow cytometry using the two fluorescent probes 2',7'-dichlorodihydrofluorescein diacetate (H_2-DCFDA) and hydroethidine (HE). Data are expressed as mean ± S.E.M. of 3 independent experiments.*

As depicted in the figure it can be observed a significative appearance of ROS. These ROS are not derived from mitochondria since as shown in the next figure, mitochondrial depolarization occur later and is a consequence of induced apoptosis.

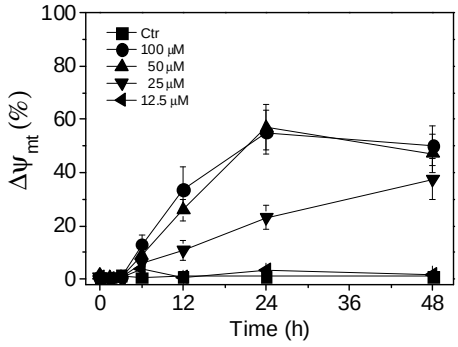

Figure 7. *Analysis of mitochondrial potential after treatment with compound DE-8 at the indicated concentrations. Jurkat cells were stained with the fluorescent probe JC-1 and analyzed by flow cytometry at different times of incubation. Data are expressed as mean ± S.E.M. of 3 independent experiments.*

To further prove the involvement of ROS in DE-8 induced cell death we performed experiments in which we analyzed the cell viability after 48 h of incubation with DE-8 (50 μM) in the presence of two well know ROS scavengers. As shown in the figure both Tocopherol acetate (TOC) and N-acetyl cysteine (NAC) significantly increase cell viability.

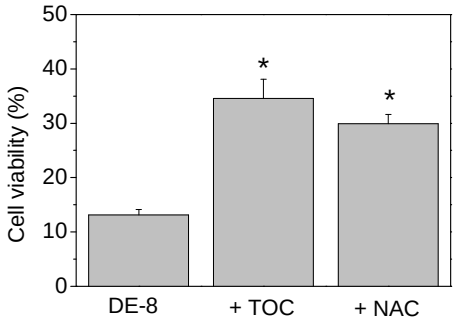

Figure 8. *Effect of Tocopherol (TOC, 100 μM) and N-acetyl cisteine (NAC 1mM) on the cell death induced by DE-8 (50 μM). Jurkat cell were incubate in the absence or in the presence of the scavengres and the after 48 h of incubation cell viability was measured by MTT test. Data are expressed as mean ± S.E.M. of 3 independent experiments. *p<0.01 vs DE-8 alone.*

4. Conclusions

This paper present the isolation and structural characterization of two new and fourteen known daucane esters together with four coumarins, two phenylpropanoids, and one polyacetylene. All the isolated compounds were tested for their antiproliferative activity against a panel of human tumour cell lines and some of the daucane esters present significant activity. On the basis of the cytotoxic effects we could trace some preliminary evaluation of structure activity relationships for the considered daucane derivatives observing that the *trans* fusion of the penta- and hepta-atomic cycles, and lipophilic ester groups linked to positions 6 are enhancing the cytotoxic activity. Moreover the isomeric derivatives (**DE-8** and **DE-9** or **DE-3**, **DE-4** and **DE-5**) present significant differences in their IC_{50} supporting that the β orientation for the ester group in the position 2 is crucial for the cytotoxic effect. Furthermore we investigated the mode of cell death induced by the two most active

compounds showing that apoptosis may be the primary cause of cell death after incubation with **DE-8** and **DE-11**. Interestingly the antiproliferative activity is moderately reduced in the presence of the pancaspase inhibitor z-VAD suggesting that induced apoptosis is partially caspase-dependent. Our results are in good agreement with that reported by Gamal-Eldeen *et al.*[23]and Macho *et al.*[24] which found that lapiferin and ferutinin two daucane derivatives induce apoptosis in MCF-7 and Jurkat cell lines respectively. Moreover they also found that apoptosis is mediated by caspase activation.

We observed a cell cycle arrest upon incubation with daucane derivatives along with a decrease of the S phase. More importantly, we detected the appearance of a hypodiploid peak (subG1). This peak represents those cells with a DNA content less than G1, usually considered as apoptotic cells, On the contrary, Poli *et al.*[11] reported that daucane esters induce an antiproliferative activity in three colon cancer cell lines and this effect was preceded by cell cycle arrest in the G1 phase that is not followed by apoptosis. Preliminary experiments indicate that the mechanism of induced cell death is a strong oxidative stress induced by the compounds. Of course further experiment are needed to evaluate in detail which are the mechanism(s) involved.

In conclusion, we have demonstrated the antiproliferative activity of some daucane derivatives isolated from different species of *Ferula* and, although at the present stage is not possible to present a precise mechanism of these compounds, our data suggest that apoptosis may be the major cause of cell death.

References

Appendino, G.; Tagliapietra, S.; Paglino, L.; Nano, G. M.; Monti, D.; Picci, V. *Phytochemistry* **1990,** *29*, 1481.

1.

2. Lamnaouer, D.; Martin, M.T.; Molho, D.; Bodo, B. *Phytochemistry* **1989,** *28*, 2711.

3. Appendino, G.; Tagliapietra, S.; Gariboldi, P.; Nano, M.G.; Picci, V. *Phytochemistry* **1988,** *27*, 3619.

4. Miski, M.; Mabry, T. J.; Saya, Ö. *J. Nat. Prod.* **1987,** *50*, 829.

5. Miski, M.; Mabry, T. J. *Phytochemistry* **1985,** *24*, 1735.

6. Abd El-Razek, M. H.; Ohta, S.; Hirata, T. *Heterocycles* **2003,** *60*, 689.

7. Al-Yahya, M. A.; Muhammad, I.; Mirza, H. H.; El-Feraly, F. S. *Phytother. Res.* **1998,** *12*, 335.

8. Arnoldi, L.; Ballero, M.; Fuzzati, N.; Maxia, A.; Mercalli, E.; Pagni, L. *Fitoterapia* **2004,** *75*, 342.

9. Miski, M.; Jakupovic, J. *Phytochemistry* **1990,** *29*, 1995.

10. Miski, M.; Mabry, T. J.; Bohlmann, F. *J. Nat. Prod.* **1986,** *49*, 916.

11. Poli, F.; Appendino, G.; Sacchetti, G.; Ballero, M.; Maggiano, N.; Ranelletti, F. O. *Phytother. Res.* **2005,** *19*, 152.

12. Dall'Acqua, S.; Maggi, F.; Minesso, P.; Salvagno, M.; Papa, F.; Vittori, S.; Innocenti, G. *Fitoterapia* **2010,** *81*, 1208.

13. Bazzaz, B. S. F.; Memariani, Z.; Khashiarmanesh, Z.; Iranshahi, M.; Naderinasab, M. *Braz. J. Microbiol.* **2010,** *41*, 574.

14. Basile, A.; Sorbo, S.; Spadaro, V.; Bruno, M.; Maggio, A.; Faraone, N.; Rosselli, S. *Molecules* **2009,** *14*, 939.

15. Iranshahi, M.; Arfa, P.; Ramezani, M.; Jaafari, M. R.; Sadeghian, H.; Bassarello, C.; Piacente, S.; Pizza, C. *Phytochemistry* **2007,** *68*, 554.

16. Iranshahi, M.; Sahebkar, A.; Hosseini, S. T.; Takasaki, M.; Konoshima, T.; Tokuda, H. *Phytomedicine* **2010,** *17*, 269.

17. Iranshahi, M.; Sahebkar, A.; Takasaki, M.; Konoshima, T.; Tokuda, H. *Eur. J. Cancer Prev.* **2009,** *18*, 412.

18. Maggi, F.; Cecchini, C.; Cresci, A.; Coman, M. M.; Tirillini, B.; Sagratini, G.; Papa, F. *Fitoterapia* **2009,** *80*, 68.

19. Maggi, F.; Tirillini, B.; Papa, F.; Sagratini, G.; Vittori, S.; Cresci, A.; Coman, M. M.; Cecchini, C. *Flavour Fragrance J.* **2009**, *24*, 309.

20. Cecchini, C.; Coman, M. M.; Cresci, A.; Tirillini, B.; Cristalli, G.; Papa, F.; Sagratini, G.; Vittori, S.; Maggi, F. *Flavour Fragrance J.* **2010**, *25*, 493.

21. Appendino, G.; Spagliardi, P.; Cravotto, G.; Pocock, V.; Milligan, S. *J. Nat. Prod.* **2002**, *65*, 1612.

22. Lee, C. -.; Chiang, L. -.; Cheng, L. -.; Liaw, C. -.; Abd El-Razek, M. H.; Chang, F. -.; Wu, Y. -. *J. Nat. Prod.* **2009**, *72*, 1568.

23. Gamal-Eldeen, A. M.; Hegazy, M. -. F. *Nat. Prod. Res.* **2010**, *24*, 246.

24. Macho, A.; Blanco-Molina, M.; Spagliardi, P.; Appendino, G.; Bremner, P.; Heinrich, M.; Fiebich, B. L.; Muñoz, E. *Biochem. Pharmacol.* **2004**, *68*, 875.

25. Lhuillier, A.; Fabre, N.; Cheble, E.; Oueida, F.; Maurel, S.; Valentin, A.; Fourasté, I.; Moulis, C. *J. Nat. Prod.* **2005**, *68*, 468.

26. Suzuki, K.; Okasaka, M.; Kashiwada, Y.; Takaishi, Y.; Honda, G.; Ito, M.; Takeda, Y.; Kodzhimatov, O. K.; Ashurmetov, O.; Sekiya, M.; Ikeshiro, Y. *J. Nat. Prod.* **2007**, *70*, 1915.

27. Alkhatib, R.; Hennebelle, T.; Joha, S.; Idziorek, T.; Preudhomme, C.; Quesnel, B.; Sahpaz, S.; Bailleul, F. *Phytochemistry* 2008, *69*, 2979.

28. Alkhatib, R.; Hennebelle, T.; Joha, S.; Roumy, V.; Güzel, Y.; Biabiany, M.; Idziorek, T.; Preudhomme, C.; Quesnel, B.; Sahpaz, S.; Bailleul, F. *J. Nat. Prod.* 2010, *73*, 780.

29. Šmejkal, K.; Svačinová, J.; Šlapetová, T.; Schneiderová, K.; Dall'Acqua, S.; Innocenti, G.; Závalová, V.; Kollár, P.; Chudík, S.; Marek, R.; Julínek, O.; Urbanová, M.; Kartal, M.; Csöllei, M.; Doležal, K. *J. Nat. Prod.* 2010, *73*, 568.

30. Šmejkal, K.; Babula, P.; Šlapetové, T.; Brognara, E.; Dall'Acqua, S.; Žemlička, M.; Innocenti, G.; Cvačka, J. *Planta Med.* 2008, *74*, 1488.

31. Dall'Acqua, S.; Viola, G.; Piacente, S.; Cappelletti, E. M.; Innocenti, G. *J. Nat. Prod.* 2004, *67*, 1588.

32. Dall'Acqua, S.; Viola, G.; Giorgetti, M.; Loi, M. C.; Innocenti, G. *Chemical and Pharmaceutical Bulletin* 2006, *54*, 1187.

33. Miski, M.; Ulubelen, A.; Mabry, T. J.; Watson, W. H.; Vickovic, I.; Holub, M. *Tetrahedron* 1984, *40*, 5197.

34. Miski, M.; Ulubelen, A.; Mabry, T. J.; Watson, W. H.; Vickovic, I.; Holub, M. *Tetrahedron* 1984, *40*, 5197.

35. Appendino, G.; Spagliardi, P.; Sterner, O.; Milligan, S. *J. Nat. Prod.* 2004, *67*, 1557.

36. Miski, M.; Mabry, T. J. *J. Nat. Prod.* 1986, *49*, 657.

37. Diaz, J. G.; Fraga, B. M.; González, A. G.; Gónzalez, P.; Hernández, M. G. *Phytochemistry* 1984, *23*, 2541.

38. Kushmuradov, A. Y.; Saidkhodzhaev, A. I.; Malikov, V. M. *Chem Nat Compd* 1986, *22*, 48.

39. Miski, M.; Ulubelen, A.; Mabry, T. J. *Phytochemistry* 1983, *22*, 2231.

40. Eshbakova, K. A.; Saidkhodzhaev, A. I. *Chem. Nat. Compd.* 2004, *40*, 194.

41. Iranshahi, M.; Shahverdi, A. R.; Mirjani, R.; Amin, G.; Shafiee, A. *Z. Naturforsch. Sect. C J. Biosci.* 2004, *59*, 506.

42. Schmiech, L.; Uemura, D.; Hofmann, T. *J. Agric. Food Chem.* 2008, *56*, 10252.

43. Miski, M.; Jakupovic, J. *Phytochemistry* 1990, *29*, 173.

44. Appendino, G.; Pollastro, F.; Verotta, L.; Ballero, M.; Romano, A.; Wyrembek, P.; Szczuraszek, K.; Mozrzymas, J. W.; Taglialatela-Scafati, O. *J. Nat. Prod.* 2009, *72*, 962.

45. Vermes, I.; Haanen, C.; Steffens-Nakken, H.; Reutelingsperger, C.P. *J. Immun. Method* 1995, *184*, 39-51.

46. Galluzzi, L., Aaronson, S.A., Abrams, J., Alnemri, E.S., Andrews, D.W., Baehrecke E.H., et al. *Cell Death Differ.* 2009, *16*, 1093-1107.

47 Viola G.; Fortunato E.; Cecconet L.; Del Giudice L., Dall'Acqua F.; Basso G. *Toxicol. Appl. Pharm.* 2008, *227*, 84-96.